



3-1981

## The Development, Implementation, and Evaluation of Depletion Perturbation Theory in a Light Water Reactor Nodal Code

Stephen M. Bowman  
*University of Tennessee, Knoxville*

Follow this and additional works at: [https://trace.tennessee.edu/utk\\_gradthes](https://trace.tennessee.edu/utk_gradthes)



Part of the [Nuclear Engineering Commons](#)

---

### Recommended Citation

Bowman, Stephen M., "The Development, Implementation, and Evaluation of Depletion Perturbation Theory in a Light Water Reactor Nodal Code. " Master's Thesis, University of Tennessee, 1981.  
[https://trace.tennessee.edu/utk\\_gradthes/3960](https://trace.tennessee.edu/utk_gradthes/3960)

This Thesis is brought to you for free and open access by the Graduate School at TRACE: Tennessee Research and Creative Exchange. It has been accepted for inclusion in Masters Theses by an authorized administrator of TRACE: Tennessee Research and Creative Exchange. For more information, please contact [trace@utk.edu](mailto:trace@utk.edu).

To the Graduate Council:

I am submitting herewith a thesis written by Stephen M. Bowman entitled "The Development, Implementation, and Evaluation of Depletion Perturbation Theory in a Light Water Reactor Nodal Code." I have examined the final electronic copy of this thesis for form and content and recommend that it be accepted in partial fulfillment of the requirements for the degree of Master of Science, with a major in Nuclear Engineering.

H. Lee Dodds, Major Professor

We have read this thesis and recommend its acceptance:

L. F. Miller, P. F. Pasqua, Paul C. Polard

Accepted for the Council:

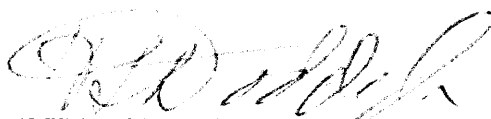
Carolyn R. Hodges

Vice Provost and Dean of the Graduate School

(Original signatures are on file with official student records.)

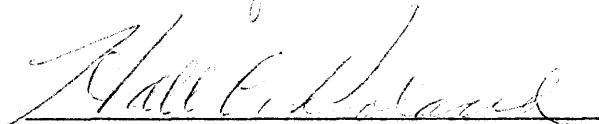
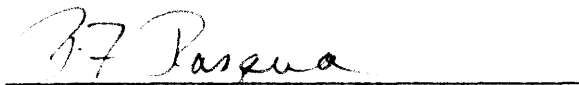
To the Graduate Council:

I am submitting herewith a thesis written by Stephen M. Bowman entitled "The Development, Implementation, and Evaluation of Depletion Perturbation Theory in a Light Water Reactor Nodal Code." I recommend that it be accepted in partial fulfillment of the requirements for the degree of Master of Science, with a major in Nuclear Engineering.



H. Lee Dodds, Major Professor

We have read this thesis  
and recommend its acceptance:



Accepted for the Council:



Vice Chancellor  
Graduate Studies and Research

THE DEVELOPMENT, IMPLEMENTATION, AND EVALUATION  
OF DEPLETION PERTURBATION THEORY IN A  
LIGHT WATER REACTOR NODAL CODE

A Thesis

Presented for the

Master of Science

Degree

The University of Tennessee, Knoxville

Stephen M. Bowman

March 1981

30419500

## ACKNOWLEDGMENTS

The author wishes to express his appreciation for the advice and encouragement of Dr. H. L. Dodds, his major professor, and the University of Tennessee staff members who served on his Graduate Committee.

The author would also like to thank Dr. M. L. Williams of the Engineering Physics Division at the Oak Ridge National Laboratory for his guidance throughout this entire work. Thanks are also due to Dr. S. H. Levine of the Pennsylvania State University, who provided data from Cycle I of Three Mile Island Unit I which were used for many of the calculations in this work. Special thanks are due to A. L. Houston and J. K. Lawhorn for the many hours they spent typing the drafts and final version of this report.

The author wishes to express his appreciation for the support and use of the facilities of the U.S. Department of Energy under contract W-7405-eng-26 with the Union Carbide Corporation Nuclear Division.

## ABSTRACT

A generalized depletion perturbation (DPT) theory formulation for light water reactor (LWR) depletion problems is developed and implemented into the three-dimensional LWR nodal code SIMULATE. This development applies the principles of the original derivation by M. L. Williams to the nodal equations solved by SIMULATE. The present formulation is first described in detail, and the nodal coupling methodology in SIMULATE is used to determine partial derivatives of the coupling coefficients. The modifications to the original code and the new DPT options available to the user are discussed. Finally, the accuracy and the applicability of the new DPT capability to LWR design analysis is examined for several LWR depletion test cases.

The cases range from simple static cases to a realistic PWR model for an entire fuel cycle. Responses of interest included  $K_{\text{eff}}$ , nodal peaking, and peak nodal exposure. The nonlinear behavior of responses with respect to perturbations of the various types of cross sections was also investigated. The time-dependence of the sensitivity coefficients for different responses were examined and compared.

Comparison of DPT results for these examples to direct calculations reveals the limited applicability of depletion perturbation theory to LWR design calculations at the present. The reasons for these restrictions are discussed, and several methods which might improve the computational accuracy of DPT are proposed for future research.

## TABLE OF CONTENTS

SECTION	PAGE
I. INTRODUCTION . . . . .	1
General Comments . . . . .	1
Scope and Organization . . . . .	2
II. DEVELOPMENT OF THE GENERALIZED AND DEPLETION ADJOINT EQUATIONS FOR <u>SIMULATE</u> . . . . .	4
Review of Perturbation Theory. . . . .	4
Formulation of Generalized Adjoint Equations for <u>SIMULATE</u> . . . . .	7
Development of Depletion Adjoint Equations for <u>SIMULATE</u> . . . . .	17
III. APPROXIMATING THE CHANGES IN THE NODAL COUPLING COEFFICIENTS . . . . .	24
<u>SIMULATE</u> Nodal Coupling Methodology. . . . .	24
Determination of the Nodal Coupling Coefficients Using Coarse Mesh Diffusion Theory. . . . .	32
The Partial Derivatives of the Nodal Coupling Coefficients with Respect to the Two-Group Cross Sections. . . . .	38
IV. COMPARISON OF GPT AND DPT RESULTS TO DIRECT CALCULATIONS . . . . .	47
Static Cases . . . . .	47
Burnup Dependent Cases . . . . .	68
V. SUMMARY. . . . .	100
Conclusions. . . . .	100
Recommendations. . . . .	102
LIST OF REFERENCES . . . . .	104
APPENDICES . . . . .	106
APPENDIX A. ADJOINT MATRIX OPERATORS. . . . .	107
APPENDIX B. FUNDAMENTAL MODE CONTAMINATION. . . . .	113
APPENDIX C. DERIVATION OF DEPLETION ADJOINT EQUATIONS . . . . .	116
APPENDIX D. IMPLEMENTATION OF DEPLETION PERTURBATION THEORY INTO <u>SIMULATE</u> . . . . .	131
VITA . . . . .	154

## LIST OF TABLES

TABLE	PAGE
2.1. Two-Group Macroscopic Cross Sections Input to SIMULATE. . . . .	8
3.1. Hierarchy for Nodal Coupling Coefficients as Functions of Two-Group Cross Sections. . . . .	39
4.1. Comparison of GPT Results with Direct Results . . . . .	49
4.2. Comparison of GPT Results with Direct Results for Changing Enrichment . . . . .	51
4.3. Comparison of GPT and SD Results to Direct Calculations for 5% Perturbations of a 2-D Model for $K_{eff}$ Response . . . . .	54
4.4. Comparison of GPT and SD Results to Direct Calculations for 10% Perturbations of a 2-D Model for $K_{eff}$ Response. . . . .	55
4.5. Comparison of GPT and SD Results to Direct Calculations for 10% Perturbations of a 2-D Model for Power Peaking in Fuel Assembly #3 . . . . .	57
4.6. Comparison of GPT Results to Direct Calculations for 10% Perturbations of a 3-D Model for $K_{eff}$ Response. . . . .	58
4.7. $K_{eff}$ Versus $\nu \sum_{f_1}$ . . . . .	61
4.8. $K_{eff}$ Versus $\sum_{a_2}$ . . . . .	61
4.9. Decrease LBP Concentration in Fuel Assembly #12 . . . . .	64
4.10. Remove Partial Control Rod from Fuel Assembly #13 . . . . .	65
4.11. Insert Partial Control Rod into Fuel Assembly #4. . . . .	66
4.12. Remove Control Rod from Fuel Assembly #24 . . . . .	67
4.13. Insert Control Rod into Fuel Assembly #22 . . . . .	68
4.14. Replacing a Low Enrichment Fuel Assembly and a Medium Enrichment Fuel Assembly with Two High Enrichment Fuel Assemblies. . . . .	69
4.15. Comparison of DPT Results to Direct Calculations for 10% Perturbations of a 3-D Model from 0-40 MWD/T for EOC $K_{eff}$ Response . . . . .	70



TABLE	PAGE
4.16. Comparison of DPT Results to Direct Calculations for 10% Perturbations of a 3-D Model from 0-40 MWD/T for Peak Exposure Response. . . . .	72
4.17. Removal of a Partial Control Rod from Fuel Assembly #13 for a Fuel Cycle of 14,000 MWD/T. . . . .	72
4.18. Cross Section Perturbations for Removal of Partial Control Rod from Fuel Assembly #13. . . . .	74
4.19. Replacing a High Enrichment Fuel Assembly with a Low Enrichment Fuel Assembly for a Fuel Cycle of 14,000 MWD/T . . .	85
4.20. Cross Section Perturbations for Replacing a High Enrichment Fuel Assembly with a Low Enrichment Fuel Assembly. . . . .	86
4.21. Removal of LBP at BOC and Insertion of Control Rod at 8,000 MWD/T in Fuel Assembly #22 for a Fuel Cycle of 14,000 MWD/T. . . . .	88
4.22. Cross Section Perturbations for Removal of LBP at BOC and Insertion of Control Rod in Fuel Assembly #22 . . . . .	89
4.23. 5% Perturbation of $\nu \sum_{f_1}$ for a Fuel Cycle of 14,000 MWD/T. . . . .	91
D.1. Macroscopic Cross Sections with Sensitivity Coefficients. . . . .	142
D.2. Identification Numbers of Available Control Variables . . . . .	144
D.3. New Subroutines Added to SIMULATE . . . . .	146
D.4. I/O Units for Forward and Backward March Through Time . . . . .	147
D.5. Control Options for Depletion Adjoint Equations . . . . .	150
D.6. Internal Flags for Depletion Adjoint Equations. . . . .	152
D.7. Edits of New Arrays . . . . .	153

## LIST OF FIGURES

FIGURE	PAGE
2.1. Quarter Core with Half-Node Boundaries . . . . .	11
3.1. SIMULATE Nodal Arrangement . . . . .	25
3.2. Neutron Partial Current Representation . . . . .	29
4.1. Two-Dimensional Top View of GPT Test Model 1/4 Core . . . . .	48
4.2. Two-Dimensional Top View of PWR Reference Case 1/8 Core. . . . .	52
4.3. $K_{\text{eff}}$ Versus $\nu \sum_{f_1}$ . . . . .	59
4.4. $K_{\text{eff}}$ Versus $\sum_{a_2}$ . . . . .	60
4.5. $\sum_{a_1}$ Sensitivity Coefficient for EOC $K_{\text{eff}}$ . . . . .	75
4.6. $\sum_{r_1}$ Sensitivity Coefficient for EOC $K_{\text{eff}}$ . . . . .	76
4.7. $\nu \sum_{f_1}$ Sensitivity Coefficient for EOC $K_{\text{eff}}$ . . . . .	77
4.8. $\sum_{a_2}$ Sensitivity Coefficient for EOC $K_{\text{eff}}$ . . . . .	78
4.9. $\nu \sum_{f_2}$ Sensitivity Coefficient for EOC $K_{\text{eff}}$ . . . . .	79
4.10. $\sum_{a_1}$ Sensitivity Coefficient for EOC Peak Exposure. . . . .	80
4.11. $\sum_{r_1}$ Sensitivity Coefficient for EOC Peak Exposure. . . . .	81
4.12. $\nu \sum_{f_1}$ Sensitivity Coefficient for EOC Peak Exposure . . . . .	82
4.13. $\sum_{a_2}$ Sensitivity Coefficient for EOC Peak Exposure. . . . .	83
4.14. $\nu \sum_{f_2}$ Sensitivity Coefficient for EOC Peak Exposure . . . . .	84
4.15. BOC Fission Source Density . . . . .	92
4.16. EOC Fission Source Density . . . . .	93
4.17. BOC Adjoint Function . . . . .	94
4.18. EOC Adjoint Function . . . . .	95
4.19. BOC Generalized Adjoint Function . . . . .	96

FIGURE	PAGE
4.20. Generalized Adjoint Function at Exposure Step ( $\lambda-1$ ). . . .	97
A.1. Half Nodes on Boundary . . . . .	109
A.2. Full Nodes on Boundary . . . . .	110
D.1. Flow Chart for the Inner and Outer Source Iteration Levels . . . . .	133
D.2. Fuel Bundle ID Numbers - Old Method. . . . .	135
D.3. Fuel Bundle ID Numbers - New Method. . . . .	136
D.4. Forward March Through Time . . . . .	139
D.5. Backward March Through Time. . . . .	140

## I. INTRODUCTION

### General Comments

Obtaining the maximum energy production from the uranium fuel in light water reactors (LWRs) before removing the fuel from the reactor core is a primary concern of the commercial nuclear power industry. With the escalating costs for all forms of energy and the shortage of resources with which to produce the energy, improvement of the uranium utilization efficiency of the LWR fuel cycle has both economic and resource management incentives. One of the most important areas under study is the improvement of fuel loading and shuffling programs.

Designing optimal fuel loading patterns requires many expensive computer calculations. Since these calculations are usually similar in nature, they are prime candidates for solution by a perturbation theory, or sensitivity analysis, approach. A perturbation theory approach replaces many repetitive calculations with a single reference calculation. This reference calculation, which contains both a forward and an adjoint calculation, is then used with the sensitivity coefficients obtained by this type of method to predict changes in the reactor performances for any number of changes in the reference design without performing any further costly design calculations. These sensitivity coefficients are determined from the forward and the adjoint solutions and from appropriate partial derivatives. They measure the relative importance of various design parameters and control variables to a certain reactor system response.

The use of perturbation theory methods has become more widespread for static reactor analysis problems in recent years. An increasing amount of attention has also been given to extending these methods to time-dependent cases. Williams<sup>1</sup> has demonstrated the applicability of sensitivity theory depletion analysis through the development of coupled adjoint equations to account for variations in the neutron and nuclide fields arising from variations in the initial conditions and the nuclear data. Solving these adjoint equations backwards in time yields sensitivity coefficients which relate the change in a certain system response of interest (e.g.,  $K_{eff}$ ) at the final time to changes in design parameters or nuclear data at the initial time. One then has the capability to study the effects of changing different design parameters without recalculating the forward equations each time. This can result in large savings in computing costs, especially if very many forward calculations are required, with a minimal loss in accuracy.

### Scope and Organization

The objectives of this work are (1) to develop the depletion adjoint equations consistent with depletion perturbation theory for the three-dimensional LWR nodal analysis code SIMULATE,<sup>2</sup> (2) to implement these equations into SIMULATE and make the necessary modifications to allow for the solution of these equations in a manner consistent with the solution of the forward equations, and (3) to verify and evaluate the modified code by comparing results obtained from the solution of the depletion adjoint equations with results obtained by direct calculations.

The accomplishment of these objectives is covered in the remainder of this report. Section II reviews the basic principles of perturbation

theory and presents the system of equations which are adjoint to the forward equations solved by SIMULATE. In Section III the derivatives needed for the Taylor Series approximation of the changes in the nodal coupling coefficients are developed. The results of several depletion perturbation cases are compared to direct calculations in Section IV. Conclusions drawn from this work and suggestions for future work are presented in Section V.

## II. DEVELOPMENT OF THE GENERALIZED AND DEPLETION ADJOINT EQUATIONS FOR SIMULATE

### Review of Perturbation Theory

One is often interested in computing the change in a reactor response such as the effective multiplication factor caused by a change in the composition of the core design. For small changes or "perturbations," it is possible to do this without performing another complete criticality calculation by applying perturbation theory techniques to approximate the response change in terms of the original calculation.

To better understand the basic principles of perturbation theory, let us study a simple example. The one-group criticality equation is<sup>3</sup>

$$-\nabla \cdot D(\bar{r})\nabla\phi(\bar{r}) + \Sigma_a(\bar{r}) = \frac{1}{K} \nu \Sigma_f(\bar{r})\phi(\bar{r}) \quad (2.1)$$

which can also be written in operator notation

$$M\phi = \frac{1}{K} F\phi \quad (2.2)$$

where

$$M = -\nabla \cdot D(\bar{r})\nabla + \Sigma_a$$

and

$$F = \nu \Sigma_f(\bar{r})$$

The adjoint of an operator  $H$  (denoted as  $H^*$ ) is defined by the equation<sup>3</sup>

$$\langle \psi, H\phi \rangle = \langle \phi, H^*\psi \rangle + \text{boundary conditions} \quad (2.3)$$

where  $\langle \rangle$  signifies the inner product of the quantities contained therein. The boundary conditions in Eq. (2.3) are generally zero.

Suppose there is a small perturbation in the macroscopic absorption cross section,  $\Delta\bar{\Sigma}_a(\bar{r})$ , caused by the addition of a lumped burnable poison. Then the perturbed cross section is

$$\bar{\Sigma}'_a(\bar{r}) = \bar{\Sigma}_a(\bar{r}) + \Delta\bar{\Sigma}_a(\bar{r})$$

The criticality equation for the perturbed system is

$$M'\phi' = \frac{1}{K'} F\phi' \quad (2.4)$$

since  $\Delta\bar{\Sigma}_a(\bar{r})$  will cause a direct change in the  $M$  operator and an indirect change in the flux. We will now attempt to predict the change in  $K$  due to the perturbed absorption cross section.

We now define the adjoint flux as the solution of the adjoint of Eq. (2.2)

$$M^*\phi^* = \frac{1}{K^*} F^*\phi^* \quad , \quad (2.5)$$

where it is easy to show that  $K^* = K$ .<sup>3</sup>

Multiplying Eq. (2.4) by the adjoint flux and taking the inner product yields

$$\langle \phi^* M' \phi' \rangle = \langle \phi^* M \phi \rangle + \langle \phi^* \Delta M \phi \rangle = \frac{1}{K'} \langle \phi^* F \phi' \rangle \quad (2.6)$$



Using the adjoint property, one obtains

$$\langle \phi^* M \phi \rangle = \langle \phi^* M^* \phi^* \rangle$$

$$\frac{1}{K} \langle \phi^* F \phi \rangle = \frac{1}{K} \langle \phi^* F^* \phi^* \rangle .$$

Multiplying Eq. (2.5) by the perturbed flux and taking the inner product yields

$$\langle \phi^* M \Delta \phi \rangle = \frac{1}{K} \langle \phi^* F^* \Delta \phi \rangle . \quad (2.7)$$

Substituting these equations into Eq. (2.6), one obtains

$$\langle \phi^* \Delta M \phi \rangle = \left( \frac{1}{K'} - \frac{1}{K} \right) \langle \phi^* F \phi \rangle$$

or

$$\Delta \lambda = \frac{1}{K'} - \frac{1}{K} = \frac{\langle \phi^* \Delta M \phi \rangle}{\langle \phi^* F \phi \rangle} \quad (2.8)$$

All terms on the right hand side of Eq. (2.8) are known, with the exception of the perturbed flux. Equation (2.8) can be expanded

$$\Delta \lambda = \frac{\langle \phi^* \Delta M \phi \rangle}{\langle \phi^* F \phi \rangle} + \frac{\langle \phi^* \Delta M \Delta \phi \rangle}{\langle \phi^* F \phi \rangle} - \frac{\langle \phi^* \Delta M \phi \rangle \langle \phi^* F \Delta \phi \rangle}{\langle \phi^* F \phi \rangle^2} - \dots \quad (2.9)$$

For small perturbations, second and higher order terms can be neglected and we obtain the following approximation for first order (or linear) perturbation theory,

$$\Delta \lambda \cong \frac{\langle \phi^* \Delta M \phi \rangle}{\langle \phi^* F \phi \rangle} . \quad (2.10)$$

But

$$\Delta\lambda = \frac{1}{K'} - \frac{1}{K} = \frac{K-K'}{K'K} = \frac{-\Delta K}{K'K} \approx \frac{-\Delta K}{K^2}$$

for small perturbations of  $K$  near 1, so

$$\frac{\Delta K}{K} \approx - \frac{\langle \phi^* \Delta M \phi \rangle}{\frac{1}{K} \langle \phi^* F \phi \rangle} \quad (2.11)$$

From this simple example one can see that perturbation theory can be a useful tool in computing response changes for small perturbations in a reactor core design.

#### Formulation of Generalized Adjoint Equations for SIMULATE

SIMULATE solves a one-group eigenvalue equation which can be written in matrix form as<sup>2</sup>

$$(\underline{M} - \lambda \underline{F}) \underline{S} = 0 \quad (2.12)$$

where  $\underline{M}, \underline{F} \equiv$  nodal coupling coefficients which are complicated functions of nodal macroscopic cross sections

$$\lambda \equiv \text{the eigenvalue} = \frac{1}{K_{\text{eff}}}$$

$\underline{S} \equiv$  the fission neutron source density.

The macroscopic cross sections are input to SIMULATE as two group cross sections (Table 2.1) which SIMULATE then collapses into a set of one group parameters, as will be shown later in this section. The nodal

Table 2.1. Two-Group Macroscopic  
Cross Sections Input to SIMULATE

Identification Number	Macroscopic Cross Section
1	$\Sigma_{tr_1}$
2	$\Sigma_{a_1}$
3	$\Sigma_r = \Sigma_{s_{1 \rightarrow 2}}$
4	$v \Sigma_{f_1}$
5	$\Sigma_{f_1}$
6	$\Sigma_{tr_2}$
7	$\Sigma_{a_2}$
8	$v \Sigma_{f_2}$
9	$K \Sigma_{f_2}$

coupling coefficients are calculated then by any one of several options in SIMULATE<sup>2</sup>

- (1) Coarse mesh diffusion theory (CMDT)
- (2) Modified coarse mesh diffusion theory (MCMDT or PRESTO)
- (3) FLARE<sup>4</sup> equivalent
- (4) Diffusion theory with Taylor Series expansion (ROCS).

This work deals only with the first method, coarse mesh diffusion theory. The CMDT and MCMDT methods are the more widely used options because they are much more general in nature than FLARE or ROCS (FLARE requires extensive user familiarity and ROCS is limited to two-dimensional

cubical node problems). Coarse mesh diffusion theory was chosen for this work because it can be used for both two-dimensional and three-dimensional calculations, whereas MCMDT can not always be used for two-dimensional problems.<sup>5</sup>

SIMULATE has been modified in this work to also solve the adjoint of Eq. (2.12)

$$(\underline{M}^* - \lambda \underline{F}^*) \underline{S}^* = 0 \quad (2.13)$$

The adjoint matrix operators  $\underline{M}^*$  and  $\underline{F}^*$  are determined by reversing the coupling of the coefficients. When the boundary conditions in Eq. (2.3) are equal to zero, the adjoint matrix operators are the transposes of the matrices. However, the boundary conditions are not equal to zero for  $\underline{M}$  and  $\underline{F}$  in some core configurations (see Appendix A for details).

The solutions of Eqs. (2.12) and (2.13) can be used to calculate the first order approximation of a change in  $K_{\text{eff}}$  caused by some perturbation. The exact solution of Eq. (2.12) for the perturbed case is

$$(\underline{M}' - \lambda' \underline{F}') \underline{S}' = 0$$

or

$$\left[ \underline{M} + \Delta \underline{M} - (\lambda + \Delta \lambda) (\underline{F} + \Delta \underline{F}) \right] (\underline{S} + \Delta \underline{S}) = 0 \quad .$$

Neglecting second order terms, one obtains

$$(\underline{M} - \lambda \underline{F}) \Delta \underline{S} + (\Delta \underline{M} - \lambda \Delta \underline{F}) \underline{S} - \Delta \lambda \underline{F} \underline{S} \approx 0 \quad .$$

Multiplying this equation by  $\underline{S}^*$  and multiplying Eq. (2.12) by  $\underline{\Delta S}$  and subtracting one from the other gives

$$\underline{S}^*(\underline{M} - \lambda \underline{F}) \underline{\Delta S} + \underline{S}^*(\underline{\Delta M} - \lambda \underline{\Delta F}) \underline{S} - \underline{\Delta S} \underline{S}^* \underline{F} \underline{S} \approx \underline{\Delta S}(\underline{M}^* - \lambda \underline{F}^*) \underline{S}^* .$$

By the adjoint property, the first term on the LHS of the equation is equal to the RHS, and the equation reduces to

$$\underline{S}^*(\underline{\Delta M} - \lambda \underline{\Delta F}) \underline{S} - \underline{\Delta S} \underline{S}^* \underline{F} \underline{S} \approx 0$$

or

$$\underline{\Delta \lambda} = \frac{1}{K_{\text{eff}}} - \frac{1}{K_{\text{eff}}} \approx \frac{\underline{S}^*(\underline{\Delta M} - \lambda \underline{\Delta F}) \underline{S}}{\underline{S}^* \underline{F} \underline{S}} \quad (2.14)$$

Once SIMULATE has solved Eqs. (2.12) and (2.13), the solutions can be used in Eq. (2.14) to calculate the first order approximation of the change in  $K_{\text{eff}}$  for any given  $\underline{\Delta M}$  and  $\underline{\Delta F}$ .

If all of the nodes in a particular problem do not have the same volume, then the adjoint source  $\underline{S}^*$  in each partial node must be weighted by the relative volume of that node before solving Eq. (2.14). For example, in the two-dimensional quarter core problem illustrated in Fig. 2.1, the adjoint source for node 1 must be multiplied by  $\frac{1}{4}$ . For nodes 2 - 8 and 9, 17, 25, 32, 39, 45, and 50, the adjoint source in each node must be multiplied by  $\frac{1}{2}$ . This volume weighting is necessary since Eq. (2.14) is essentially an inner product over the volume as in Eq. (2.10).

The changes in the nodal coupling coefficients in Eq. (2.14) due to a perturbation in some design parameter can be approximated by a first-order Taylor Series expansion

0	2	10	18	26	33	40	46	51	0
9	1	9	17	25	32	39	45	50	0
10	2	10	18	26	33	40	46	51	0
11	3	11	19	27	34	41	47	52	0
12	4	12	20	28	35	42	48	0	0
13	5	13	21	29	36	43	49	0	0
14	6	14	22	30	37	44	0	0	0
15	7	15	23	31	38	0	0	0	0
16	8	16	24	0	0	0	0	0	0
0	0	0	0	0	0	0	0	0	0

Fig. 2.1. Quarter Core with Half-Node Boundaries

$$\underline{\Delta M} \cong \frac{\partial \underline{M}}{\partial p} \Delta P \quad (2.15)$$

$$\underline{\Delta F} \cong \frac{\partial \underline{F}}{\partial p} \Delta P \quad (2.16)$$

where  $P \equiv$  the design parameter that is changed.

The derivatives in Eqs. (2.15) and (2.16) are derived in Section III for coarse mesh diffusion theory. Combining Eqs. (2.14), (2.15), and (2.16), one can obtain the first order approximation of the effect of any design parameter change on  $K_{\text{eff}}$ .

Predicting changes in responses other than  $K_{\text{eff}}$  with perturbation theory requires the solution of the generalized, or fixed source, adjoint equation<sup>6</sup>

$$(\underline{M}^* - \lambda \underline{F}^*) \underline{I}^* = \underline{Q}^* \quad , \quad (2.17)$$

where  $\underline{Q}^*$  is defined to be orthogonal to the forward source

$$\underline{S}^T \underline{Q}^* = 0 \quad , \quad (2.18)$$

and  $\lambda$  is the eigenvalue of the homogeneous equation. SIMULATE has also been modified to solve Eq. (2.17), using the method of successive approximations

$$\underline{M}^* \underline{I}^*_{n+1} = \lambda \underline{F}^* \underline{I}^*_n + \underline{Q}^* \quad ,$$

where the subscript  $n$  is the iteration index.

Some care must be exercised in solving Eq. (2.17), because the matrix on the LHS is singular. A routine has been added to sweep out the "fundamental mode contamination"<sup>7</sup> at the end of each outer iteration (see Appendix B)

$$\underline{\tilde{\Gamma}}^* = \underline{\Gamma}^* - \begin{bmatrix} \underline{\Gamma}^{*T} \underline{F} \underline{S} \\ \underline{S}^{*T} \underline{F} \underline{S} \end{bmatrix} \cdot \underline{S}^* \quad (2.19)$$

To predict the change in some response ratio

$$R = \frac{H_1 \cdot \underline{S}}{H_2 \cdot \underline{S}} \quad , \quad (2.20)$$

$\underline{Q}^*$  is set equal to <sup>6</sup>

$$\underline{Q}^* = \frac{dR}{d\underline{S}} = \frac{(H_2 \cdot \underline{S}) H_1 - (H_1 \cdot \underline{S}) H_2}{(H_2 \cdot \underline{S})^2}$$

or

$$\underline{Q}^* = R \left[ \frac{H_1}{(H_1 \cdot \underline{S})} - \frac{H_2}{(H_2 \cdot \underline{S})} \right] \quad (2.21)$$

Substituting Eq. (2.21) into Eq. (2.17) yields

$$(\underline{M}^* - \lambda \underline{F}^*) \underline{\Gamma}^* = R \left[ \frac{H_1}{H_1 \cdot \underline{S}} - \frac{H_2}{H_2 \cdot \underline{S}} \right] \cdot$$

The forward eigenvalue equation for a perturbed case is

$$(\underline{M}' - \lambda' \underline{F}') \underline{S}' = 0 \quad ,$$

which previously has been shown to have the first order approximation



$$(\underline{M} - \lambda \underline{F}) \underline{\Delta S} + (\underline{\Delta M} - \lambda \underline{\Delta F}) \underline{S} - \Delta \lambda \underline{F} \underline{S} \cong 0 \quad .$$

Multiplying this equation by  $\underline{\Gamma}^*$  and Eq. (2.17) by  $\underline{\Delta S}$  and subtracting one from the other gives

$$\underline{\Delta S}(\underline{M}^* - \lambda \underline{F}^*) \underline{\Gamma}^* - \underline{\Gamma}^*(\underline{M} - \lambda \underline{F}) \underline{\Delta S} - \underline{\Gamma}^*(\underline{\Delta M} - \lambda \underline{\Delta F}) \underline{S} \cong \underline{Q}^* \cdot \underline{\Delta S}$$

The term containing  $\Delta \lambda$  has vanished because  $\underline{\Gamma}^*$  is orthogonal to  $\underline{F} \underline{S}$ . The first two terms in this equation will cancel by the adjoint property, and the equation reduces to

$$-\underline{\Gamma}^*(\underline{\Delta M} - \lambda \underline{\Delta F}) \underline{S} \cong \frac{\partial R}{\partial \underline{S}} \underline{\Delta S} \quad ,$$

since

$$\underline{Q}^* = \frac{\partial R}{\partial \underline{S}} \quad .$$

For a perturbed case, the first order approximation of the change in the response ratio R is

$$\Delta R \cong \frac{\partial R}{\partial \underline{H}} \underline{\Delta H} + \frac{\partial R}{\partial \underline{S}} \underline{\Delta S} \quad .$$

Calculating the first term on the RHS of the equation

$$\begin{aligned} \frac{\partial R}{\partial \underline{H}} \underline{\Delta H} &= \frac{\partial R}{\partial \underline{H}_1} \underline{\Delta H}_1 + \frac{\partial R}{\partial \underline{H}_2} \underline{\Delta H}_2 = \frac{\underline{\Delta H}_1 \cdot \underline{S}}{\underline{H}_1 \cdot \underline{S}} - \frac{(\underline{H}_1 \cdot \underline{S})(\underline{\Delta H}_2 \cdot \underline{S})}{(\underline{H}_2 \cdot \underline{S})^2} \\ &= R \left[ \frac{\underline{\Delta H}_1 \cdot \underline{S}}{\underline{H}_1 \cdot \underline{S}} - \frac{\underline{\Delta H}_2 \cdot \underline{S}}{\underline{H}_2 \cdot \underline{S}} \right] \quad , \end{aligned}$$

and substituting the expression for  $\frac{\partial R}{\partial \underline{S}} \Delta \underline{S}$ , one obtains

$$\frac{\Delta R}{R} \cong \left[ \frac{\Delta H_1 \cdot \underline{S}}{H_1 \cdot \underline{S}} - \frac{\Delta H_2 \cdot \underline{S}}{H_2 \cdot \underline{S}} \right] - \frac{\Gamma^*(\Delta \underline{M} - \lambda \Delta \underline{F}) \underline{S}}{R} \quad (2.22)$$

The first term on the RHS of Eq. (2.20) accounts for the direct effect of the perturbation, while the second term is the first-order generalized perturbation theory approximation of the indirect effect (i.e., the change in  $\underline{S}$ ) of the perturbation. Once again,  $\Delta \underline{M}$  and  $\Delta \underline{F}$  can be approximated by Eqs. (2.15) and (2.16), respectively.

As an illustrative example, let us define a response ratio for the relative power peak in a node. The response ratio is

$$R \equiv \frac{H_m \cdot \underline{S}}{H_{TOT} \cdot \underline{S}} = \frac{\text{power peak in node } m}{\text{total power}} \quad (2.23)$$

where

$$H_m \equiv \begin{cases} V_m K \sum_f / \nu \sum_f & \text{for node } m \\ 0 & \text{for all other nodes} \end{cases}$$

and

$$H_{TOT} \equiv V_i K \sum_f / \nu \sum_f \quad \text{for all nodes}$$

and

$$V_i \equiv \text{volume of node } i$$

$$K = \text{energy released per fission (MeV)}$$

Because  $\underline{S}$  is the fission neutron source density, it must be divided by  $v\sum_f$  to obtain the flux. Using Eq. (2.23) to define R, the fixed source is

$$\underline{Q}^* = \frac{\partial R}{\partial \underline{S}} = R \left[ \frac{H_m}{(H_m \cdot \underline{S})} - \frac{H_{TOT}}{H_{TOT} \cdot \underline{S}} \right],$$

according to Eq. (2.21). Once this equation is solved for  $\underline{Q}^*$ , SIMULATE can solve Eq. (2.17) for  $\underline{\Gamma}^*$ . Then the change in magnitude of the power peak in node m may be computed from Eq. (2.22) for any number of perturbations.

Therefore, SIMULATE can solve the K-adjoint Eq. (2.13) and then calculate the sensitivity coefficient for some design parameter p

$$\alpha_p = \frac{\underline{S}^{*T} \left( \frac{\partial \underline{M}}{\partial p} - \lambda \frac{\partial \underline{F}}{\partial p} \right) \underline{S}}{\underline{S}^{*T} \underline{F} \underline{S}}, \quad (2.24)$$

which can then be used to calculate the approximate change in  $K_{eff}$  due to a perturbation in the value of the design parameter p

$$\frac{\Delta K_{eff}}{K_{eff}} \cong - \frac{\alpha_p \Delta p}{1/K_{eff}}. \quad (2.25)$$

Likewise, SIMULATE can solve the generalized adjoint Eq. (2.17) and then calculate the sensitivity coefficient for some design parameter p

$$\alpha_p = - \underline{\Gamma}^{*T} \left( \frac{\partial \underline{M}}{\partial p} - \lambda \frac{\partial \underline{F}}{\partial p} \right) \underline{S},$$

which can then be used to compute the approximate change in the defined response due to a perturbation in the value of the design parameter  $p$

$$\frac{\Delta R}{R} = \left[ \frac{\Delta H_1 \cdot S}{H_1 \cdot S} - \frac{\Delta H_2 \cdot S}{H_2 \cdot S} \right] - \frac{\alpha_p \Delta p}{R} \quad (2.26)$$

Thus, the above equations provide the basis for SIMULATE to perform generalized perturbation theory (GPT) calculations for static (time-independent) cases.

#### Development of Depletion Adjoint Equations for SIMULATE

For burnup-dependent (time-dependent) cases, one may use a variational principle to develop the depletion adjoint equations, such as Williams<sup>1</sup> used to derive the original depletion perturbation theory (DPT) equations. Since the development of these equations is rather involved, it is only outlined here. The entire development is presented in Appendix C.

There are five governing equations solved by SIMULATE for the case of no thermal-hydraulic feedback. These equations are:

(1) Forward Eigenvalue Equation

$$(\underline{M}_i - \lambda_i \underline{E}_i) \underline{S}_i = 0 \quad , \quad (i = 0, 1, \dots, \lambda) \quad (2.27)$$

where the subscript  $i$  denotes timestep  $i$  and  $\lambda$  is the final timestep;

(2) Exposure (Burnup) Equation

$$\underline{E}_{i+1} = \underline{E}_i + (R_i \cdot \underline{A}_i \underline{S}_i) \cdot T_i \quad , \quad (i = 0, 1, \dots, \lambda) \quad (2.28)$$

where  $\underline{E}_i \equiv$  nodal exposure (GWD/T) at exposure step  $i$

$T_i \equiv$  length (GWD/T) of exposure step  $i$

$(R_i \cdot \underline{A}_i \cdot \underline{S}_i) = P_i \equiv$  relative nodal power at exposure step  $i$

[see Eq. (2.31)];

### (3) Cross Section Fitting Equation

$$\begin{aligned} \underline{\Sigma}_i^x &= \underline{f}^x(\underline{E}_i, \underline{C}_1, \dots, \underline{C}_K, \dots) \quad (i = 0, 1, \dots, \ell) \\ & \quad (\chi = 1, 2, \dots, 9) \end{aligned} \quad (2.29)$$

where  $\underline{\Sigma}_i^x =$  nodal macroscopic cross section of type  $\chi$  at exposure step  $i$  (see Table 2.1)

$\underline{f}^x =$  polynomial expression for  $\underline{\Sigma}_i^x$  fitted against exposure  $\underline{E}_i$  and control variables  $\underline{C}_1, \dots, \underline{C}_K, \dots$

$\underline{C}_K \equiv$  concentration of  $K^{\text{th}}$  control variable (e.g. boron concentration);

### (4) Source Normalization Equation

$$\underline{h}_i \cdot \underline{S}_i = N_i \quad i = (0, 1, \dots, \ell) \quad (2.30)$$

where  $\underline{h}_i \equiv$  fission source normalization vector

$$= (V_1, V_2, \dots, V_m)$$

$V_j \equiv$  relative volume of node  $j$

$N_i \equiv$  magnitude of integrated fission source

$$= \sum_{i=1}^m V_i$$

$m \equiv$  total number of nodes;

## (5) Power Normalization Equation

$$R_i \cdot \underline{h}_i \underline{A}_i \underline{S}_i = \underline{h}_i \underline{P}_i = N_i \quad (i = 0, 1, \dots, L) \quad (2.31)$$

where  $R_i \equiv$  power normalization constant for exposure step  $i$

$\underline{A}_i \equiv$  diagonal matrix of  $\left( \frac{K_{\Sigma f, i}^{\Sigma}}{\nu \Sigma_{f, i}} \right)_{\text{node}}$  for conversion of

nodal fission source to relative nodal power.

The source and power normalizations yield an average value of 1.0 for both  $\underline{S}_i$  and  $\underline{P}_i$  for each full node.

These five governing equations are then used to form the functional

$$\begin{aligned} K = & \sum_{i=0}^L \underline{S}_i^* (\underline{M}_i - \lambda_i \underline{F}_i) \underline{S}_i \\ & + \sum_{i=1}^L \underline{E}_i^* (\underline{E}_i - \underline{E}_{i-1} - R_{i-1} \underline{A}_{i-1} \underline{S}_{i-1} \underline{T}_{i-1}) \\ & + \sum_{i=0}^L \left\{ \sum_{x=1}^9 \underline{S}_i^x \left( \underline{\Sigma}_i^x - \underline{f}^x(\underline{E}_i, \underline{C}_1, \dots, \underline{C}_K, \dots) \right) \right\} \\ & + \sum_{i=0}^L a_i (\underline{h}_i \cdot \underline{S} - N_i) \\ & + \sum_{i=0}^L b_i (R_i \cdot \underline{h}_i \underline{A}_i \underline{S}_i - N_i) \quad , \end{aligned} \quad (2.32)$$

where the parameters  $\underline{S}_i^*$ ,  $\underline{E}_i^*$ ,  $\underline{S}_i^x$ ,  $a_i$ , and  $b_i$  are as yet unspecified.

The first order estimate for  $\Delta K$  is then obtained, and after several simplifications, the final conditions ( $i=L$ ) for the end of cycle (EOC)  $k_{\text{eff}}$  response are determined to be

$$(\underline{M}^* - \lambda_2 \underline{F}^*) \underline{S}_2^* = 0 \quad (2.33)$$

$$\underline{s}_2^X = -\underline{S}_2^* \left( \frac{\partial \underline{M}}{\partial \underline{\Sigma}_2^X} - \lambda_2 \frac{\partial \underline{F}}{\partial \underline{\Sigma}_2^X} \right) \underline{S}_2 \quad (2.34)$$

$$\underline{E}_2^* = \sum_{x=1}^9 \left[ \underline{s}_2^X \left( \frac{\partial f}{\partial \underline{E}_2} \right) c_K \right] \quad (2.35)$$

$$a_2 = 0 \quad (2.36)$$

$$b_2 = 0 \quad (2.37)$$

The  $\underline{S}_2^*$  in Eq. (2.33) corresponds to  $\underline{S}_2^*$  in Eq. (2.13). The final conditions for a response ratio R at the final time ( $i=2$ )

$$(\underline{M}^* - \lambda_2 \underline{F}^*) \underline{S}_2^* = \frac{\partial R}{\partial \underline{S}_2} = \underline{Q}_2^* \quad (2.38)$$

$$\underline{S}_2 \cdot \underline{Q}_2^* = \underline{S}_2 \cdot \frac{\partial R}{\partial \underline{S}_2} = 0 \quad (2.39)$$

$$\underline{s}_2^X = -\underline{S}_2^* \left( \frac{\partial \underline{M}}{\partial \underline{\Sigma}_2^X} - \lambda_2 \frac{\partial \underline{F}}{\partial \underline{\Sigma}_2^X} \right) \underline{S}_2 + \left( \frac{\partial R}{\partial \underline{H}_2} \right) \left( \frac{\partial \underline{H}}{\partial \underline{\Sigma}_2^X} \right) \quad (2.40)$$

$$\underline{E}_2^* = \sum_{x=1}^9 \left[ \underline{s}_2^X \left( \frac{\partial f^X}{\partial \underline{E}_2} \right) c_K \right] \quad (2.41)$$

$$a_2 = 0 \quad (2.42)$$

$$b_2 = 0 \quad (2.43)$$

where  $R = R(\underline{S}_2, \underline{H}_2)$ .

The depletion adjoint equations for all preceding exposure steps ( $i < \ell$ ) are identical for both the EOC  $k_{\text{eff}}$  response and the final time response ratio R:

$$(\underline{M}_i^* - \lambda_i \underline{F}_i^*) \underline{S}_i^* = R_i T_i A_i^* E_{i+1}^* - b_i R_i A_i^* h_i = \underline{Q}_i^* \quad (2.44)$$

$$b_i = \frac{T_i E_{i+1}^* A_i S_i}{h_i A_i S_i} \quad (2.45)$$

$$\underline{S}_{i=i}^* F_i S_i = 0 \quad (2.46)$$

$$\underline{S}_i^X = -\underline{S}_i^* \left( \frac{\partial \underline{M}_i}{\partial \underline{\Sigma}_i^X} - \lambda_i \frac{\partial \underline{F}_i}{\partial \underline{\Sigma}_i^X} \right) \underline{S}_i \quad (2.47)$$

$$\underline{E}_i^* = \underline{E}_{i+1}^* + \sum_{x=1}^9 \underline{S}_i^X \left( \frac{\partial f_j^X}{\partial \underline{E}_i} \right) \quad (2.48)$$

The  $\underline{S}_i^*$  in Eqs. (2.38) and (2.44) correspond to  $\underline{\Gamma}^*$  in Eq. (2.17).

For all exposure steps ( $i=0,1,\dots,\ell$ ),  $\underline{E}_i^*$  is the importance of the exposure at exposure step  $i$ , and  $\underline{S}_i^X$  is the cross section sensitivity coefficient for the macroscopic cross section of type  $X$  at exposure step  $i$ .

Once Eqs. (2.33) - (2.37) and (2.44) - (2.48) have been solved, one can predict the effect of any combination of perturbations at the beginning of cycle (BOC) on the EOC  $k_{\text{eff}}$  response. For perturbations in the control variables, the change in the EOC  $k_{\text{eff}}$  response is approximated by



$$\left( \frac{\Delta k_{\text{eff}}}{k_{\text{eff}}} \right)_{\ell} \cong \frac{\sum_K \alpha_{C_K} \cdot \Delta C_K}{\left( 1/k_{\text{eff}} \right)_{\ell} \frac{S^* F_{\ell} S_{\ell}}{\ell}} \quad (2.49)$$

where

$$\alpha_{C_K} \cong \sum_{i=0}^{\ell} \sum_{x=1}^g \left[ s_i^x \left( \frac{\partial f^x}{\partial C_K} \right) E_i \right]$$

$\equiv$  sensitivity coefficient for control variable K.

For perturbations in the nodal macroscopic cross sections (e.g. changes in enrichment or lumped burnable poison), the change in the EOC  $k_{\text{eff}}$  response is approximated by

$$\left( \frac{\Delta k_{\text{eff}}}{k_{\text{eff}}} \right)_{\ell} \cong \frac{\sum_{i=0}^{\ell} \left( \sum_{x=1}^g s_i^x \Delta \sum_i^x \right)}{\left( 1/k_{\text{eff}} \right)_{\ell} \left( \frac{S^* F_{\ell} S_{\ell}}{\ell} \right)} \quad (2.50)$$

When Eqs. (2.38) - (2.48) have been solved, one can predict the effect of any combination of perturbations at BOC on a final time response ratio R. For control variable perturbations, the change in the final time response is approximately

$$\left( \frac{\Delta R}{R} \right)_{\ell} \cong \frac{\sum_K \alpha_{C_K} \cdot \Delta C_K}{R} \quad (2.51)$$

For perturbations in the nodal macroscopic cross sections, the change in the final time response is

$$\left(\frac{\Delta R}{R}\right)_\ell \cong \frac{\sum_{i=0}^{\ell} \left( \sum_{x=1}^9 \frac{s_i^x}{\Delta \sum_i^x} \right)}{R} \quad (2.52)$$

SIMULATE has been modified to solve the depletion adjoint Eqs. (2.33) - (2.48). It now contains the capabilities of both generalized (static) perturbation theory (GPT) and depletion perturbation theory (DPT). For perturbations of static cases, Eqs. (2.25) and (2.26) may be used to predict the effects of the perturbations, and for burnup-dependent cases, Eqs. (2.49) - (2.51) may be used to predict the effect on EOC responses due to BOC perturbations.

### III. APPROXIMATING THE CHANGES IN THE NODAL COUPLING COEFFICIENTS

#### SIMULATE Nodal Coupling Methodology

In SIMULATE, each node of the reactor model is a rectangular parallelepiped with a square base (Fig. 3.1), i.e., the X and Y dimensions of each node are equal while the Z dimension is independent. Every full node in the model is the same size. Each node is coupled to the neighboring nodes on each of its six faces. If a node lies on a reactor boundary (core-reflector interface), and thus has no neighboring node on one or more of its six faces, the node is coupled to itself on each boundary face by the albedo for that boundary,

$$\rho_{ij} = \frac{J_i^{\text{in}}}{J_i^{\text{out}}} = \frac{J_j^{\text{out}}}{J_i^{\text{out}}} \quad (3.1)$$

where  $J_i^{\text{out}}$  is the one group current leaving node i and  $J_j^{\text{in}}$  is the one group current reflected into node i.

The nodal coupling coefficient matrices  $\underline{M}$  and  $\underline{F}$  are seven-stripped matrices then, since each node is coupled to itself and its six adjacent neighbors. For a two-dimensional problem, the matrices have five non-zero stripes because the nodes have no neighbors above or below themselves. The matrix equation presented in the previous section

$$(\underline{M} - \lambda \underline{F}) \underline{S} = 0 \quad (3.2)$$

can be written as a set of coupled equations for each node  $i^2$ :

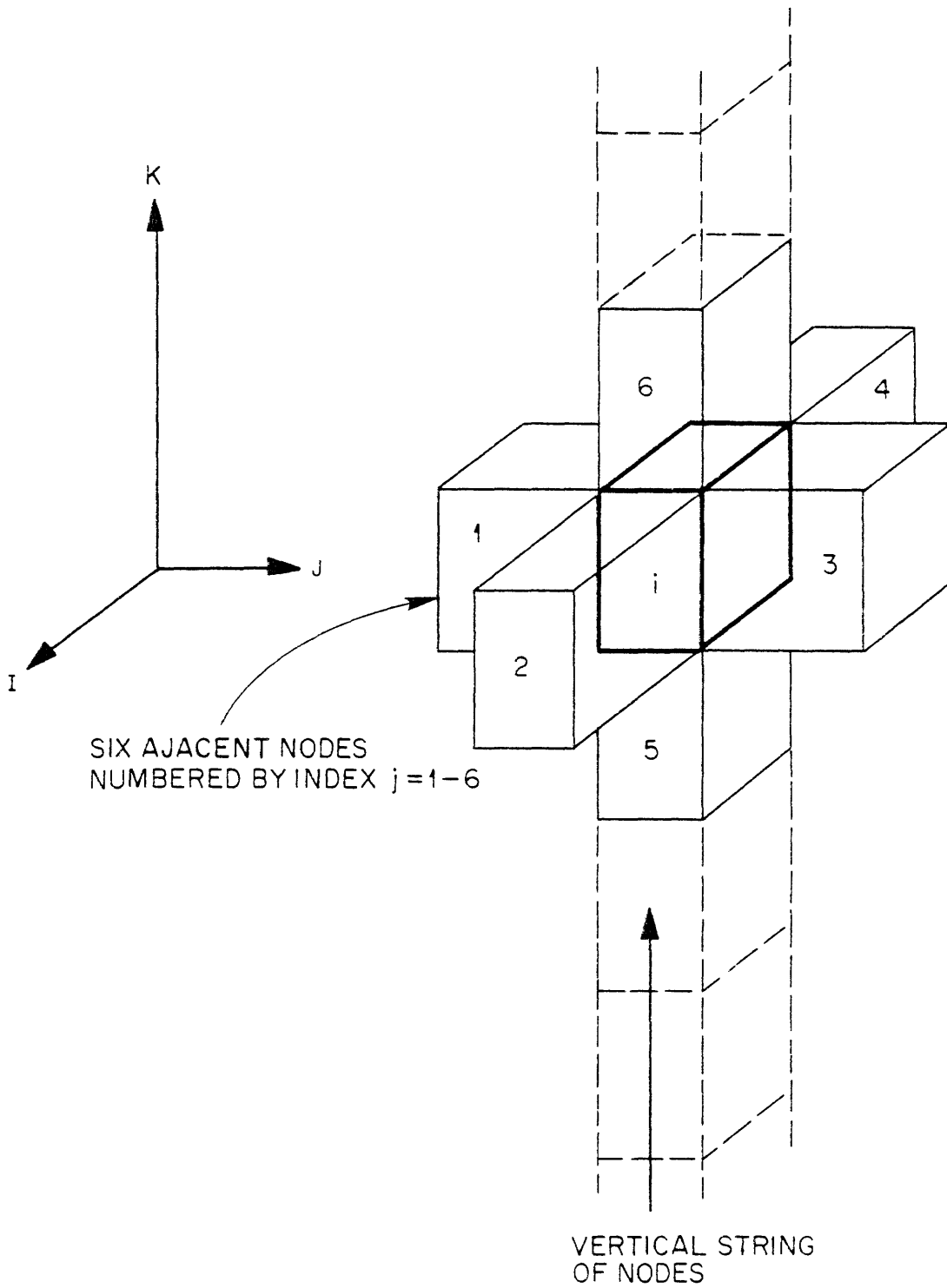


Fig. 3.1. SIMULATE Nodal Arrangement

$$\begin{aligned}
& \left\{ \Gamma_i \sum_j v_{ij+1} \right\} S_i - \sum_j \frac{K_i}{K_j} \Gamma_j v_{ji} S_j \\
& = \frac{K_i}{K_{\text{eff}}} \left\{ \left[ 1 - \alpha_i \Gamma_i \sum_j v_{ij} \right] S_i + \sum_j \alpha_j \Gamma_j v_{ji} S_j \right\} , \tag{3.3}
\end{aligned}$$

where the summation over  $j$  is a simple summation over the six nodes adjacent to node  $i$ . The first term on the LHS of Eq. (3.3) is the diagonal coupling coefficient of  $\underline{M}$  for node  $i$ , and the second term represents the off-diagonal coupling coefficients of  $\underline{M}$  for the six neighbor nodes of  $i$ . Likewise, the first term on the RHS of the equation is the diagonal coupling coefficient of  $\underline{F}$  for node  $i$ , and the second term represents the off-diagonal coupling coefficients of  $\underline{F}$  for the six neighbor nodes of  $i$ .

The nodal coupling coefficients then are defined as follows:

$$M_{ii} = 1 + \Gamma_i \sum_j v_{ij} \tag{3.4}$$

$$M_{ij} = - \frac{K_i}{K_j} \Gamma_j v_{ji} \tag{3.5}$$

$$F_{ii} = K_i (1 - \alpha_i \Gamma_i \sum_j v_{ij}) \tag{3.6}$$

$$F_{ij} = K_i \alpha_j \Gamma_j v_{ji} , \tag{3.7}$$

where  $K_i = K_\infty$  of node  $i$  and the parameters  $\alpha_i$ ,  $\Gamma_i$ , and  $v_{ij}$  will now be defined.

First we examine the parameter  $\alpha_i$ , which is the ratio of neutrons which enter node  $i$  from node  $j$  and are absorbed in node  $i$  to those which enter node  $i$  from node  $j$  and behave like neutrons born in node  $i$ . This is stated mathematically as<sup>2</sup>

$$\alpha_i \equiv \frac{\beta_{ji}}{\mu_{ji}} \quad (3.8)$$

where  $\beta_{ji} \equiv$  the direct absorption probability of a neutron crossing into  $i$  from  $j$

$\mu_{ji} \equiv$  the scattering probability of a neutron crossing into  $i$  from  $j$ .

These two probabilities are related to the reflection probability of a neutron crossing into  $i$  from  $j$ ,  $\rho_{ji}$ , which was defined in Eq. (3.1),

$$\rho_{ji} + \beta_{ji} + \mu_{ji} = 1 \quad (3.9)$$

All three of these quantities are assumed to be properties of node  $i$  only.

The parameter  $\Gamma_i$  is defined as<sup>2</sup>

$$\Gamma_i \equiv \frac{1 - \sigma_i}{\alpha_i + \sigma_i} \quad (3.10)$$

where  $\sigma_i \equiv$  non-escape probability. The parameter  $\nu_{ij}$  is defined as<sup>2</sup>

$$\nu_{ij} = \frac{r_{ij} (1 - \rho_{ij})}{1 - \rho_{ij} \rho_{ji}} \quad (3.11)$$

where  $r_{ij}$  = probability that a neutron leaking from node  $i$  will leak into node  $j$ , so that  $\sum_j r_{ij} = 1$ , and  $\rho_{ij}$  is defined in Eq. (3.1).

Therefore, if node is a cube, the probability of leakage out all faces is equal, and  $r_{ij} = 1/6$  for all six faces. The probability  $r_{ij}$  is also considered to be a property of only node  $i$ .

In an attempt to better understand the significance of these coupling parameters, let us examine a reactor node (Fig. 3.2) using a response matrix approach.<sup>8</sup> Let  $u$  denote one nodal face ( $x$ ,  $y$ , or  $z$ ) where a uniform incoming current is imposed and let  $v$  denote each of the other faces where outgoing partial currents occur in response to the incoming current at  $u$ . A "trans-emission factor,"<sup>8</sup>  $t_{uv}$ , is then defined

$$t_{uv} = \frac{J_{v+}^{\text{out}} A_v}{J_{u-}^{\text{in}} A_u} = \frac{J_{v-}^{\text{out}} A_v}{J_{u-}^{\text{in}} A_u} = \frac{J_{v+}^{\text{out}} A_v}{J_{u+}^{\text{in}} A_u} = \frac{J_{v-}^{\text{out}} A_v}{J_{u+}^{\text{in}} A_u}$$

$$\equiv \frac{\text{outgoing partial current on } v \text{ face}}{\text{incoming current on } u \text{ face}}, \quad (3.12)$$

where  $A$  is the area and  $J$  is the current per unit area.

The reflection of the incoming current plus the outgoing partial current in the direction opposite that of the incoming current is contained in another term<sup>8</sup>

$$a_{uu} = \frac{J_{u-}^{\text{out}}}{J_{u-}^{\text{in}}} = \frac{J_{u+}^{\text{out}}}{J_{u+}^{\text{in}}} = t_{uu} + \rho_u, \quad (3.13)$$

ORNL-DWG 80-18171

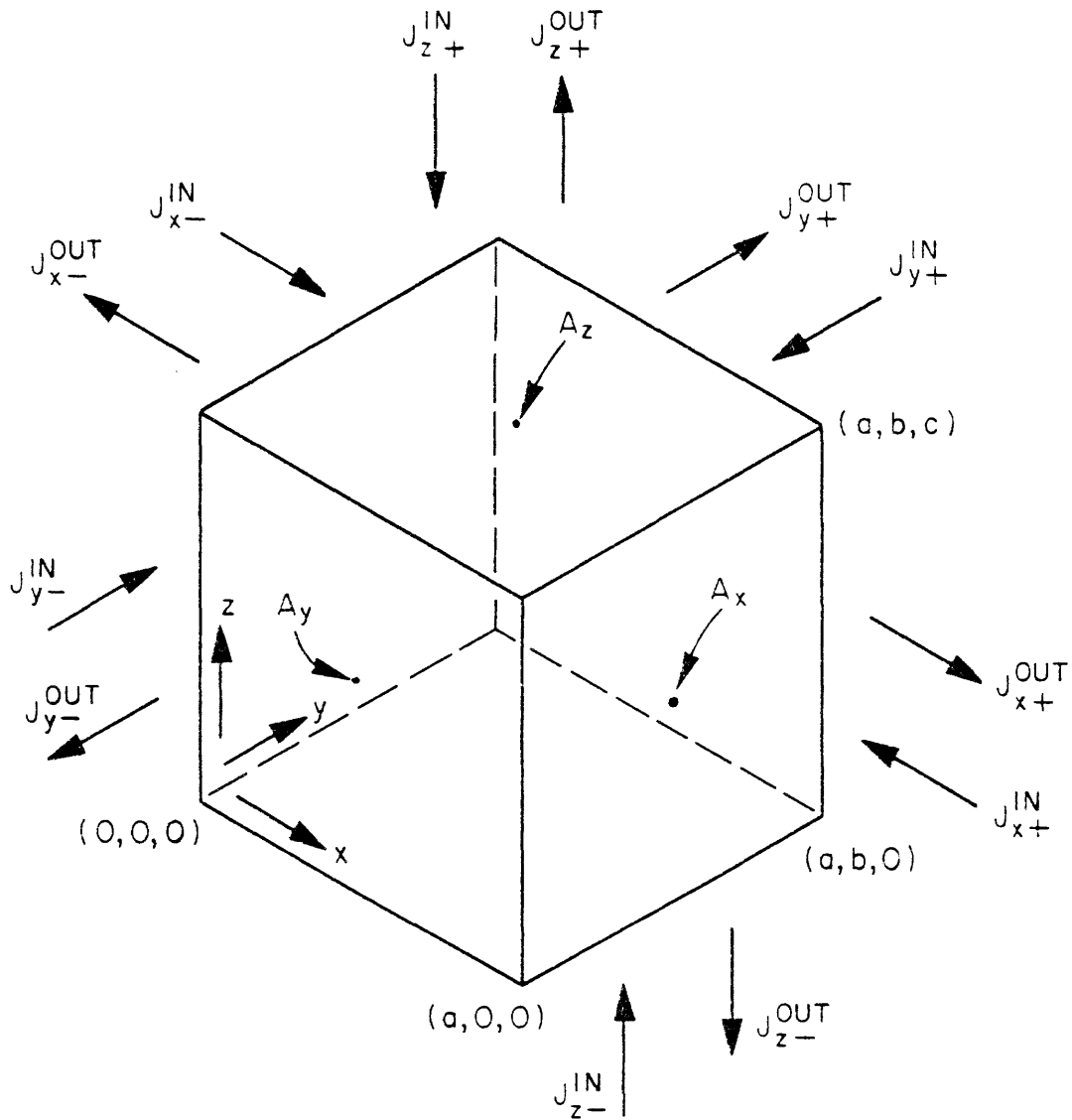


Fig. 3.2. Neutron Partial Current Representation



where  $\rho_u$  is the reflection probability. There are now four factors for each direction ( $a_{uu}$ ,  $t_{uu}$ , and  $t_{uv}$  for  $v = x, y, z \neq u$ ) and three directions ( $x, y, z$ ), or twelve factors for each node. In order to reduce the number of factors which must be stored for each node, it is assumed that  $t_{uv}$  can be separated into two independent functions  $\rho_u$  and  $r_v$

$$t_{uv} = (1 - \rho_u) t r_v \quad (3.14)$$

where

$$\rho_u = a_{uu} - t_{uu}$$

and

$$2 \sum_{v=x,y,z} r_v = 1.$$

The number of factors has now been reduced from twelve to six:  $t$  (a directionless property),  $\rho_u$  ( $u=x, y, z$ ) and  $r_v$  ( $v=x, z$ ). Recall that the  $x$  and  $y$  dimensions are equal, and therefore,  $r_x = r_y$ .

We now seek to correlate the parameters  $\rho_{ji}$ ,  $r_{ij}$ ,  $\alpha_i$ ,  $\Gamma_i$  to  $t$ ,  $\rho_{uv}$ ,  $r_v$ . By their definitions,

$$\rho_{ji} = \rho_u$$

$$r_{ij} = r_v$$

and it has been shown in reference (8) that

$$\frac{t-1}{t} = \frac{(K_i-1) (\alpha_i + \sigma_i)}{(1 + \alpha_i K_i) (1 - \sigma_i)} \quad (3.15)$$

or, after some manipulation,

$$\alpha_i = \frac{\left(\frac{t}{t-1}\right) (K_\infty - 1) \left(\frac{\sigma_i}{\sigma_i - 1}\right) + 1}{- \left[ K_\infty + \left(\frac{t}{t-1}\right) \left(\frac{K_\infty - 1}{\sigma_i - 1}\right) \right]} \quad (3.16)$$

In addition, it has been shown in the same derivation that

$$t = \frac{2 \sum_{u=x,y,z} \sum_{v=x,y,z} t_{uv} A_u}{\sum_{u=x,y,z} (1 - \rho_u) A_u} \quad (3.17)$$

and

$$r_u = \frac{\sum_{v=x,y,z} t_{vu} A_v}{t \sum_{v=x,y,z} (1 - \rho_v) A_v} \quad (3.18)$$

For the non-escape probability  $\sigma$ , we will use the Wigner rational approximation

$$\sigma = \frac{\sum_a \frac{4V}{A}}{1 + \sum_a \frac{4V}{A}} \quad (3.19)$$

where  $V$  is the node volume and  $A$  is the node surface area.

If solutions can be found for  $t_{uv}$  and  $a_{uu}$ , we can then solve for  $\alpha_j$ ,  $\Gamma_j$ , and  $\nu_{ij}$  in order to obtain the nodal coupling coefficients as

functions of the collapsed one group cross sections. We now proceed to solve for  $t_{uv}$  and  $a_{uu}$  using coarse mesh diffusion theory (CMDT).

### Determination of the Nodal Coupling Coefficients Using Coarse Mesh Diffusion Theory

In coarse mesh diffusion theory, the value used for the flux,  $\phi$ , in the integral solution of the one group diffusion theory equation

$$-\int_A \bar{J} \cdot \bar{n} dA - \int_V \sum_a (1-K_\infty) \phi dV = 0 \quad (3.20)$$

is the node center flux,  $\phi_c$ .<sup>2</sup> In this equation  $\bar{J}$  represents the net outward current from the node surface area  $A$ ,  $\bar{n}$  is the outward normal vector to  $A$ , and  $V$  is the node volume. Eq. (3.20) can be written using summations rather than integrals

$$\sum_{j=1}^6 J_j^{\text{in}} A_j - \sum_{j=1}^6 J_j^{\text{out}} A_j - \sum_a (1-K_\infty) \phi_c V = 0 \quad , \quad (3.21)$$

where  $J_j^{\text{in}}$  and  $J_j^{\text{out}}$  are the partial currents going in and coming out face  $j$  of the node, respectively. The partial currents are approximated by Fick's Law:<sup>3</sup>

$$J_x^\pm = \frac{\phi}{4} \mp \frac{D}{2} \phi'_x \quad , \quad (3.22)$$

where  $J_x^+$  and  $J_x^-$  are the forward and backward currents in the  $X$  direction, respectively,  $D$  is the diffusion coefficient, and

$$\phi'_x = \frac{\Delta\phi}{\Delta x} = \frac{\phi_c - \phi(0,b/2,c/2)}{a/2} \quad (3.23)$$

is the partial derivative of the flux with respect to  $X$  approximated by coarse mesh methodology for a node with dimensions  $a$ ,  $b$ , and  $c$  (Fig. 3.2). Note that  $\phi(0,b/2,c/2)$  is the flux at the center of the  $X = 0$  face.

We now proceed to solve for the node center flux  $\phi_c$  by applying a unit current to the  $X = 0$  face and zero current to all other faces. On the  $X = 0$  face,

$$J_{x-}^{in} = 1 = \frac{\phi(0,b/2,c/2)}{4} - \frac{D}{2} \frac{\phi_c - \phi(0,b/2,c/2)}{a/2} \quad (3.24)$$

is obtained by substituting Eq. (3.23) into Eq. (3.22). The flux at the center of  $X = 0$  face is

$$\phi(0,b/2,c/2) = a/D + \phi_c \quad (3.25)$$

Likewise, on the opposite face ( $X=a$ ),

$$J_{x+}^{in} = 0 = \frac{\phi(a,b/2,c/2)}{4} - D/2 \frac{\phi(a,b/2,c/2) - \phi_c}{a/2}$$

and

$$\phi(a,b/2,c/2) = \frac{\phi_c}{1 + a/4D} \quad (3.26)$$

Solutions for the fluxes on the other four faces can be obtained in a similar manner. These are then used in Eq. (3.22) to determine the partial currents as functions of  $\phi_c$ :

$$j_{x-}^{\text{out}} = \frac{a/4D - 1 + \phi_c/2}{1 + a/4D} \quad (3.27)$$

$$j_{x+}^{\text{out}} = \frac{\phi_c/2}{1 + a/4D} \quad (3.28)$$

$$j_{y+}^{\text{out}} = j_{y-}^{\text{out}} = \frac{\phi_c/2}{1 + b/4D} \quad (3.29)$$

$$j_{z+}^{\text{out}} = j_{z-}^{\text{out}} = \frac{\phi_c/2}{1 + c/4D} \quad (3.30)$$

Equations (3.27) - (3.30) are then substituted into Eq. (3.21) to obtain the solution for the center node flux<sup>2</sup>

$$\phi_c = \frac{\frac{2}{a(1+a/4D)}}{\sum_{u=a,b,c} \frac{1}{u(1+u/4D)} + \sum_a (1-K_\infty)} \quad (3.31)$$

This is actually  $\phi_{cx}$  because it is the flux resulting from a unit incoming current in the X-direction. The node center fluxes  $\phi_{cy}$  and  $\phi_{cz}$  resulting from incoming currents from the other two directions are obtained by substituting b and c, respectively, for a in the numerator of Eq. (3.31).

Next, let us examine the reflection and trans-emission factors. Substituting Eq. (3.27) into Eq. (3.13) gives

$$a_{xx} = \frac{j_{x-}^{\text{out}}}{j_{x-}^{\text{in}}} = j_{x-}^{\text{out}} = \frac{a/4D - 1 + \phi_c/2}{1 + a/4D} \quad (3.32)$$

The trans-emission factors are obtained by substituting Eqs. (3.28), (3.29) and (3.30) into Eq. (3.12):

$$t_{xx} = \frac{j_{x+}^{\text{out}} A_x}{j_{x-}^{\text{in}} A_x} = j_{x+}^{\text{out}} = \frac{\phi_{cx}/2}{1 + a/4D} \quad (3.33)$$

$$t_{xy} = \frac{j_{y+}^{\text{out}} A_y}{j_{x-}^{\text{in}} A_x} = j_{y+}^{\text{out}} \frac{ac}{bc} = \frac{\phi_{cx}/2}{1 + b/4D} (a/b) \quad (3.34)$$

$$t_{xz} = \frac{j_{z+}^{\text{out}} A_z}{j_{x-}^{\text{in}} A_x} = j_{z+}^{\text{out}} \frac{ab}{bc} = \frac{\phi_{cx}/2}{1 + c/4D} (a/c) \quad (3.35)$$

The  $a_{uu}$  and  $t_{uv}$  factors for the y and z directions can be obtained in the same manner. The general expressions for these factors are:<sup>2</sup>

$$a_{uu} = \frac{u/4D - 1 + \phi_{cu}/2}{1 + u/4D} \quad (3.36)$$

and

$$t_{uv} = \frac{\phi_{cu}/2}{1 + u/4D} \frac{A_u}{A_v} \quad (3.37)$$

From these expressions we can solve for the reflection probability

$$\rho_u = a_{uu} - t_{uu} = \frac{u/4D - 1}{u/4D + 1} \quad (3.38)$$

These solutions are then substituted into Eqs. (3.17) and (3.18) to obtain

$$t = 1/2 \sum_u \phi_{cu} = \frac{F}{F + \sum_a (1 - K_\infty)} \quad (3.39)$$

and

$$r_u = \frac{1}{2Fu(1+u/4D)} \quad (3.40)$$

where

$$F = \sum_{u=a,b,c} \frac{1}{u(1+u/4D)} \quad (3.41)$$

It is now possible to compute the nodal coupling coefficients directly from the one group collapsed cross sections ( $\sum_a$ ,  $K_\infty$ ,  $D$ ) and the nodal dimensions using Eqs. (3.4) - (3.7), (3.10), (3.11), (3.16), (3.19), and (3.39) - (3.41). Expressing the collapsed one group cross sections in terms of the two group cross sections which are input to SIMULATE will then give the nodal coupling coefficients as functions of the two group cross sections.

The two group equations for an infinite system are used to determine  $K_\infty$ :

$$\sum_{a_1} \phi_{a_1} + \sum_{r_1} \phi_{r_1} = \frac{\nu \sum_{f_1} \phi_{f_1} + \nu \sum_{f_2} \phi_{f_2}}{K_\infty} \quad (3.42)$$

$$\sum a_2 \phi_2 = \sum r_1 \phi_1 \quad (3.43)$$

Then,

$$K_\infty = \frac{v \sum f_1 \phi_1 + v \sum f_2 \phi_2}{\sum a_1 \phi_1 + \sum a_2 \phi_2} = \frac{v \sum f_1 + v \sum f_2 (\phi_2 / \phi_1)}{\sum a_1 + \sum a_2 (\phi_2 / \phi_1)} \quad (3.44)$$

Using the following expression for the flux ratio<sup>2</sup>

$$\phi_2 / \phi_1 = T \sum r_1 / \sum a_2 \quad , \quad (3.45)$$

where T is the thermal leakage correction (T is unity for no leakage between nodes)

$$K_\infty = \frac{v \sum f_1 + (T \sum r_1 / \sum a_2) v \sum f_2}{\sum a_1 + T \sum r_1} \quad (3.46)$$

The absorption cross section is simply collapsed from the two group absorption cross sections

$$\sum a = \frac{\sum a_1 \phi_1 + \sum a_2 \phi_2}{\phi_1 + \phi_2} = \frac{\sum a_1 + \sum a_2 (\phi_2 / \phi_1)}{1 + (\phi_2 / \phi_1)} \quad (3.47)$$

Substituting Eq. (3.45) into (3.47) yields

$$\sum a = \frac{\sum a_1 + T \sum r_1}{1 + T \sum r_1 / \sum a_2} \quad (3.48)$$



Finally, the one group diffusion coefficient is defined as<sup>2</sup>

$$D = \sum_a M^2 \quad (3.49)$$

where

$$M^2 = \tau + L^2$$

where

$$\tau = \left( \frac{1}{3} \sum_{tr_1} \right) \left( \frac{1}{\sum_{a_1} + \sum_{r_1}} \right) \text{ and } L^2 = \left( \frac{1}{3} \sum_{tr_2} \right) \left( \frac{1}{\sum_{a_2}} \right) \quad (3.50)$$

Thus, by combining Eqs. (3.46) and (3.48) - (3.50) with the equations mentioned previously, one can express the nodal coupling coefficients as functions of the two group input cross sections. We shall now use these equations to derive the partial derivatives of the nodal coupling coefficients with respect to the two group cross sections.

#### The Partial Derivatives of the Nodal Coupling Coefficients with Respect to the Two Group Cross Sections

In Section II of this report, it was shown that the partial derivatives of the nodal coupling coefficients were needed to compute the sensitivity coefficients for both the static case [Eq. (2.24)] and the burnup-dependent case [Eqs. (2.34), (2.40), and (2.47)]. Since the relationship between the nodal coupling coefficients and the cross sections have been established in the preceding part of this section, it is now possible to derive the partial derivatives.

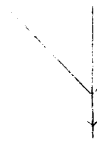
Expressing the nodal coupling coefficients as functions of the two group cross sections was performed in a three step "hierarchy" as illustrated in Table 3.1. A reverse procedure will be followed, beginning at the bottom of the hierarchy (the one group cross sections as functions of the two group cross sections) and moving toward the top, in deriving the partial derivatives.

Table 3.1. Hierarchy for Nodal Coupling Coefficients as Functions of Two-Group Cross Sections

---

Nodal Coupling Coefficients

$$\underline{M}, \underline{F} = f_1 (\underline{\alpha}, \underline{\Gamma}, \underline{\nu}, \underline{K}) \quad [\text{Eqs. (3.4)-(3.7)}]$$



Intermediate Coupling Coefficients

$$\underline{\alpha}, \underline{\Gamma}, \underline{\nu} = f_2 (\underline{K}, \underline{\Sigma a}, \underline{D}) \quad [\text{Eqs. (3.10), (3.16), (3.19), (3.39)-(3.41)}]$$



One Group Cross Sections

$$\underline{K}, \underline{\Sigma a}, \underline{D} = f_3 (\underline{\Sigma tr}_1, \underline{\Sigma a}_1, \underline{\Sigma r}_1, \underline{\nu \Sigma f}_1, \underline{\Sigma tr}_2, \underline{\Sigma a}_2, \underline{\nu \Sigma f}_2)$$

[Eqs. (3.46), (3.48)-(3.50)]

---

We will begin by taking derivatives of the one group absorption cross section from Eq. (3.48). Throughout the derivatives,  $T$  will be assumed to be constant. Then the derivatives are:

$$\frac{\partial \bar{\Sigma}_a}{\partial \bar{\Sigma}_{a_1}} = \frac{1}{1+r} \quad (3.51)$$

$$\frac{\partial \bar{\Sigma}_a}{\partial \bar{\Sigma}_{a_2}} = \frac{\bar{\Sigma}_a}{\bar{\Sigma}_{a_2}} \left( \frac{r}{1+r} \right) \quad (3.52)$$

$$\frac{\partial \bar{\Sigma}_a}{\partial \bar{\Sigma}_{r_1}} = \left( \frac{T}{1+r} \right) \left( 1 - \frac{\bar{\Sigma}_a}{\bar{\Sigma}_{a_2}} \right), \quad (3.53)$$

where  $r \equiv T\bar{\Sigma}_{r_1}/\bar{\Sigma}_{a_2}$ .

From Eq. (3.46), the derivatives of  $K_\infty$  are:

$$\frac{\partial K_\infty}{\partial \bar{\Sigma}_{a_1}} = \frac{-K_\infty}{\bar{\Sigma}_a(1+r)} = \left( \frac{-K_\infty}{\bar{\Sigma}_a} \right) \frac{\partial \bar{\Sigma}_a}{\partial \bar{\Sigma}_{a_1}} \quad (3.54)$$

$$\frac{\partial K_\infty}{\partial \bar{\Sigma}_{a_2}} = \frac{-v\bar{\Sigma}_{f_2} T\bar{\Sigma}_{r_1} / (\bar{\Sigma}_{a_2})^2}{\bar{\Sigma}_{a_1} + T\bar{\Sigma}_{r_1}} \quad (3.55)$$

$$\frac{\partial K_\infty}{\partial \bar{\Sigma}_{r_1}} = K_\infty \left[ \frac{Tv\bar{\Sigma}_{f_2}/\bar{\Sigma}_{a_2}}{v\bar{\Sigma}_{f_1} + (T\bar{\Sigma}_{r_1}/\bar{\Sigma}_{a_2})v\bar{\Sigma}_{f_2}} - \frac{T}{\bar{\Sigma}_{a_1} + T\bar{\Sigma}_{r_1}} \right] \quad (3.56)$$

$$\frac{\partial K_\infty}{\partial v\bar{\Sigma}_{f_1}} = \frac{1}{\bar{\Sigma}_a(1+r)} = \left( \frac{1}{\bar{\Sigma}_a} \right) \frac{\partial \bar{\Sigma}_a}{\partial \bar{\Sigma}_{a_1}} \quad (3.57)$$

$$\frac{\partial K_\infty}{\partial v\bar{\Sigma}_{f_2}} = \frac{r}{\bar{\Sigma}_{a_1} + T\bar{\Sigma}_{r_1}} = \frac{r}{\bar{\Sigma}_a} \frac{\partial \bar{\Sigma}_a}{\partial \bar{\Sigma}_{a_1}} = r \frac{\partial K_\infty}{\partial v\bar{\Sigma}_{f_1}} \quad (3.58)$$

Using Eqs. (3.49) and 3.50), we obtain the following derivatives:

$$\frac{\partial D}{\partial \Sigma_{a_1}} = M^2 \frac{\partial \Sigma_a}{\partial \Sigma_{a_1}} - 3 \left( \Sigma_a \tau^2 \Sigma_{tr_1} \right) \quad (3.59)$$

$$\frac{\partial D}{\partial \Sigma_{a_2}} = \frac{\Sigma_a}{\Sigma_{a_2}} \left[ M^2 \left( \frac{r}{1+r} \right) + \tau - M^2 \right] \quad (3.60)$$

$$\frac{\partial D}{\partial \Sigma_{r_1}} = M^2 \frac{\partial \Sigma_a}{\partial \Sigma_{r_1}} - 3 \left( \Sigma_a \tau^2 \Sigma_{tr_1} \right) \quad (3.61)$$

$$\frac{\partial D}{\partial \Sigma_{tr_1}} = -3 \Sigma_a \tau^2 \left( \Sigma_{a_1} + \Sigma_{r_1} \right) \quad (3.62)$$

$$\frac{\partial D}{\partial \Sigma_{tr_2}} = \frac{\Sigma_a}{\Sigma_{tr_2}} \left( \tau - M^2 \right) \quad (3.63)$$

Having derived the partial derivatives of the one group cross sections with respect to the two group cross sections, we now proceed to determine the partial derivatives of the intermediate coupling coefficients  $(\alpha, \Gamma, \nu)$  with respect to the one group cross sections. Combining Eqs.(3.16), (3.19) and (3.39), we obtain the following equation for  $\alpha_j$ :

$$\alpha_j = \frac{(F\bar{\kappa} - 1) \Sigma_a}{\left[ K_\infty \Sigma_a - F(1 + \Sigma_a \bar{\kappa}) \right]} \quad (3.64)$$

where  $\bar{\kappa} = 4V/S$ .

The derivatives of  $\alpha_i$  are:

$$\frac{\partial \alpha_i}{\partial K_\infty} = \frac{-\alpha_i^2}{[F\bar{\ell} - 1]} \quad (3.65)$$

$$\frac{\partial \alpha_i}{\partial \sum_a} = \frac{\alpha_i}{\sum_a} \left[ 1 + \frac{(F\bar{\ell} - K_\infty) \alpha_i}{(F\bar{\ell} - 1)} \right] \quad (3.66)$$

$$\frac{\partial \alpha_i}{\partial D} = \alpha_i \left( \frac{\partial F}{\partial D} \right) \left[ \frac{\bar{\ell} - \alpha_i / \sum_a (\sigma_i - 1)}{(F\bar{\ell} - 1)} \right], \quad (3.67)$$

where

$$\frac{\partial F}{\partial D} = \frac{8(DX/4D)^2}{[DX(1 + DX/4D)]^2} + \frac{4(DZ/4D)^2}{[DZ(1 + DZ/4D)]^2} \quad (3.68)$$

and DX is the nodal dimension in the X and Y directions and DZ is the nodal dimension in the Z direction.

The derivatives of  $\Gamma_i$  are determined from Eqs. (3.10) and (3.19):

$$\frac{\partial \Gamma_i}{\partial K_\infty} = \frac{-\Gamma_i \left( \frac{\partial \alpha_i}{\partial K_\infty} \right)}{(\alpha_i + \sigma_i)} \quad (3.69)$$

$$\frac{\partial \Gamma_i}{\partial \sum_a} = \frac{-\left[ \bar{\ell} + \Gamma_i \left( \frac{\partial \alpha_i}{\partial \sum_a} + (\sigma_i - 1)^2 \bar{\ell} \right) \right]}{\alpha_i + \sigma_i} \quad (3.70)$$

$$\frac{\partial \Gamma_i}{\partial D} = \frac{-\Gamma_i \left( \frac{\partial \alpha_i}{\partial D} \right)}{[\alpha_i + \sigma_i]} \quad (3.71)$$

Since  $v_{ij}$  is dependent on the cross sections of both  $i$  and  $j$ , we will take two sets of derivatives – one for  $v_{ij}$  and one for  $v_{ji}$ . Equations (3.11), (3.38) and (3.40) are combined to obtain the following derivatives:

$$\frac{\partial v_{ij}}{\partial D_i} = v_{ij} \left[ \frac{1}{r_{ij}} \left( \frac{\partial r_{ij}}{\partial D_i} \right) + \frac{\rho_{ij}}{(1 - \rho_{ij}\rho_{ji})} \left( \frac{\partial \rho_{ji}}{\partial D_i} \right) \right] \quad (3.72)$$

where

$$\frac{\partial \rho_{ji}}{\partial D_i} = -\frac{\rho_{ji}}{D_i} \left[ \frac{1}{(u/4D_i - 1)} + \frac{1}{(u/4D_i + 1)} \right] \quad (3.73)$$

and

$$\frac{\partial r_{ij}}{\partial D_i} = 2(r_{ij})^2 u \left[ \frac{Fu}{4D_i^2} - (1 + DZ/4D_i) \frac{\partial F_i}{\partial D_i} \right] \quad (3.74)$$

and  $u = \begin{matrix} DX & \text{if node } j \text{ lies in the horizontal plane with } i \\ DZ & \text{if node } j \text{ lies in the vertical plane with } i \end{matrix}$

$$\frac{\partial v_{ji}}{\partial D_i} = v_{ji} \left[ \frac{(\rho_{ij} - 1)}{(1 - \rho_{ij}\rho_{ji})(1 - \rho_{ji})} \right] \quad (3.75)$$

Note that  $v_{ij}$  is not a function of  $\sum_a$  or  $K_\infty$ .

The final step in the hierarchy of derivatives is taking the derivatives of the nodal coupling coefficients with respect to the one group cross sections. The definitions of the nodal coupling coefficients given in Eqs. (3.4)-(3.7) are used to derive the following equations. For the coefficients of  $\underline{M}$  we obtain:

$$\frac{\partial M_{ij}}{\partial K_i} = \frac{M_{ij}}{K_i} \quad (3.76)$$

$$\frac{\partial M_{ji}}{\partial K_i} = M_{ji} \left[ \frac{1}{r_i} \left( \frac{\partial r_i}{\partial K_i} \right) - \frac{1}{K_i} \right] \quad (3.77)$$

$$\frac{\partial M_{ii}}{\partial K_i} = \sum_j v_{ij} \left( \frac{\partial r_i}{\partial K_i} \right) \quad (3.78)$$

$$\frac{\partial M_{ij}}{\partial \sum a_1} = 0 \quad (3.79)$$

$$\frac{\partial M_{ji}}{\partial \sum a_1} = \frac{M_{ji}}{r_i} \left( \frac{\partial r_i}{\partial \sum a_1} \right) \quad (3.80)$$

$$\frac{\partial M_{ii}}{\partial \sum a_1} = \sum_j v_{ij} \left( \frac{\partial r_i}{\partial \sum a_1} \right) \quad (3.81)$$

$$\frac{\partial M_{ij}}{\partial D_i} = \frac{M_{ij}}{v_{ji}} \left( \frac{\partial v_{ji}}{\partial D_i} \right) \quad (3.82)$$

$$\frac{\partial M_{ji}}{\partial D_i} = M_{ji} \left[ \frac{1}{r_i} \left( \frac{\partial r_i}{\partial D_i} \right) + \frac{1}{v_{ij}} \left( \frac{\partial v_{ij}}{\partial D_i} \right) \right] \quad (3.83)$$

$$\frac{\partial M_{ii}}{\partial D_i} = \left( \sum_j v_{ij} \right) \frac{\partial r_i}{\partial D_i} + r_i \sum_j \left( \frac{\partial v_{ij}}{\partial D_i} \right) \quad (3.84)$$

$$\frac{\partial M_{jj}}{\partial D_i} = r_j \left( \frac{\partial v_{ji}}{\partial D_i} \right) \quad (3.85)$$

For the coefficients of  $\underline{F}$  we obtain:

$$\frac{\partial F_{ij}}{\partial K_i} = \frac{F_{ij}}{K_i} \quad (3.86)$$

$$\frac{\partial F_{ji}}{\partial K_i} = F_{ji} \left[ \frac{1}{\alpha_i} \left( \frac{\partial \alpha_i}{\partial K_i} \right) + \frac{1}{\Gamma_i} \left( \frac{\partial \Gamma_i}{\partial K_i} \right) \right] \quad (3.87)$$

$$\frac{\partial F_{ii}}{\partial K_i} = \frac{F_{ii}}{K_i} - K_i \sum_j (v_{ij}) \left[ \Gamma_i \left( \frac{\partial \alpha_i}{\partial K_i} \right) + \alpha_i \left( \frac{\partial \Gamma_i}{\partial K_i} \right) \right] \quad (3.88)$$

$$\frac{\partial F_{ij}}{\partial \bar{\Sigma}_{a_1}} = 0 \quad (3.89)$$

$$\frac{\partial F_{ji}}{\partial \bar{\Sigma}_{a_1}} = F_{ji} \left[ \frac{1}{\alpha_i} \left( \frac{\partial \alpha_i}{\partial \bar{\Sigma}_{a_1}} \right) + \frac{1}{\Gamma_i} \frac{\partial \Gamma_i}{\partial \bar{\Sigma}_{a_1}} \right] \quad (3.90)$$

$$\frac{\partial F_{ii}}{\partial \bar{\Sigma}_{a_1}} = -K_i \sum_j v_{ij} \left[ \Gamma_i \left( \frac{\partial \alpha_i}{\partial \bar{\Sigma}_{a_1}} \right) + \alpha_i \left( \frac{\partial \Gamma_i}{\partial \bar{\Sigma}_{a_1}} \right) \right] \quad (3.91)$$

$$\frac{\partial F_{ij}}{\partial D_i} = \frac{F_{ij}}{v_{ji}} \left( \frac{\partial v_{ji}}{\partial D_i} \right) \quad (3.92)$$

$$\frac{\partial F_{ji}}{\partial D_i} = F_{ji} \left[ \frac{1}{\alpha_i} \left( \frac{\partial \alpha_i}{\partial D_i} \right) + \frac{1}{\Gamma_i} \left( \frac{\partial \Gamma_i}{\partial D_i} \right) + \frac{1}{v_{ij}} \left( \frac{\partial v_{ij}}{\partial D_i} \right) \right] \quad (3.93)$$

$$\begin{aligned} \frac{\partial F_{ii}}{\partial D_i} = & -K_i \left[ \Gamma_i \sum_j v_{ij} \left( \frac{\partial \alpha_i}{\partial D_i} \right) + \alpha_i \sum_j v_{ij} \left( \frac{\partial \Gamma_i}{\partial D_i} \right) \right. \\ & \left. + \alpha_i \Gamma_i \sum_j \left( \frac{\partial v_{ij}}{\partial D_i} \right) \right] \quad (3.94) \end{aligned}$$



$$\frac{\partial F_{jj}}{\partial D_j} = -\alpha_j \frac{\partial v_{ji}}{\partial D_j} \quad (3.95)$$

Now that the derivatives of the nodal coupling coefficients with respect to the one group cross sections have been established, the derivatives of the nodal coupling coefficients with respect to the two group cross sections may be computed by using the chain rule of calculus. For example, in order to obtain the derivative of the diagonal coupling coefficient  $M_{ij}$  with respect to the thermal absorption cross section  $\Sigma_{a_2}$ , one would calculate it as follows:

$$\frac{\partial M_{ij}}{\partial \Sigma_{a_2}} = \frac{\partial M_{ij}}{\partial K_j} \frac{\partial K_j}{\partial \Sigma_{a_2}} + \frac{\partial M_{ij}}{\partial \Sigma_{a_j}} \frac{\partial \Sigma_{a_j}}{\partial \Sigma_{a_2}} + \frac{\partial M_{ij}}{\partial D_j} \frac{\partial D_j}{\partial \Sigma_{a_2}} \quad (3.96)$$

All of the terms on the RHS of Eq. (3.96) are known. Every other derivative of the nodal coupling coefficients with respect to the two group input cross sections can be computed in a similar manner.

We have successfully defined the relationship between nodal coupling coefficients and the two group cross sections which are input to SIMULATE using response matrix methods and coarse mesh diffusion theory Eqs. (3.1)-(3.50). Using these definitions, we have derived the partial derivatives of the nodal coupling coefficients with respect to the two group cross sections Eqs. (3.51)-(3.96). With these equations and the ones developed in Section II, we have established the foundation for SIMULATE to perform depletion perturbation calculations.

#### IV. COMPARISON OF GPT AND DPT RESULTS TO DIRECT CALCULATIONS

The purpose of this section is to examine the validity of depletion perturbation theory for a LWR nodal code by comparing the DPT results with those obtained by performing direct calculations with SIMULATE for several different perturbation cases. The cases range from simple static problems to a realistic PWR model for an entire fuel cycle. Responses of interest included  $K_{\text{eff}}$ , nodal power peaking, and nodal exposure. Most cases studied were concerned with the  $K_{\text{eff}}$  response, because it is the most simple for performing DPT calculations and it is of more general interest than any other single response. Throughout this section, the percentage error is calculated as

$$\% \text{ Error (DPT)} = \frac{\text{DPT value} - \text{Direct value}}{\text{Direct value}} \times 100.$$

##### Static Cases

The results of several static cases are examined first, in order that the accuracy of the GPT results may be compared to the accuracy of the DPT results for several burnup-dependent cases, which will be presented later in this section. This will allow one to see the differences between using perturbation theory to predict a change in a response due to a perturbation at a specific point in time and a response change due to a perturbation over a period of time.

The first static case is a simple quarter core model of eleven (11) fuel assemblies. A two-dimensional top view of the fuel loading pattern is shown in Fig. 4.1. For this problem, a three-dimensional model was used. Each assembly was broken into six axial nodes of equal size, yielding a total of 66 nodes. The inner assemblies

ORNL-DWG 80-18172

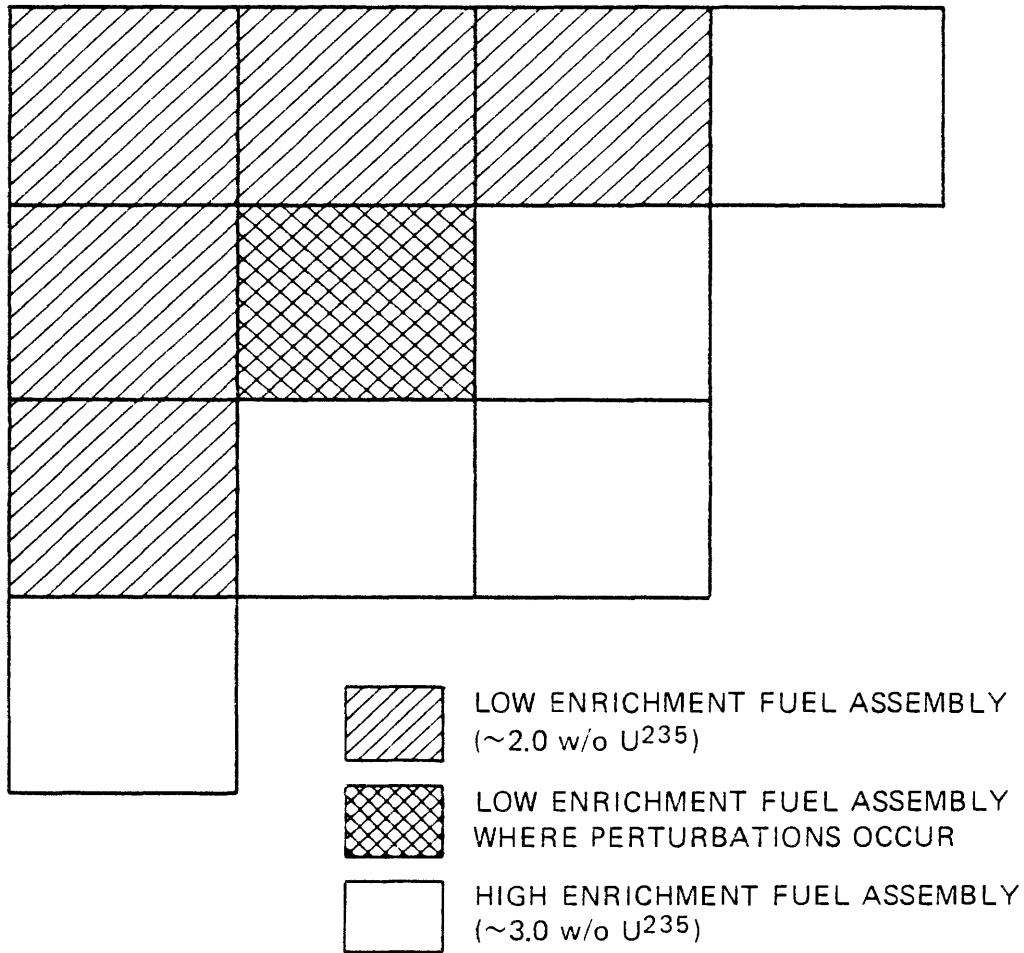


Fig. 4.1. Two-Dimensional Top View of GPT Test Model 1/4 Core

(shaded in Fig. 4.1) contain low enrichment fuel (approximately 2.0 w/o  $U^{235}$ ) and the outer assemblies contain high enrichment fuel (approximately 3.0 w/o  $U^{235}$ ). The value of  $K_{eff}$  for the reference case was 0.9994. Perturbations of 5%, 10%, and 15% were made to  $\nu_{f_1}$  and  $\nu_{f_2}$  in node (2,2,4), the fourth axial node in the fuel assembly which is cross hatched in Fig. 4.1. Sensitivity coefficients from the reference case were used to then predict the changes in both  $K_{eff}$  and the power peak in node (2,2,4). The results are given in Table 4.1. The results for the  $K_{eff}$  response are obviously more

Table 4.1. Comparison of GPT Results  
with Direct Results

$k_{eff}$			
% Perturbation of Fission Cross Sections	$\Delta K/K$ (GPT)	$\Delta K/K$ (Direct)	% Error $\Delta K/K$ (GPT)
5	0.0017	0.0018	-5.56
10	0.0036	0.0039	-7.64
15	0.0055	0.0063	-12.7

(Reference value:  $k_{eff} = 0.9994$ )

Power peaking in node (2,2,4)

% Perturbation of Fission Cross Sections	$\Delta R/R$ (GPT)	$\Delta R/R$ (Direct)	% Error $\Delta R/R$ (GPT)
5	0.1263	0.1340	-5.75
10	0.2523	0.2900	-13.0
15	0.3814	0.4742	-19.6

accurate than those for the power peaking response. Generally, perturbation theory predicts changes in  $K_{\text{eff}}$  more accurately than changes in other responses, because  $K_{\text{eff}}$  is a more global response, for which there is usually a cancellation of errors due to competing effects.

Two other perturbations were made to the reference problem. The fuel enrichment was changed from the lower enrichment to the higher enrichment in: (a) node (2,2,4) only and (b) in the entire fuel assembly (2,2). This second change is equivalent to swapping a low-enrichment fuel bundle for a high-enrichment fuel bundle in location (2,2). The GPT results are compared to the results of direct calculations in Table 4.2, and the magnitude of the perturbations of the individual cross sections for these two cases are also listed there. Although the error is rather large, it does not seem so unreasonable for perturbations of this magnitude.

The remaining cases are adapted from Three Mile Island Unit 1 data for its first fuel cycle.<sup>9</sup> These problems constitute realistic examples for a commercial pressurized water reactor (PWR). A two-dimensional top view of the fuel loading pattern for this 1/8 core model is shown in Fig. 4.2. The first set of perturbations which will be examined for this model is individual perturbation cases of 5% and 10% to each cross section type in fuel assembly 13. The model for these calculations is a two-dimensional model which has a reference value for  $K_{\text{eff}}$  of 1.00377. The changes in  $K_{\text{eff}}$  for each of these perturbations is calculated by two different methods. The first method uses the conventional GPT sensitivity coefficients:

Table 4.2. Comparison of GPT Results with Direct Results for Changing Enrichment

Case	$\frac{\Delta K}{K}$ (GPT)	$\frac{\Delta K}{K}$ (Direct)	% Error in $\frac{\Delta K}{K}$ (GPT)
One node	0.0075	0.0092	-18.5
Fuel Assembly	0.0258	0.0339	-23.9

(Reference value:  $k_{eff} = 0.9994$ )

Perturbation in Cross Sections  
for Changing Enrichment

Cross Section	% Perturbation
$\Sigma_{tr1}$	+2.17
$\Sigma_{a1}$	-5.37
$\Sigma_{r1}$	-2.01
$\nu\Sigma_{f1}$	+35.96
$\Sigma_{tr2}$	+1.53
$\Sigma_{a1}$	+8.07
$\nu\Sigma_{f2}$	+24.06

$$\frac{\Delta K}{K} \approx \frac{\sum_{x=1}^7 \underline{S}^x \Delta \underline{\Sigma}^x}{(1/K) \underline{S}^* \underline{F} \underline{S}} = \frac{-\sum_{x=1}^7 \underline{S}^* \left( \frac{\partial \underline{M}}{\partial \underline{\Sigma}^x} - \lambda \frac{\partial \underline{F}}{\partial \underline{\Sigma}^x} \right) \underline{S} \cdot \Delta \underline{\Sigma}^x}{(1/K) \underline{S}^* \underline{F} \underline{S}} \quad (4.1)$$

Equation (4.1) is taken from Eqs. (2.47) and (2.50). This equation is simply the first-order Taylor Series approximation for the following equation:

KEY:

A- 2.06%

B- 2.747%

C- LBPA, 2.747%, 0.047g/in Boron

D- LBPA, 2.747%, 0.054 g/in Boron

E- LBPA, 2.747%, 0.062 g/in Boron

F- LBPA, 3.05%, 0.054 g/in Boron

G- 3.05%

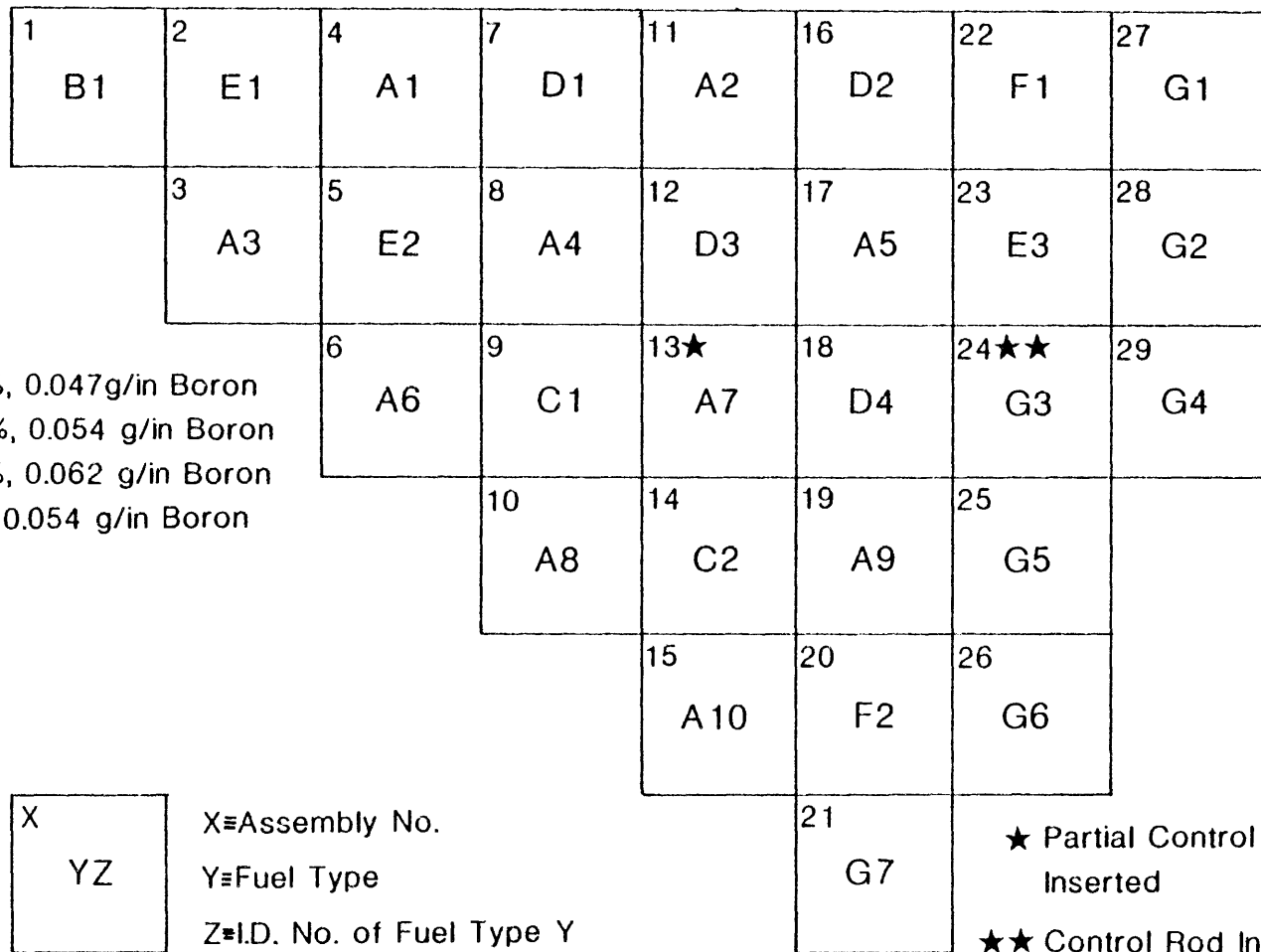


Fig. 4.2. Two-Dimensional Top View of PWR Reference Case 1/8 Core

$$\frac{\Delta K}{K} \cong \frac{- \underline{S}^* (\Delta \underline{M} - \lambda \Delta \underline{F}) \underline{S}}{(1/K) \underline{S}^* \underline{F} \underline{S}} \quad (4.2)$$

This is the second method, which we will call the "semi-direct method." This method is not ordinarily used for two reasons. First, the matrix coefficients for  $\underline{M}$  and  $\underline{F}$  are not usually calculated because of the large volume of computer storage required. Second, the perturbed values of  $\underline{M}$  and  $\underline{F}$  are not usually known, because they would have to be calculated from the perturbed cross sections in a separate calculation. Since it was necessary to perform the direct calculations for the perturbed cases in order to determine the GPT error, the perturbed values of  $\underline{M}$  and  $\underline{F}$  were calculated, too. By comparing the error of the semi-direct (SD) method with the error of the conventional GPT method, one can determine the additional error incurred by the first-order Taylor Series approximation. The two-dimensional model was used in order to reduce the amount of computer storage required for the explicit calculation of the matrix coupling coefficients.

The GPT and SD results for the 5% and the 10% perturbations are compared to the direct calculations in Table 4.3 and Table 4.4, respectively. Examining the errors for each cross section type in these two tables reveal that  $K_{\text{eff}}$  has a nearly linear behavior with respect to  $\nu \sum_{f_1}$ , while it behaves in a very nonlinear manner with respect to  $\sum_{a_2}$  and  $\nu \sum_{f_2}$ . Perturbing  $\sum_{\text{tr}_1}$  or  $\sum_{\text{tr}_2}$  has only a slight effect on  $K_{\text{eff}}$ . The data show that although these two perturbations are the largest in magnitude, they produce the smallest changes in the response. In fact, the perturbations of  $\sum_{\text{tr}_2}$  create such small changes in  $K_{\text{eff}}$  that they



Table 4.3. Comparison of GPT and SD Results to Direct Calculations  
for 5% Perturbations of a 2-D Model for  $K_{\text{eff}}$  Response

Perturbed Cross Section, $\Sigma^x$	$\Delta\Sigma^x$ ( $\text{cm}^{-1}$ )	$\Delta K/K$			% Error	
		(GPT)	(SD)	(Direct)	(GPT)	(SD)
$\Sigma_{\text{tr}1}$	$1.140 \times 10^{-2}$	$1.816 \times 10^{-5}$	$1.806 \times 10^{-5}$	$1.786 \times 10^{-5}$	1.68	1.04
$\Sigma_{\text{a}1}$	$4.396 \times 10^{-4}$	$-6.867 \times 10^{-4}$	$-6.6181 \times 10^{-5}$	$-6.475 \times 10^{-4}$	6.05	2.21
$\Sigma_{\text{r}1}$	$8.894 \times 10^{-4}$	$1.854 \times 10^{-4}$	$2.045 \times 10^{-4}$	$2.074 \times 10^{-4}$	-10.6	-1.40
$\nu\Sigma_{\text{f}1}$	$2.603 \times 10^{-4}$	$3.964 \times 10^{-4}$	$3.989 \times 10^{-4}$	$4.068 \times 10^{-4}$	-2.55	-1.94
$\Sigma_{\text{tr}2}$	$4.224 \times 10^{-2}$	$1.562 \times 10^{-6}$	$1.631 \times 10^{-6}$	$1.985 \times 10^{-6}$	-4.23*	†
$\Sigma_{\text{a}2}$	$3.449 \times 10^{-3}$	$-1.308 \times 10^{-3}$	$-1.231 \times 10^{-3}$	$-1.180 \times 10^{-3}$	10.9	4.27
$\nu\Sigma_{\text{f}2}$	$4.689 \times 10^{-3}$	$1.531 \times 10^{-3}$	$1.5657 \times 10^{-3}$	$1.6646 \times 10^{-3}$	-8.06	-5.94

† Not calculated since  $\Delta K/K$  is so small that  $\Delta K/K$  (SD) is probably more accurate than  $\Delta K/K$  (Direct).

\* Error compared to  $\Delta K/K$  (SD).

[Reference value:  $K_{\text{eff}} = 1.00377$ ]

Table 4.4. Comparison of GPT and SD Results to Direct Calculations for 10% Perturbations of a 2-D Model for  $K_{\text{eff}}$  Response

Perturbed Cross Section, $\Sigma^x$	$\Delta\Sigma^x(\text{cm}^{-1})$	$\Delta K/K$			% Error	
		(GPT)	(SD)	(Direct)	(GPT)	(SD)
$\Sigma_{\text{tr}1}$	$2.280 \times 10^{-2}$	$3.360 \times 10^{-5}$	$3.510 \times 10^{-5}$	$3.470 \times 10^{-5}$	4.50	1.04
$\Sigma_{\text{a}1}$	$8.792 \times 10^{-4}$	$-1.373 \times 10^{-3}$	$-1.303 \times 10^{-3}$	$-1.252 \times 10^{-3}$	9.66	4.07
$\Sigma_{\text{r}1}$	$1.779 \times 10^{-3}$	$3.708 \times 10^{-4}$	$4.047 \times 10^{-4}$	$4.137 \times 10^{-4}$	-10.4	-2.18
$\nu\Sigma_{\text{f}1}$	$5.206 \times 10^{-4}$	$7.928 \times 10^{-4}$	$8.026 \times 10^{-4}$	$8.231 \times 10^{-4}$	-3.68	-2.49
$\Sigma_{\text{tr}2}$	$8.448 \times 10^{-2}$	$3.120 \times 10^{-6}$	$2.880 \times 10^{-6}$	$4.960 \times 10^{-6}$	-8.33*	†
$\Sigma_{\text{a}2}$	$6.899 \times 10^{-3}$	$-2.615 \times 10^{-3}$	$-2.329 \times 10^{-3}$	$-2.158 \times 10^{-3}$	21.2	7.92
$\nu\Sigma_{\text{f}2}$	$9.378 \times 10^{-3}$	$3.061 \times 10^{-3}$	$3.196 \times 10^{-3}$	$3.647 \times 10^{-3}$	-16.1	-12.4

† Not calculated since  $\Delta K/K$  is so small that  $\Delta K/K$  (SD) is probably more accurate than  $\Delta K/K$  (Direct).

\* Error compared to  $\Delta K/K$  (SD).

[Reference value:  $K_{\text{eff}} = 1.00377$ ]

cannot be measured accurately from direct calculations, because they are the same order of magnitude as the convergence criterion. For this reason, the SD result is considered to be the correct value for  $\sum_{tr_2}$  perturbations in Tables 4.3 and 4.4.

Comparing the GPT and SD errors shows that, in general, the Taylor Series approximation [Eq. (4.1)] introduces a second error that is approximately equal to the first error which appears in the SD method. In the case of  $\sum_{r_1}$ , it introduces an error which is much larger than the original error in the SD method. Another unusual phenomenon in the  $\sum_{r_1}$  case is the slight decrease in the GPT error when the perturbation is increased from 5% to 10%.

The same direct calculations for the 10% perturbations were used to test the ability of the GPT and SD methods to predict changes in the power peaking response in fuel assembly #3. The comparison of these results is tabulated in Table 4.5. The value of this response for the reference case was 1.390. The semi-direct method gives better results in every case except  $\sum_{tr_1}$  and  $\sum_{a_1}$ . The only case where there is a significant difference between the two methods is that of  $\sum_{a_2}$ . Once again, the errors in the power peaking perturbations are generally much larger than those in the  $K_{eff}$  perturbations, since the power peaking response is a localized, and therefore, more nonlinear response.

A series of 10% perturbation cases was also performed for a three-dimensional model of the reactor core pictured in Fig. 4.2. Each assembly was divided into seven (7) axial nodes of equal size. This model contained 203 fueled nodes and required too much computer storage to use the semi-direct method. The GPT calculations were performed and

Table 4.5. Comparison of GPT and SD Results to Direct Calculations  
for 10% Perturbations of a 2-D Model for  
Power Peaking in Fuel Assembly #3

Perturbed Cross Section, $\Sigma^x$	$\Delta\Sigma^x(\text{cm}^{-1})$	$\Delta R/R$			% Error	
		(GPT)	(SD)	(Direct)	(GPT)	(SD)
$\Sigma_{\text{tr}_1}$	$2.280 \times 10^{-2}$	$1.159 \times 10^{-3}$	$1.088 \times 10^{-3}$	$1.439 \times 10^{-3}$	-19.4	-24.4
$\Sigma_{\text{a}_1}$	$8.792 \times 10^{-4}$	$1.723 \times 10^{-2}$	$1.664 \times 10^{-2}$	$1.799 \times 10^{-2}$	-4.21	-7.50
$\Sigma_{\text{r}_1}$	$1.779 \times 10^{-3}$	$-9.847 \times 10^{-3}$	$-9.650 \times 10^{-3}$	$-7.914 \times 10^{-3}$	24.4	21.9
$\nu\Sigma_{\text{f}_1}$	$5.206 \times 10^{-4}$	$-1.073 \times 10^{-2}$	$-1.084 \times 10^{-2}$	$-1.223 \times 10^{-2}$	-12.2	-11.3
$\Sigma_{\text{tr}_2}$	$8.448 \times 10^{-2}$	$9.970 \times 10^{-5}$	$9.154 \times 10^{-5}$	0.0	—	—
$\Sigma_{\text{a}_2}$	$6.899 \times 10^{-3}$	$3.711 \times 10^{-2}$	$3.354 \times 10^{-2}$	$3.309 \times 10^{-2}$	12.1	1.37
$\nu\Sigma_{\text{f}_2}$	$9.378 \times 10^{-3}$	$-4.144 \times 10^{-2}$	$-4.299 \times 10^{-2}$	$-4.964 \times 10^{-2}$	-16.5	-13.4

[Reference value:  $R = 1.390$ ]

appear in Table 4.6 with the results of the direct calculations. The errors are approximately the same for the three-dimensional model as for the two-dimensional model (Table 4.4). The  $K_{\text{eff}}$  response behaves most linearly with respect to  $\nu \sum_{f_1}$  and most nonlinearly with respect to  $\sum_{a_2}$ . In order to better understand the differences between the linear and nonlinear behavior patterns, additional direct calculations were performed for +5%, -5%, and -10% perturbations in the base cross sections for  $\nu \sum_{f_1}$  and  $\sum_{a_2}$ . The  $K_{\text{eff}}$  response as a function of  $\nu \sum_{f_1}$  is tabulated in Table 4.7 and plotted in Fig. 4.3. Table 4.8 and Figure 4.4 give  $K_{\text{eff}}$  as a function of  $\sum_{a_2}$ . These results confirm that  $K_{\text{eff}}$  varies

Table 4.6. Comparison of GPT Results to Direct Calculations for 10% Perturbations of a 3-D Model for  $K_{\text{eff}}$  Response

Perturbed Cross Section, $\sum^x$	$\Delta \sum^x$ ( $\text{cm}^{-1}$ )	$\Delta K/K$		% Error (GPT)
		(GPT)	(Direct)	
$\sum_{\text{tr}_1}$	$2.280 \times 10^{-2}$	$4.533 \times 10^{-5}$	$4.194 \times 10^{-5}$	8.10
$\sum_{a_1}$	$8.792 \times 10^{-4}$	$-1.368 \times 10^{-3}$	$-1.257 \times 10^{-3}$	8.85
$\sum_{r_1}$	$1.779 \times 10^{-3}$	$3.832 \times 10^{-4}$	$4.204 \times 10^{-4}$	-8.84
$\nu \sum_{f_1}$	$5.206 \times 10^{-4}$	$7.983 \times 10^{-4}$	$8.317 \times 10^{-4}$	-4.02
$\sum_{\text{tr}_2}$	$8.448 \times 10^{-2}$	$8.044 \times 10^{-6}$	$2.995 \times 10^{-6}$	†
$\sum_{a_2}$	$6.899 \times 10^{-3}$	$-2.623 \times 10^{-3}$	$-2.161 \times 10^{-3}$	21.4
$\nu \sum_{f_2}$	$9.378 \times 10^{-3}$	$3.061 \times 10^{-3}$	$3.671 \times 10^{-3}$	-16.6

†  $\Delta K/K$  is so small that  $\Delta K/K$  (GPT) is probably more accurate than  $\Delta K/K$  (Direct).

[Reference value:  $K_{\text{eff}} = 1.00154$ ]

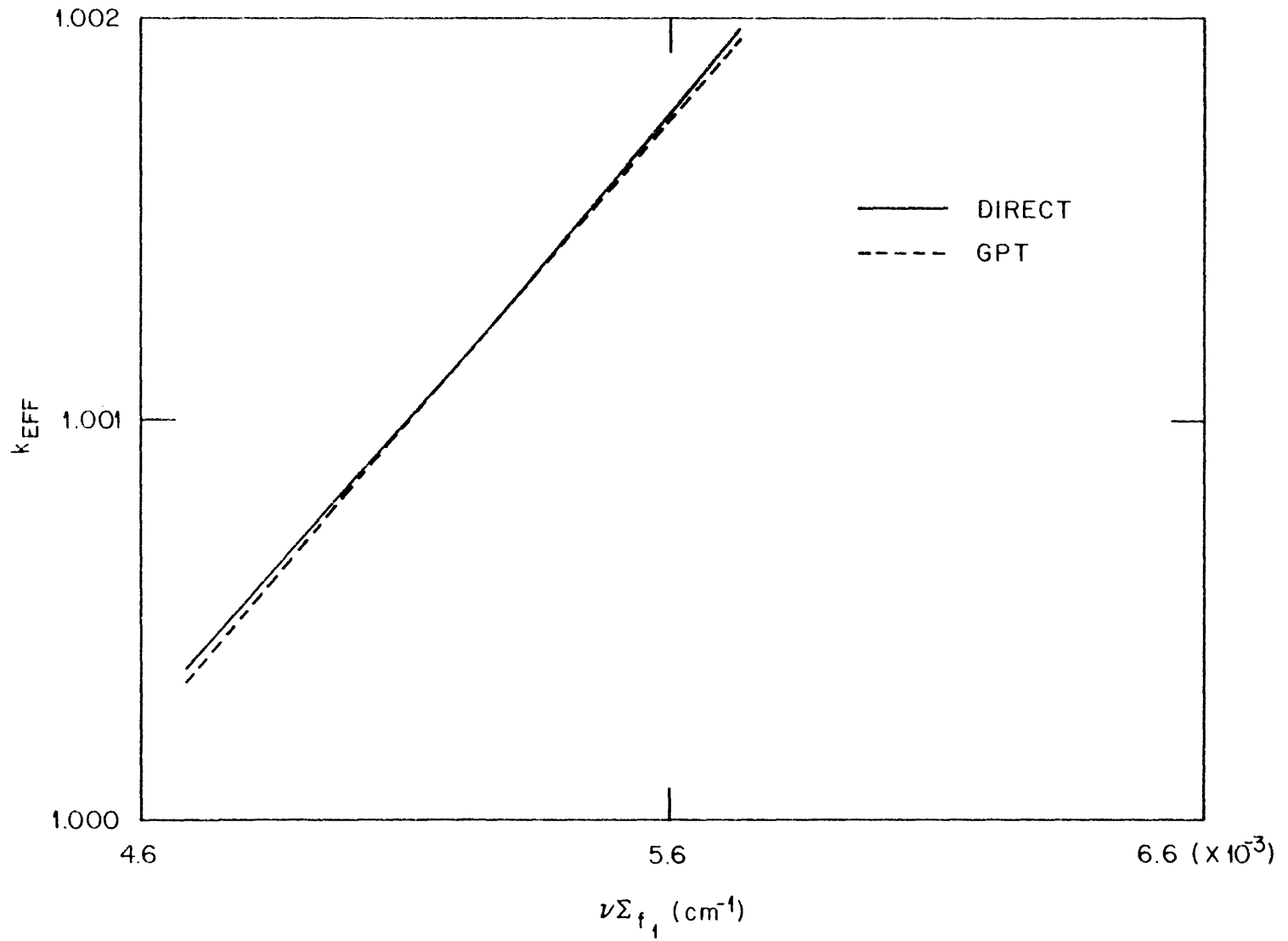


Fig. 4.3.  $k_{eff}$  Versus  $\nu \Sigma_{f_1}$

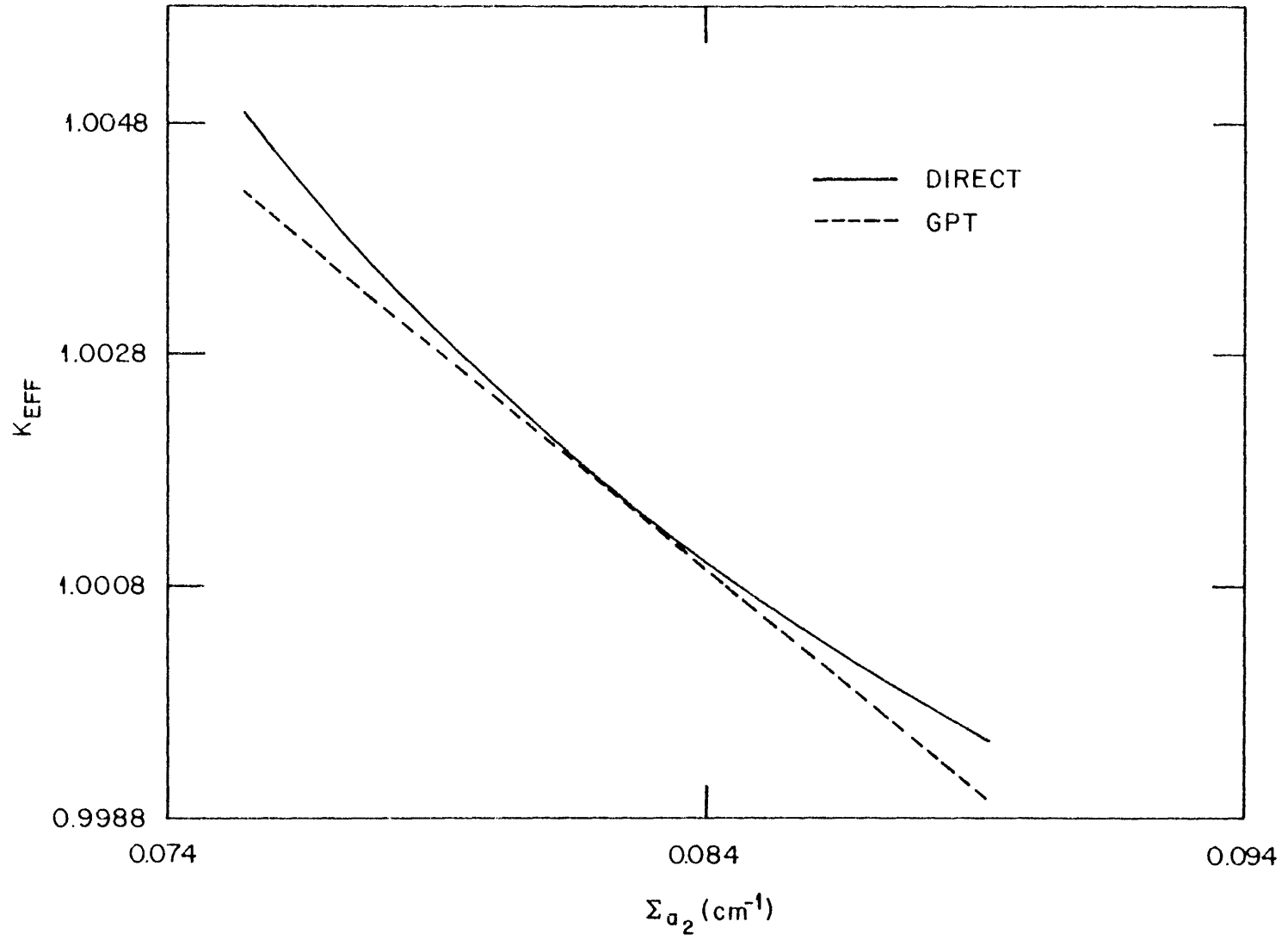


Fig. 4.4.  $K_{\text{eff}}$  Versus  $\Sigma_{a_2}$

Table 4.7.  $K_{\text{eff}}$  vs.  $\bar{\nu}_{f_1}$ 

$\bar{\nu}_{f_1}$ ( $\text{cm}^{-1}$ )	$K_{\text{eff}}$	$\Delta\bar{\nu}_{f_1}$ ( $\text{cm}^{-1}$ )	$\Delta K/K$	Sensitivity Coefficient (Direct)	% Error in GPT Sensitivity Coefficient
$.4686 \times 10^{-2}$	1.000775	$-.5200 \times 10^{-3}$	$-.7638 \times 10^{-3}$	1.467	4.29
$.4946 \times 10^{-2}$	1.001149	$-.2600 \times 10^{-3}$	$-.3904 \times 10^{-3}$	1.500	2.00
$.5206 \times 10^{-2}$	1.001540	0.0	0.0	—	—
$.5467 \times 10^{-2}$	1.001947	$.2610 \times 10^{-3}$	$.4064 \times 10^{-3}$	1.561	-1.99
$.5727 \times 10^{-2}$	1.002373	$.5210 \times 10^{-3}$	$.8317 \times 10^{-3}$	1.594	-4.02

[GPT Sensitivity Coefficient = 1.530]

Table 4.8.  $K_{\text{eff}}$  vs.  $\bar{\nu}_{a_2}$ 

$\bar{\nu}_{a_2}$ ( $\text{cm}^{-1}$ )	$K_{\text{eff}}$	$\Delta\bar{\nu}_{a_2}$ ( $\text{cm}^{-1}$ )	$\Delta K/K$	Sensitivity Coefficient (Direct)	% Error in GPT Sensitivity Coefficient
$.7544 \times 10^{-1}$	1.004842	$-.6900 \times 10^{-2}$	$.3297 \times 10^{-2}$	-0.4771	-20.5
$.7889 \times 10^{-1}$	1.003000	$-.3450 \times 10^{-2}$	$.1458 \times 10^{-2}$	-0.4219	-9.93
$.8234 \times 10^{-1}$	1.001540	0.0	0.0	—	—
$.8579 \times 10^{-1}$	1.000355	$.3450 \times 10^{-2}$	$-.1183 \times 10^{-2}$	-.3430	10.8
$.8924 \times 10^{-1}$	0.999376	$.6900 \times 10^{-2}$	$-.2161 \times 10^{-2}$	-.3127	21.4

[GPT Sensitivity Coefficient = -.3795]



almost linearly, as assumed by generalized perturbation theory, with respect to  $v_{\sum f_1}$ , and that  $K_{\text{eff}}$  varies in a nonlinear manner with respect to  $\sum a_2$ . Thus, perturbation theory is valid over a much wider range for  $v_{\sum f_1}$  than for  $\sum a_2$ . The errors tabulated in the final column of both Tables 4.7 and 4.8 measure the difference between the actual sensitivity coefficient obtained from direct calculations

$$\underline{\alpha}^x = \frac{1}{K} \frac{\Delta K/K}{\underline{\Delta \sum^x}}, \quad (4.3)$$

and the sensitivity coefficient calculated using generalized perturbation theory for the reference case

$$\underline{\alpha}^x = \frac{\underline{s}^x}{\underline{s}^* \underline{F} \underline{S}} \cong \frac{1}{K} \frac{\Delta K/K}{\underline{\Delta \sum^x}}, \quad (4.4)$$

or

$$\frac{\Delta K}{K} \cong \frac{\underline{s}^x \underline{\Delta \sum^x}}{(1/K) \underline{s}^* \underline{F} \underline{S}} = \frac{\underline{\alpha}^x \underline{\Delta \sum^x}}{(1/K)}, \quad (4.5)$$

which is equivalent to Eq. (2.50).

The data contained in Tables 4.7 and 4.8 also provide us with the means to check for any errors in the SIMULATE perturbation theory methodology for calculating the GPT sensitivity coefficients. Averaging the actual sensitivity coefficients for two perturbations of equal magnitude in the opposite directions should give approximately the same value as the corresponding GPT sensitivity coefficient. The average of the  $v_{\sum f_1}$  sensitivity coefficients for perturbations of +5% and -5% is 1.5305, only .03% from the GPT value of 1.530. The average of the  $\sum a_2$

sensitivity coefficients for similar perturbations is  $-0.38245$ , which varies only  $0.78\%$  from the GPT value of  $-0.3795$ . From this, one can conclude that the sensitivity coefficients calculated by SIMULATE are, in fact, the sensitivity coefficients predicted by perturbation theory. Thus, the errors in the GPT predictions for  $\Delta K/K$  are due entirely to nonlinear effects and not to any error in the SIMULATE perturbation theory methodology.

Six "realistic" static perturbation cases were studied using this PWR model to test the validity of generalized perturbation theory for LWR design modifications. The first perturbation was to decrease the lumped burnable poison (LBP) concentration in fuel assembly #12 from  $0.054$  gm/in. of boron to  $0.047$  gm/in. of boron. This a very small perturbation, as can be seen from the cross section changes in Table 4.9. For small perturbations such as this one, perturbation theory should give very accurate results, which it does, as shown in Table 4.9.

The second perturbation is removing a partial control rod from fuel assembly #13. Table 4.10 shows that the only significant change is in  $\Sigma_{a_2}$ . However, this cross section has an extremely nonlinear effect on  $K_{eff}$ , as was discussed earlier. The large error is consistent with the results in Table 4.8.

The next perturbation is the converse of the previous perturbation. It is the insertion of a partial control rod into fuel assembly #4 (Table 4.11). The changes in the cross sections for this case have the same approximate absolute values and the opposite signs as those in the previous problem. Likewise, the error is approximately the same magnitude and has the opposite sign as the error in the previous case. This is also consistent with the data in Table 4.8.

Table 4.9. Decrease LBP Concentration  
in Fuel Assembly #12

$\Delta K/K$		% Error in GPT
(Direct)	(GPT)	
$.5092 \times 10^{-3}$	$.5022 \times 10^{-3}$	-1.37
[Reference Value: $K_{\text{eff}} = 1.00154$ ]		
$\sum^x$	% $\Delta \sum^x$	$\alpha^x$ (GPT)
$\sum_{\text{tr}_1}$	0.0	$1.26 \times 10^{-3}$
$\sum_{\text{a}_1}$	-0.30	-2.28
$\sum_{\text{r}_1}$	-0.13	0.526
$\nu \sum_{\text{f}_1}$	-0.07	2.28
$\sum_{\text{tr}_2}$	0.0	$2.56 \times 10^{-5}$
$\sum_{\text{a}_2}$	-0.86	0.465
$\nu \sum_{\text{f}_2}$	0.17	0.378

The fourth and the fifth perturbation cases deal with the removal of a control rod (Table 4.12) and the insertion of a control rod (Table 4.13), respectively. The changes in  $\sum_{\text{a}_2}$  are twice as large for these perturbations as they were for the two previous cases. The thermal absorption is the dominating effect, and causes very serious errors in predicting the changes in  $K_{\text{eff}}$  for these two cases. These examples demonstrate that the validity of perturbation theory is severely restricted for perturbations in the thermal absorption due to the strong nonlinearity of  $K_{\text{eff}}$  with respect to  $\sum_{\text{a}_2}$ . It should be noted that these

Table 4.10. Remove Partial Control Rod  
from Fuel Assembly #13

$\Delta K/K$		% Error in GPT
(Direct)	(GPT)	
$.4137 \times 10^{-2}$	$.32330 \times 10^{-2}$	-21.9
[Reference Value: $K_{\text{eff}} = 1.00154$ ]		
$\Sigma^x$	% $\Delta \Sigma^x$	$\alpha^x$ (GPT)
$\Sigma_{\text{tr}_1}$	-0.92	$1.99 \times 10^{-3}$
$\Sigma_{\text{a}_1}$	-2.67	-1.55
$\Sigma_{\text{r}_1}$	-1.13	0.219
$\nu \Sigma_{\text{f}_1}$	-0.52	1.53
$\Sigma_{\text{tr}_2}$	0.08	$4.61 \times 10^{-5}$
$\Sigma_{\text{a}_2}$	-8.29	-0.380
$\nu \Sigma_{\text{f}_2}$	1.12	0.327

errors would have been approximately one-half as great with the semi-direct method.

A general trend about the importance of the different cross section types can be observed from the sensitivity coefficients in Tables 4.9 through 4.14. The most important cross sections are usually  $\Sigma_{\text{a}_1}$  and  $\nu \Sigma_{\text{f}_1}$ . The importance of  $\Sigma_{\text{r}_1}$ ,  $\Sigma_{\text{a}_2}$  and  $\nu \Sigma_{\text{f}_2}$  are typically an order of magnitude less than the first two cross sections. The transport cross sections,  $\Sigma_{\text{tr}_1}$  and  $\Sigma_{\text{tr}_2}$ , have a negligible effect on  $K_{\text{eff}}$ . The

Table 4.11. Insert Partial Control Rod  
into Fuel Assembly #4

$\Delta K/K$		% Error in GPT
(Direct)	(GPT)	
$-.2596 \times 10^{-2}$	$-.3205 \times 10^{-2}$	23.5
[Reference Value $K_{eff} = 1.00154$ ]		
$\Sigma^x$	% $\Delta \Sigma^x$	$\alpha^x$ (GPT)
$\Sigma_{tr_1}$	0.93	$9.52 \times 10^{-5}$
$\Sigma_{a_1}$	2.74	-1.66
$\Sigma_{r_1}$	1.15	-0.051
$\nu \Sigma_{f_1}$	0.52	1.18
$\Sigma_{tr_2}$	-0.08	$2.32 \times 10^{-6}$
$\Sigma_{a_2}$	9.05	-0.371
$\nu \Sigma_{f_2}$	-1.11	0.272

sensitivities of the fission cross sections are always positive and those of absorption cross sections are always negative. The removal cross section generally has a positive sensitivity coefficient, but it can be negative occasionally (Table 4.11).

The final static perturbation case consists of two perturbations, replacing a 2.06 w/o enriched fuel assembly and a 2.747 w/o enriched fuel assembly with two 3.05 w/o enriched fuel assemblies. The cross section changes and the sensitivity coefficients for each assembly are listed in Table 4.14. The greatest perturbations in the cross sections

Table 4.12. Remove Control Rod  
from Fuel Assembly #24

$\Delta K/\%$		% Error in GPT
(Direct)	(GPT)	
$.11243 \times 10^{-1}$	$.03531 \times 10^{-1}$	-68.6%
[Reference Value: $K_{\text{eff}} = 1.00154$ ]		
$\Sigma^x$	% $\Delta \Sigma^x$	$\alpha^x$ (GPT)
$\Sigma_{\text{tr}1}$	-2.0	$2.16 \times 10^{-3}$
$\Sigma_{\text{a}1}$	-9.00	-0.664
$\Sigma_{\text{r}1}$	3.60	0.043
$\nu \Sigma_{\text{f}1}$	-0.92	0.544
$\Sigma_{\text{tr}2}$	2.43	$3.70 \times 10^{-5}$
$\Sigma_{\text{a}2}$	-21.52	-0.094
$\nu \Sigma_{\text{f}2}$	4.89	0.086

occur in  $\nu \Sigma_{\text{f}1}$ ,  $\Sigma_{\text{a}2}$  and  $\nu \Sigma_{\text{f}2}$  in fuel assembly #13, where a low enrichment assembly has been replaced. The error for this case is obviously dominated by  $\nu \Sigma_{\text{f}2}$  and  $\Sigma_{\text{a}2}$ , both of which have been shown to have substantial nonlinear effects on  $K_{\text{eff}}$ . Because perturbation theory assumes that the response varies linearly with respect to the perturbed variables, it is possible to use perturbation theory to approximate the effects of two or more perturbations simultaneously, as was done for this case. Doing this can have the effect of adding error to error or

Table 4.13. Insert Control Rod  
into Fuel Assembly #22

$\Delta K/K$		% Error in GPT
(Direct)	(GPT)	
$-.2097 \times 10^{-2}$	$-.3373 \times 10^{-2}$	60.9
[Reference Value: $K_{\text{eff}} = 1.00154$ ]		
$\Sigma^x$	% $\Delta \Sigma^x$	$\alpha^x$ (GPT)
$\Sigma_{\text{tr}1}$	1.57	$-8.46 \times 10^{-4}$
$\Sigma_{\text{a}1}$	6.01	-0.929
$\Sigma_{\text{r}1}$	1.34	0.020
$\nu \Sigma_{\text{f}1}$	0.93	0.700
$\Sigma_{\text{tr}2}$	0.723	$-1.62 \times 10^{-5}$
$\Sigma_{\text{a}2}$	17.0	-0.145
$\nu \Sigma_{\text{f}2}$	-2.61	0.108

cancelling errors, depending upon the signs of the errors for each individual perturbation.

#### Burnup-Dependent Cases

The results of several burnup-dependent cases are now presented in order to determine the validity of depletion perturbation theory for LWRs. The model used for all these cases is the 1/8 core PWR model illustrated in Fig. 4.2.

The first set of perturbations of a depletion problem is individual perturbations of 10% to each of the five most important cross section

Table 4.14. Replacing a Low Enrichment Fuel Assembly and a Medium Enrichment Fuel Assembly with Two High Enrichment Fuel Assemblies

	$\Delta K/K$		% Error in GPT	
	(Direct)	(GPT)		
	$.2413 \times 10^{-1}$	$.1546 \times 10^{-1}$	-35.9	
[Reference Value: $K_{\text{eff}} = 1.00377$ ]				
$\Sigma^x$	Assembly #2		Assembly #13	
	% $\Delta \Sigma^x$	$\alpha^x$ (GPT)	% $\Delta \Sigma^x$	$\alpha^x$ (GPT)
$\Sigma_{\text{tr}1}$	-0.57	$2.15 \times 10^{-3}$	-0.04	$1.59 \times 10^{-3}$
$\Sigma_{\text{a}1}$	-2.11	-1.33	3.73	-1.56
$\Sigma_{\text{r}1}$	2.95	0.433	-7.03	0.208
$\nu \Sigma_{\text{f}1}$	6.24	1.46	24.01	1.52
$\Sigma_{\text{tr}2}$	3.32	$4.32 \times 10^{-5}$	0.04	$3.70 \times 10^{-5}$
$\Sigma_{\text{a}2}$	-4.17	-0.289	13.04	-0.379
$\nu \Sigma_{\text{f}2}$	11.76	0.240	41.82	0.326

types. The two transport cross sections were omitted since perturbing them has virtually no effect. The burnup calculations covered a short cycle of 40 MWD/T, with calculations at 0, 20, and 40 MWD/T. The DPT results for the  $K_{\text{eff}}$  response at the end of cycle (EOC) are compared to direct calculations in Table 4.15. The results in this table may be compared with the data in Table 4.6 to realize the difference in accuracy of perturbation theory for static and burnup-dependent cases.



Table 4.15. Comparison of DPT Results to Direct Calculations for 10% Perturbations of a 3-D Model from 0-40 MWD/T for EOC  $K_{\text{eff}}$  Response

Perturbed Cross Section, $\Sigma^x$	$\frac{\Delta K}{K}$		% Error in DPT
	(DPT)	(Direct)	
$\Sigma_{a_1}$	$-.1294 \times 10^{-2}$	$-.1244 \times 10^{-2}$	4.06
$\Sigma_{r_1}$	$.3791 \times 10^{-3}$	$.4040 \times 10^{-3}$	-6.18
$\nu \Sigma_{f_1}$	$.8024 \times 10^{-3}$	$.8577 \times 10^{-3}$	-6.44
$\Sigma_{a_2}$	$-.2380 \times 10^{-2}$	$-.2129 \times 10^{-2}$	11.8
$\nu \Sigma_{f_2}$	$.2937 \times 10^{-2}$	$.3722 \times 10^{-2}$	-21.1

[Reference Value:  $K_{\text{eff}} = 0.955355$ ]

The DPT errors in Table 4.15 are less than the GPT errors in Table 4.6 except for the fission cross section, especially  $\nu \Sigma_{f_2}$ . The reduction in error of the thermal absorption is the most significant change, decreasing from 21.4% in the GPT case to 11.8% in the DPT case. The decreased error for a depletion case is a common phenomenon which is caused by the cancellation of errors from the terms of the different timesteps.

Another set of DPT calculations were performed for the EOC peak exposure response for the same depletion problem. The sensitivity coefficients for this response are determined by setting

$$\underline{S}_l^* = 0$$

$$\underline{E}_l^* = \begin{cases} 1 & \text{for the node with the exposure peak} \\ 0 & \text{for all other nodes} \end{cases}$$

in Eq. (C.16) of Appendix C. Equation (C.34) then becomes

$$\Delta E_{p\ell} \cong \sum_{i=0}^{\ell-1} \sum_{x=1}^7 \underline{s}_i^x \Delta \sum_i^x, \quad (4.6)$$

where  $\underline{s}_i^x \equiv$  EOC peak exposure sensitivity coefficient for exposure step  $i$  and cross section type  $x$  and

$E_{p\ell} \equiv$  peak exposure at the final exposure step.

The DPT results for the same set of perturbations are compared to direct calculations for the EOC peak exposure response in Table 4.16. The error for each one of these is much greater than that for the  $K_{\text{eff}}$  response. The reason for the increased amount of error may be attributed to the fact that these perturbations have only an indirect effect on the peak exposure, since it occurs in another fuel assembly. This type of effect is more difficult to predict in LWRs because localized perturbations are hardly felt in other regions of the reactor.

The results of several "realistic cases" will now be presented to test the applicability of depletion perturbation theory to PWR design problems for an entire fuel cycle. These problems all have a fuel cycle of 14,000 MWD/T, calculated in 22 exposure steps. The first test case consists of the same perturbation as that presented in Table 4.10, i.e., the removal of a partial control rod from fuel assembly #13. However, in this case the perturbation occurs throughout an entire fuel cycle, rather than for a static BOC calculation. The DPT and SD results for this burnup-dependent case are compared to direct calculations in Table 4.17. Notice that the DPT error in  $\Delta K/K$  in Table 4.17 is almost half as large as the GPT error in  $\Delta K/K$  in Table 4.10. The agreement of

Table 4.16. Comparison of DPT Results to Direct Calculations for 10% Perturbations of a 3-D Model from 0-40 MWD/T for Peak Exposure Response

Perturbed Cross Section, $\Sigma^x$	$\frac{\Delta E(1,3,4)}{(\text{DPT})}$ GWD/T	$\frac{\Delta E(1,3,4)}{(\text{Direct})}$ GWD/T	% Error in DPT
$\Sigma_{a_1}$	.0008	.0011	-27.3
$\Sigma_{r_1}$	-.0003	-.0005	-40.0
$\nu \Sigma_{f_1}$	-.0005	-.0007	-28.6
$\Sigma_{a_2}$	.0015	.0020	-25.0
$\nu \Sigma_{f_2}$	-.0019	-.0029	-34.5

[Reference Value:  $E(1,3,4) = 0.0677$  GWD/T = 67.7 MWD/T]

Table 4.17. Removal of a Partial Control Rod from Fuel Assembly #13 for a Fuel Cycle of 14,000 MWD/T

EOC $K_{\text{eff}}$ Response				
$\frac{\Delta K}{K}$			% Error	
(DPT)	(SD)	(Direct)	(DPT)	(SD)
$.2632 \times 10^{-2}$	$.2976 \times 10^{-2}$	$.2945 \times 10^{-2}$	-10.6	1.05

[Reference Value:  $K_{\text{eff}} = 0.985176$ ]

EOC Peak Exposure Response				
$\Delta E_p$ (GWD/T)			% Error	
(DPT)	(SD)	(Direct)	(DPT)	(SD)
-0.288	-0.320	-0.410	-29.8	-22.0

[Reference Value:  $E_p = E(1,7,2) = 17.861$  GWD/T]

the semidirect method approximation for  $\Delta K/K$  with the direct calculation is excellent. Once again, the DPT and the SD errors in the change in peak exposure are much greater than the errors in  $\Delta K/K$ . This occurs because the peak exposure is a localized response, and because the perturbation is made in a different assembly than the one in which the peak exposure is found. The magnitudes of the cross section perturbations are given in Table 4.18 for the beginning and the end of cycle.

The values of the five significant cross section sensitivity coefficients for  $K_{eff}$  are shown for the entire fuel cycle in Figs. 4.5 - 4.9. These sensitivity coefficients are almost zero for every exposure step except the final one. Thus, the greatest contribution to the change in EOC  $K_{eff}$  is made at the EOC calculation, which is a static calculation. Unlike  $K_{eff}$ , the EOC peak exposure is not affected by a static perturbation at the end of cycle, since it is a response which is purely dependent on perturbations at previous exposure steps. This can be seen by examining graphs (Figs. 4.10 - 4.14) of the peak exposure sensitivity coefficients over the course of the fuel cycle. These are the sensitivity coefficients for perturbations in fuel assembly #22, where the next two perturbations occur. These coefficients differ greatly in character from those in Figs. 4.5 - 4.9 for the  $K_{eff}$  response. Increases in the absorption cross sections will decrease the EOC exposure since they will increase the self-shielding of the fuel. Increasing the removal or the fission cross sections will increase the EOC peak exposure, since it will increase the fission density of the fuel.

The next depletion case is the replacement of the F type fuel assembly (3.05 w/o and 0.054 g/in boron) with an A type assembly

Table 4.18. Cross Section Perturbations  
for Removal of Partial Control Rod  
from Fuel Assembly #13

BOC		
Perturbed Cross Section, $\Sigma^x$	$\Delta\Sigma^x$ ( $\text{cm}^{-1}$ )	% $\Delta\Sigma^x$
$\Sigma_{tr_1}$	$-.2124 \times 10^{-2}$	-0.92
$\Sigma_{a_1}$	$-.2429 \times 10^{-3}$	-2.67
$\Sigma_{r_1}$	$-.1977 \times 10^{-3}$	-1.13
$\nu\Sigma_{f_1}$	$-.2771 \times 10^{-4}$	-0.52
$\Sigma_{tr_2}$	$.6340 \times 10^{-3}$	0.08
$\Sigma_{a_2}$	$-.6821 \times 10^{-2}$	-8.29
$\nu\Sigma_{f_2}$	$.1050 \times 10^{-2}$	1.12
EOC		
$\Sigma_{tr_1}$	$-.2176 \times 10^{-2}$	-0.96
$\Sigma_{a_1}$	$-.2762 \times 10^{-3}$	-2.70
$\Sigma_{r_1}$	$-.1056 \times 10^{-3}$	-0.63
$\nu\Sigma_{f_1}$	$-.9956 \times 10^{-4}$	-2.12
$\Sigma_{tr_2}$	$-.5167 \times 10^{-3}$	-0.06
$\Sigma_{a_2}$	$-.9565 \times 10^{-2}$	-10.5
$\nu\Sigma_{f_2}$	$-.3507 \times 10^{-2}$	-3.20

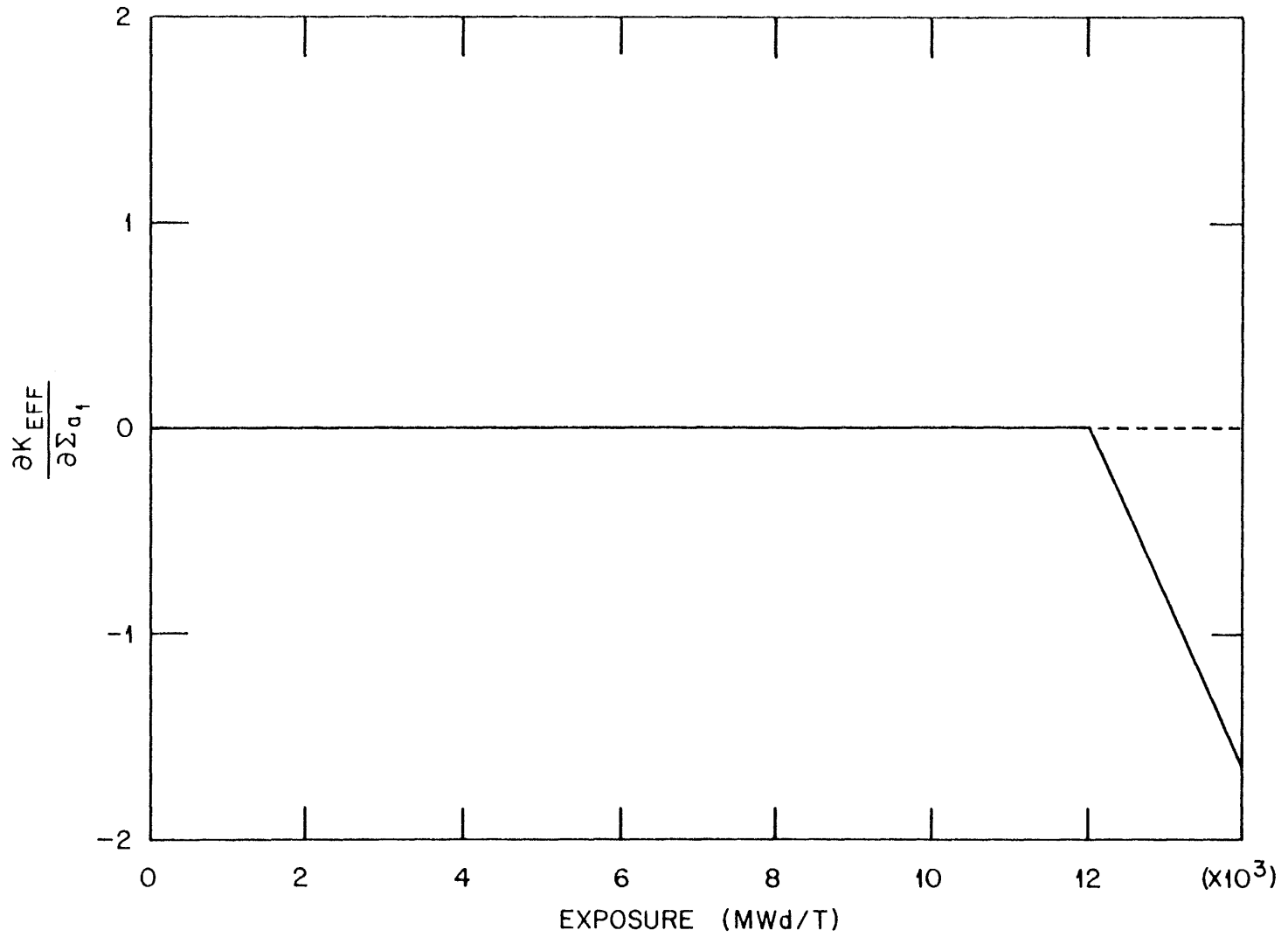


Fig. 4.5.  $\Sigma_{a1}^{-1}$  Sensitivity Coefficient for EOC  $K_{eff}$

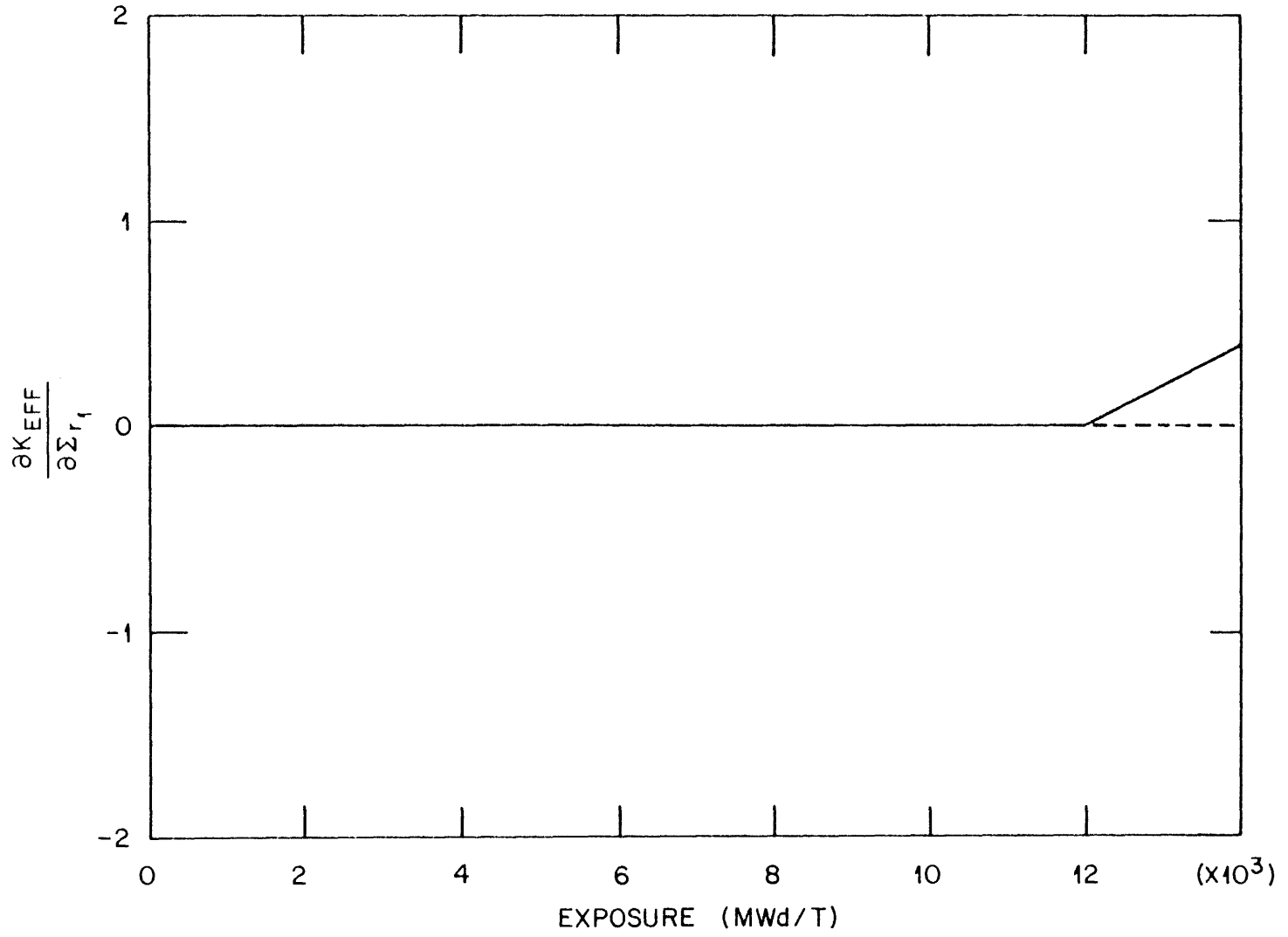


Fig. 4.6.  $\sum_{r_1}$  Sensitivity Coefficient for EOC  $K_{eff}$

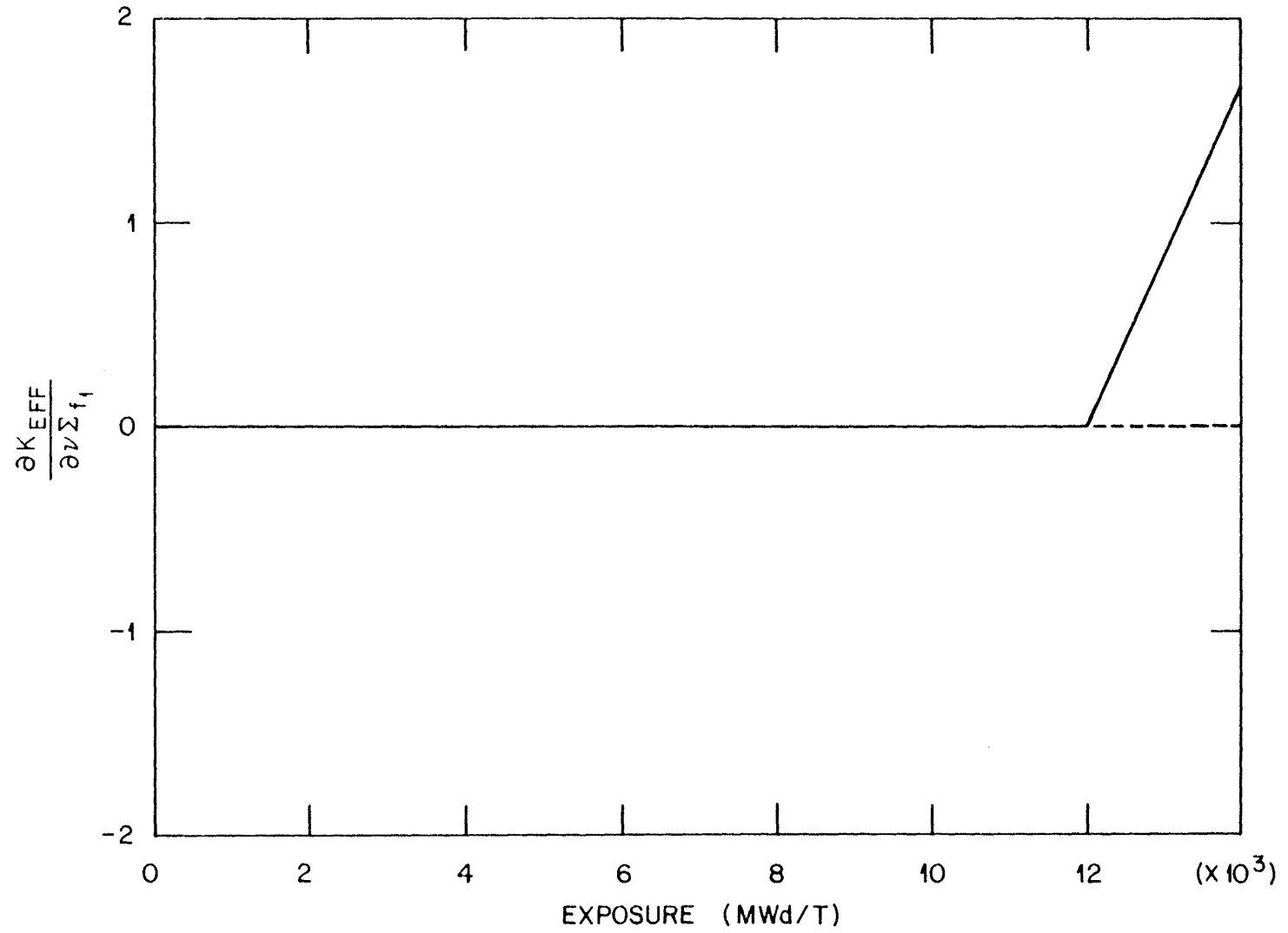


Fig. 4.7.  $\nu \Sigma f_1$  Sensitivity Coefficient for EOC  $K_{eff}$



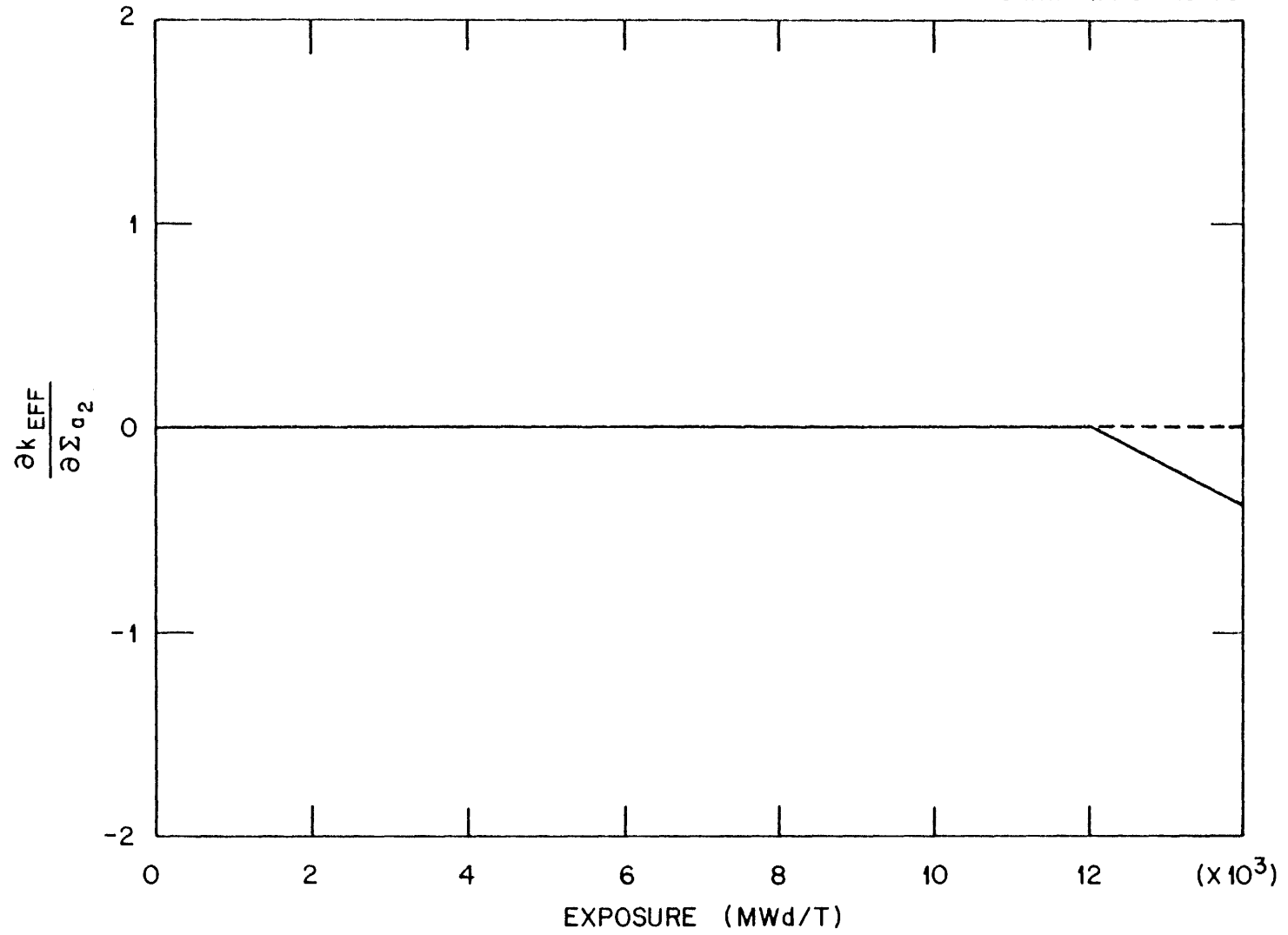


Fig. 4.8.  $\sum_{a2}$  Sensitivity Coefficient for EOC  $K_{eff}$

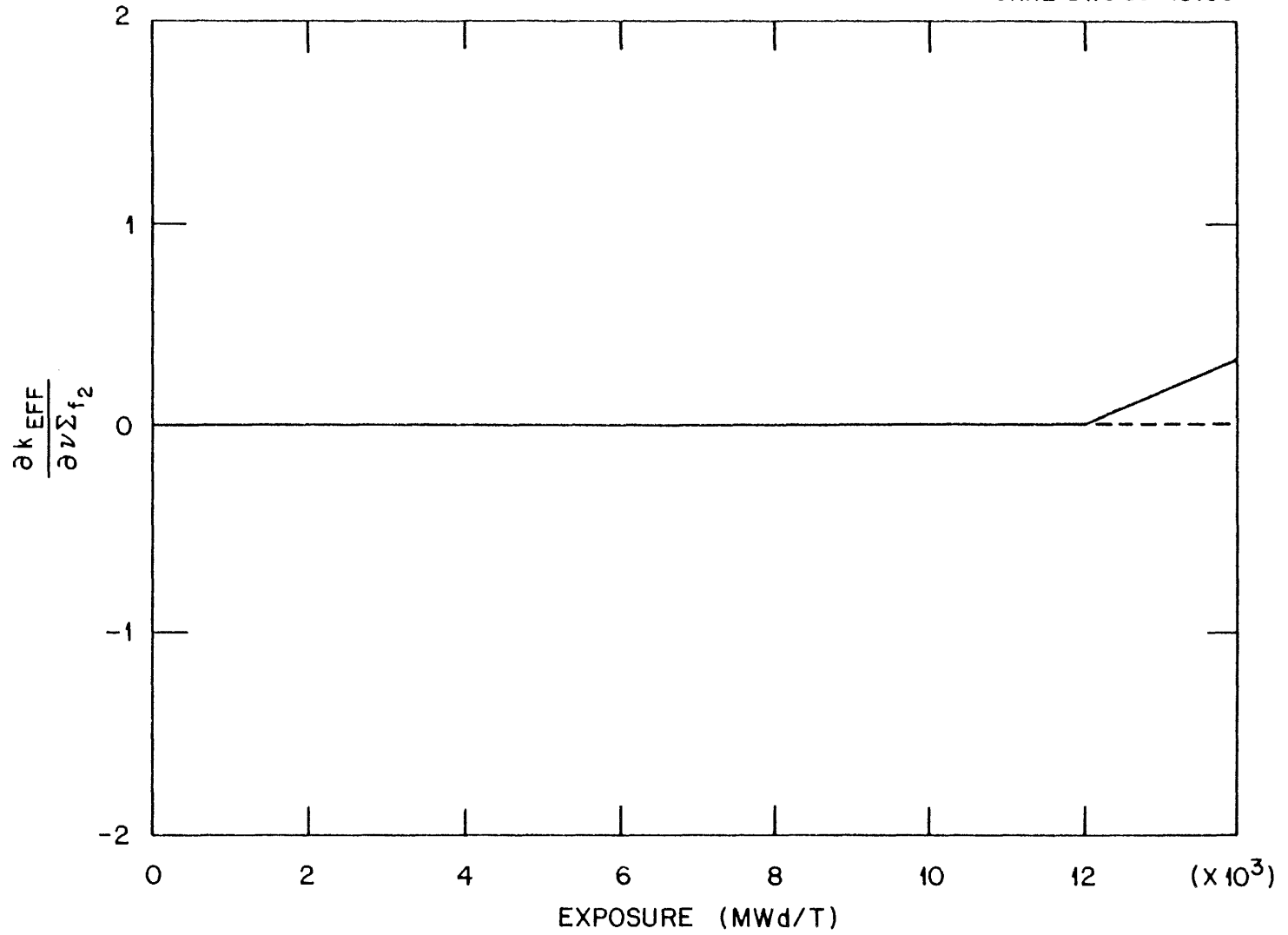


Fig. 4.9.  $\nu \Sigma_{f_2}$  Sensitivity Coefficient for EOC  $K_{eff}$

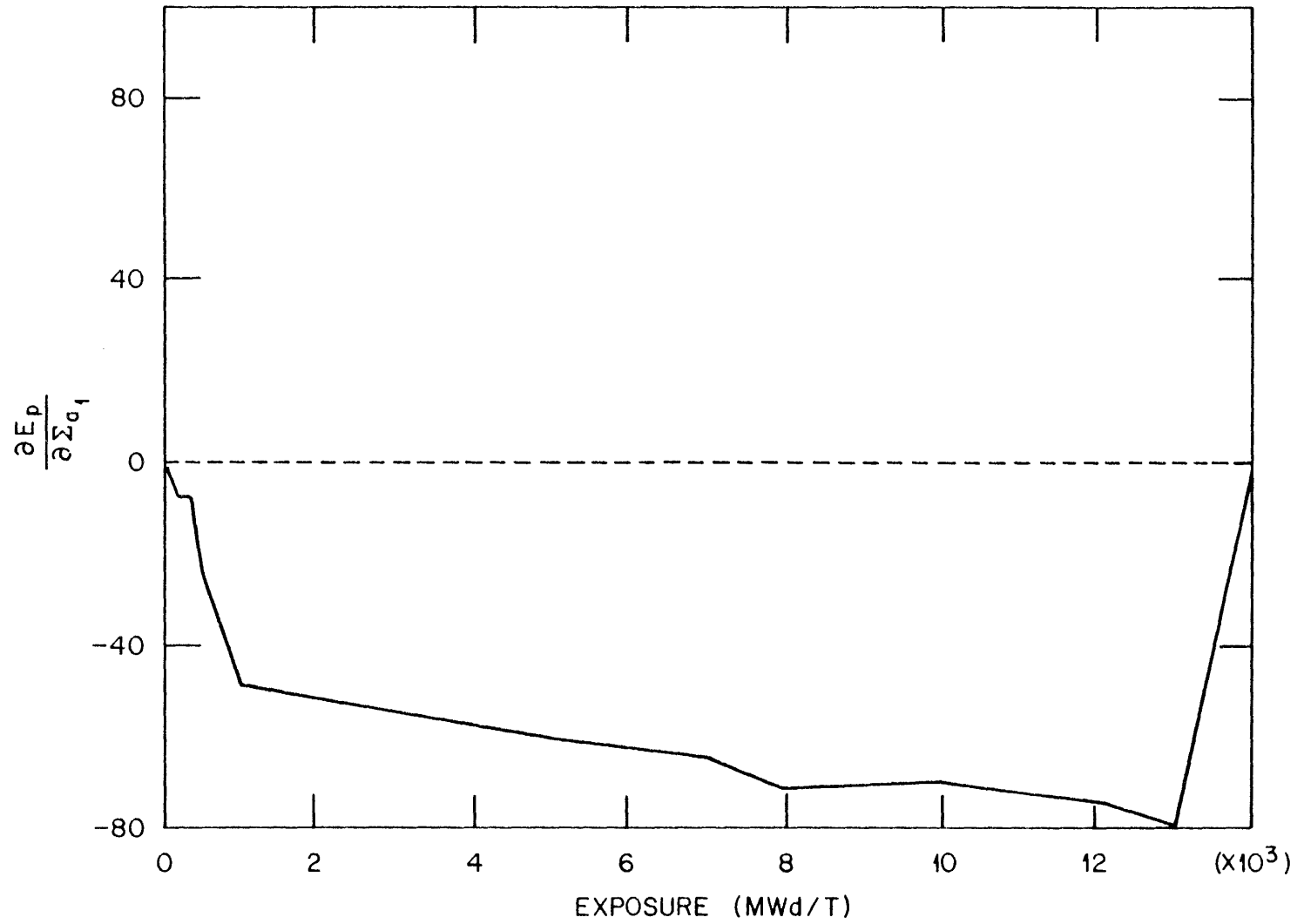


Fig. 4.10.  $\sum_{a_1}$  Sensitivity Coefficient for EOC Peak Exposure

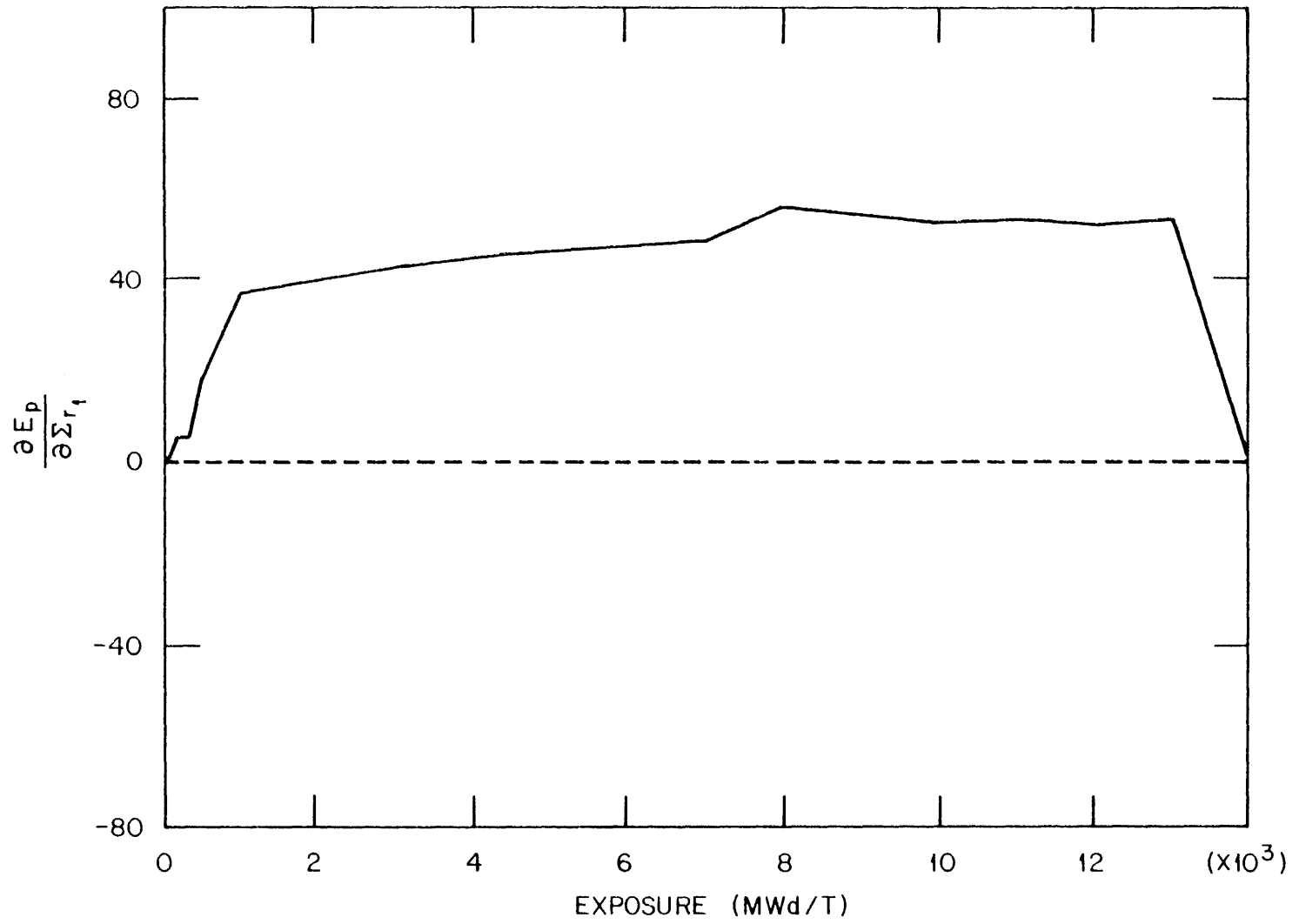


Fig. 4.11.  $\sum r_i$  Sensitivity Coefficient for EOC Peak Exposure

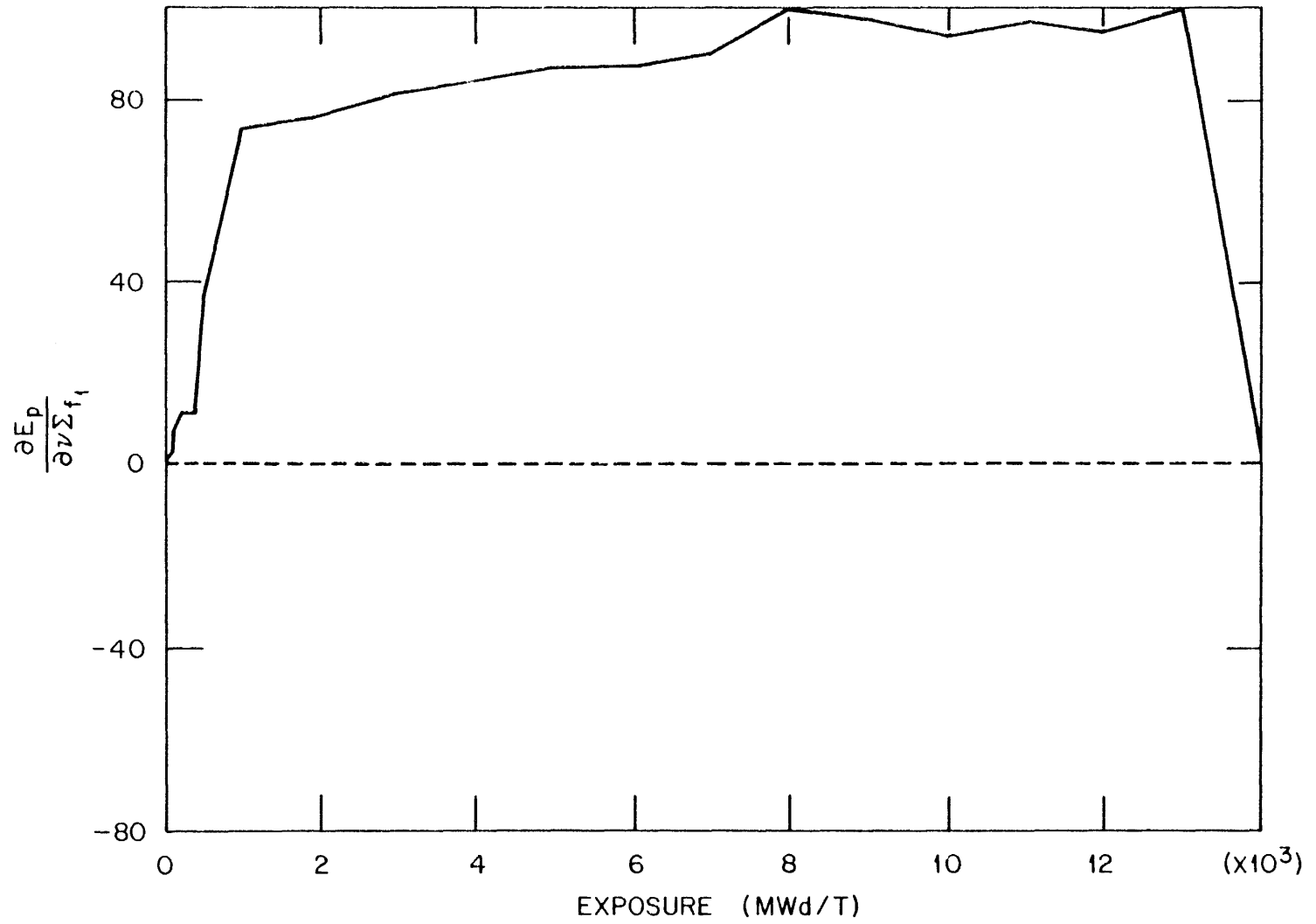


Fig. 4.12.  $\nu \Sigma_{f_1}$  Sensitivity Coefficient for EOC Peak Exposure

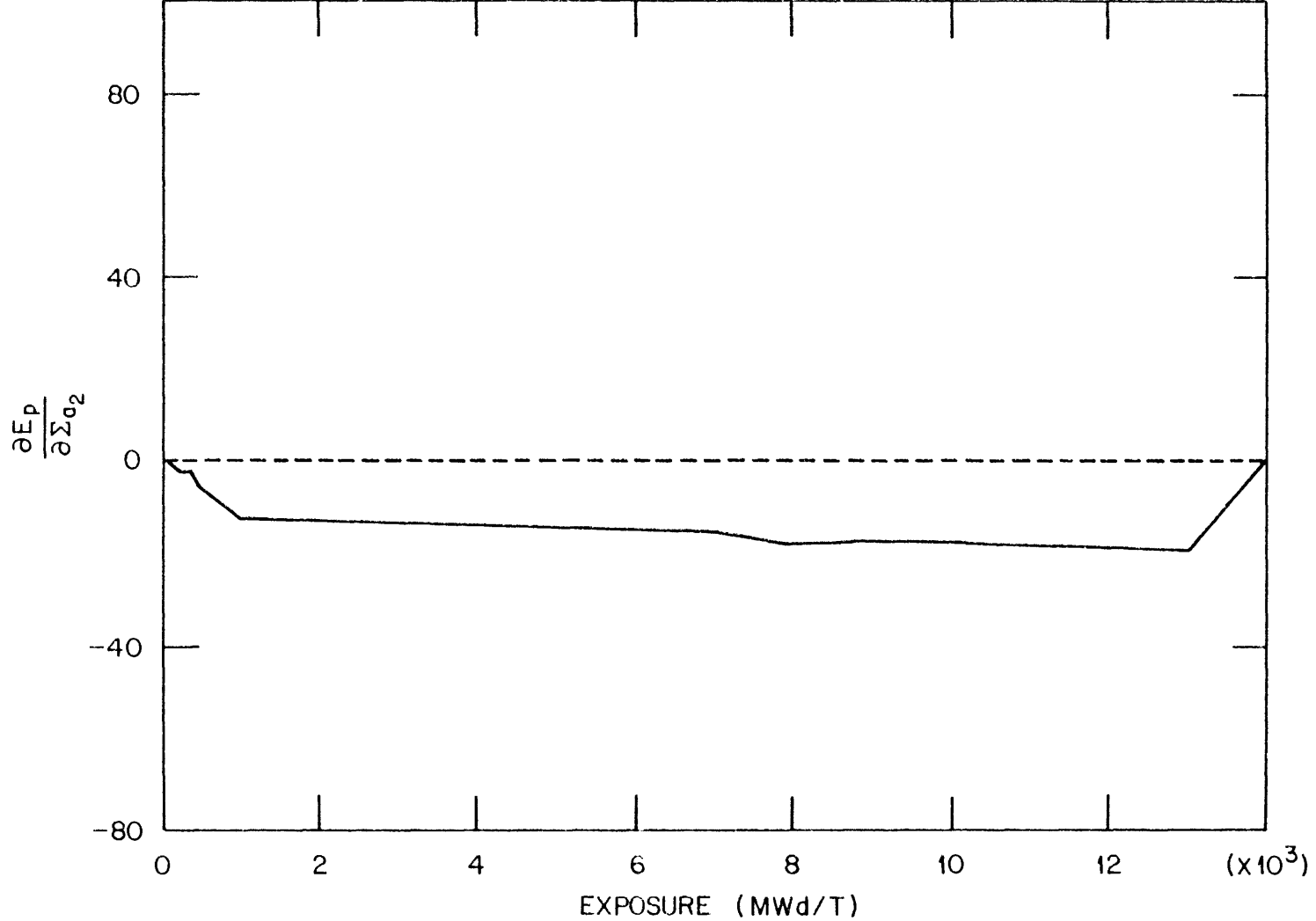


Fig. 4.13.  $\sum a_2$  Sensitivity Coefficient for EOC Peak Exposure

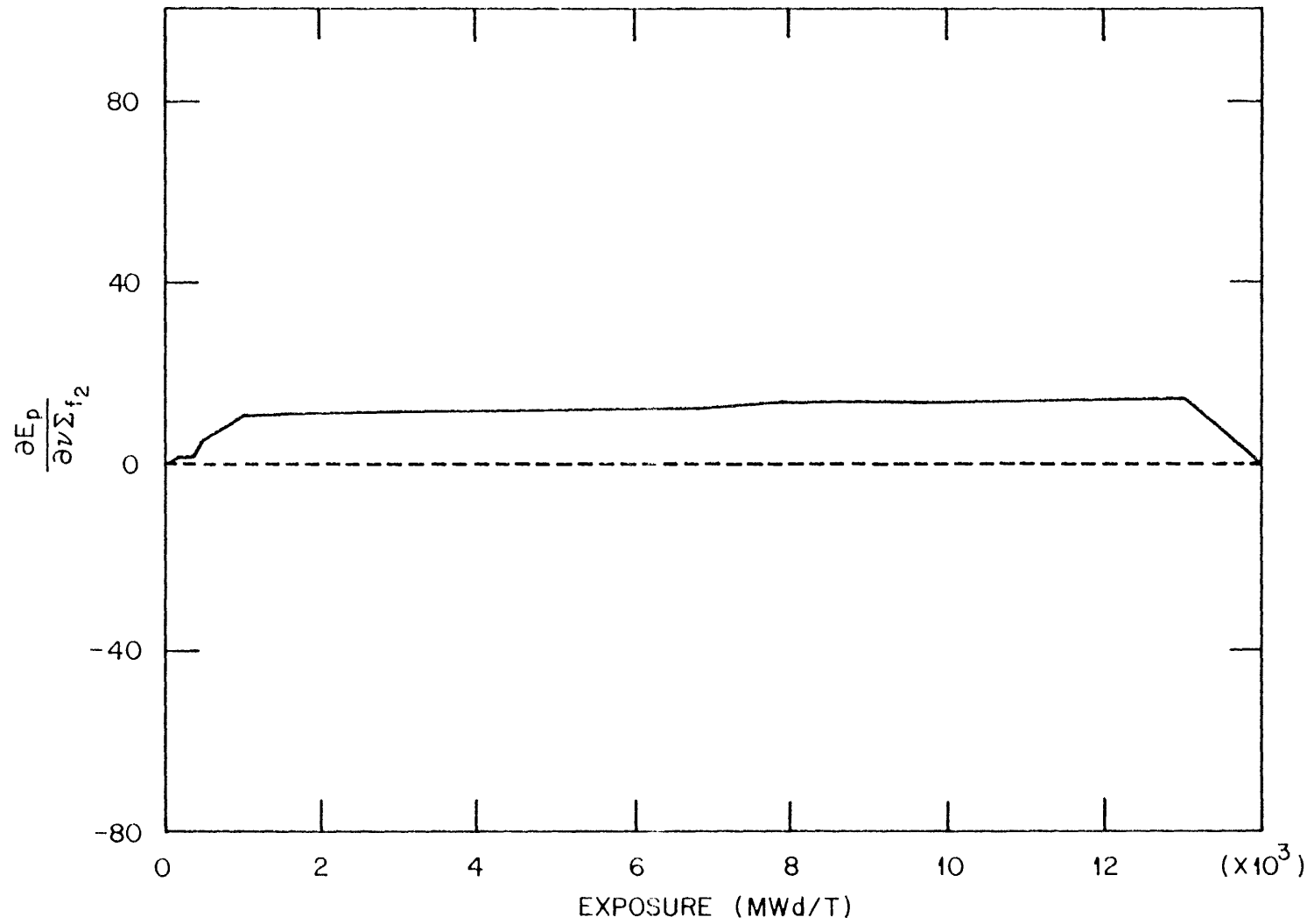


Fig. 4.14.  $\nu \Sigma_{f_2}$  Sensitivity Coefficient for EOC Peak Exposure

(2.06 w/o) in location #13. The results of DPT, SD, and direct calculations are presented in Table 4.19. The Error in the DPT and SD approximations of  $\Delta K/K$  are much larger than for the previous case, due to the larger perturbations of  $\sum a_2$ ,  $v\sum f_1$ , and  $v\sum f_2$ , as shown in Table 4.20. The magnitude of the DPT error is only slightly greater than the SD error, but the errors have opposite signs. Thus, the error due to the Taylor Series approximation of the change in the matrix coupling coefficients is partially offset by the error due to linear perturbation theory.

The error in the DPT and SD approximations of the changes in the EOC peak exposure are also larger for this case because of the much larger cross section perturbations.

Table 4.19. Replacing a High Enrichment Fuel Assembly with a Low Enrichment Fuel Assembly for a Fuel Cycle of 14,000 MWD/T

EOC $K_{eff}$ Response				
$\Delta K/K$			% Error	
(DPT)	(SD)	(Direct)	(DPT)	(SD)
$-.1449 \times 10^{-2}$	$-.2331 \times 10^{-2}$	$-.1913 \times 10^{-2}$	-24.3	21.9

[Reference Value:  $K_{eff} = 0.985176$ ]

EOC Peak Exposure Response				
$\Delta E_p$ (GWD/T)			% Error	
(DPT)	(SD)	(Direct)	(DPT)	(SD)
-1.376	-1.966	-3.009	-54.3	-34.7

[Reference Value:  $E_p = E(1,7,2) = 17.861$  GWD/T]



Table 4.20. Cross Section Perturbations for Replacing  
a High Enrichment Fuel Assembly with a  
Low Enrichment Fuel Assembly

BOC		
Perturbed Cross Section, $\Sigma^x$	$\Delta\Sigma^x$ ( $\text{cm}^{-1}$ )	% $\Delta\Sigma^x$
$\Sigma_{tr_1}$	$-.3372 \times 10^{-2}$	-1.47
$\Sigma_{a_1}$	$-.9257 \times 10^{-3}$	-9.45
$\Sigma_{r_1}$	$.1821 \times 10^{-2}$	11.7
$\nu\Sigma_{f_1}$	$-.1277 \times 10^{-2}$	-19.8
$\Sigma_{tr_2}$	$.2384 \times 10^{-1}$	2.87
$\Sigma_{a_2}$	$-.2582 \times 10^{-1}$	-25.4
$\nu\Sigma_{f_2}$	$-.3538 \times 10^{-1}$	-27.2
EOC		
$\Sigma_{tr_1}$	$-.3311 \times 10^{-2}$	-1.45
$\Sigma_{a_1}$	$-.3756 \times 10^{-3}$	-3.54
$\Sigma_{r_1}$	$.1635 \times 10^{-2}$	11.1
$\nu\Sigma_{f_1}$	$-.1044 \times 10^{-2}$	-19.0
$\Sigma_{tr_2}$	$.2344 \times 10^{-1}$	2.74
$\Sigma_{a_1}$	$-.1870 \times 10^{-1}$	-18.7
$\nu\Sigma_{f_2}$	$-.3611 \times 10^{-1}$	-26.0

Another perturbation made to this depletion fuel cycle calculation is the removal of the lumped burnable poison in fuel assembly #13 at the beginning of the cycle and the insertion of the control rod into that assembly at 8,000 MWD/T for the remainder of the fuel cycle. The DPT results for this case (Table 4.21) are much worse than for the previous burnup-dependent examples. The reason for this can be found in Table 4.22. The cross section perturbations at the BOC, when the LBP is removed, and at 8,000 MWD/T, when the control rod is inserted, are relatively small. However, the thermal absorption cross section perturbation at the EOC, where  $K_{eff}$  is much more sensitive, is 35.8%. Referring to the static perturbation case in Table 4.13, the DPT error for this case is less than the GPT error for a static perturbation of only 17.0% of  $\sum a_2$ . Thus, depletion perturbation theory consistently has less error than generalized perturbation theory for perturbations of equal magnitude.

The error in the semi-direct method is less than half that of the DPT approximation, and is only slightly larger than the SD error in the previous case. If the change in the matrix coupling coefficients could be calculated without performing a direct calculation and without storing the entire matrices in core, the accuracy of the depletion perturbation theory predictions could be greatly improved without a significant increase in computing cost. This would entail writing a code separate from SIMULATE which could calculate the changes in the coupling coefficients without storing the zero elements of the matrices.

Notice that the SD error for the change in the EOC peak exposure is significantly less for this case. As previously stated, the cross

Table 4.21. Removal of LBP at BOC and Insertion of Control Rod at 8,000 MWD/T in Fuel Assembly #22 for a Fuel Cycle of 14,000 MWD/T

EOC $K_{eff}$ Response				
$\Delta K/k$			% Error	
(DPT)	(SD)	(Direct)	(DPT)	(SD)
$-0.6919 \times 10^{-2}$	$-0.5559 \times 10^{-2}$	$-0.4253 \times 10^{-2}$	62.7	30.7
[Reference Value: $K_{eff} = 0.985176$ ]				
EOC Peak Exposure Response				
$\Delta E_p$ (GWD/T)			% Error	
(DPT)	(SD)	(Direct)	(DPT)	(SD)
-2.276	-1.508	-1.351	68.5	11.6
[Reference Value: $E_p = E(1,7,2) = 17.861$ GWD/T]				

perturbations prior to the end of cycle are relatively small. Since the EOC exposure is not affected by the static EOC cross section perturbations, the SD approximation of the change in the EOC peak exposure is very good.

The final perturbation case is a simple 5% perturbation of the first-group fission cross section in fuel assembly #13. The purpose of this case is to demonstrate that the error in the DPT calculation approaches zero for relatively small perturbations. This is similar to the example in Table 4.9, which was performed to show that the error in the GPT calculation approached zero for small perturbations. This example does indeed demonstrate that the error approaches zero for relatively small perturbations, (Table 4.23) when one uses the depletion

Table 4.22. Cross Section Perturbations for  
Removal of LBP at BOC and Insertion of  
Control Rod in Fuel Assembly #22

BOC		
Perturbed Cross Section, $\Sigma$	$\Delta\Sigma^x$ ( $\text{cm}^{-1}$ )	% $\Delta\Sigma^x$
$\Sigma_{tr1}$	$.1283 \times 10^{-2}$	-0.57
$\Sigma_{a1}$	$.3447 \times 10^{-3}$	-3.52
$\Sigma_{r1}$	$.7804 \times 10^{-3}$	4.99
$\nu\Sigma_{f1}$	0.0	0.0
$\Sigma_{tr2}$	$.2640 \times 10^{-1}$	3.18
$\Sigma_{a2}$	$-.8262 \times 10^{-2}$	-8.13
$\nu\Sigma_{f2}$	$.2763 \times 10^{-2}$	2.15
8,000 MWD/T		
$\Sigma_{tr1}$	$-.1145 \times 10^{-2}$	-0.50
$\Sigma_{a1}$	$-.8742 \times 10^{-3}$	-8.48
$\Sigma_{r1}$	$.1455 \times 10^{-2}$	9.70
$\nu\Sigma_{f1}$	$.5356 \times 10^{-3}$	9.08
$\Sigma_{tr2}$	$.5690 \times 10^{-2}$	0.67
$\Sigma_{a2}$	$-.7870 \times 10^{-2}$	-7.35
$\nu\Sigma_{f2}$	$-.1026 \times 10^{-1}$	-7.12

Table 4.22 (Continued)

Perturbed Cross Section, $\Sigma$	EOC	
	$\Delta\Sigma^x$ ( $\text{cm}^{-1}$ )	% $\Delta\Sigma^x$
$\Sigma_{tr_1}$	$.4393 \times 10^{-2}$	1.93
$\Sigma_{a_1}$	$.1030 \times 10^{-2}$	9.71
$\Sigma_{r_1}$	$.1835 \times 10^{-3}$	1.24
$\nu\Sigma_{f_1}$	$.2772 \times 10^{-3}$	5.05
$\Sigma_{tr_2}$	$.9659 \times 10^{-2}$	1.13
$\Sigma_{a_2}$	$.3574 \times 10^{-1}$	35.8
$\nu\Sigma_{f_2}$	$.8532 \times 10^{-2}$	6.13

equations which have been implemented into SIMULATE. The error in the EOC peak exposure is greater than the error for  $\Delta K/K$ , since the perturbation does occur in a different fuel assembly. However, the error in this case is significantly smaller than for the previous cases, thus demonstrating that the error tends toward zero as the size of the perturbation decreases.

Plots of the fission source density,  $\underline{S}$ , at the beginning and the end of the fuel cycle are shown in Figs. 4.15 and 4.16, respectively. Similar plots of the adjoint function  $\underline{S}^*$  are given in Figs. 4.17 and 4.18. Plots of the generalized adjoint function  $\underline{\Gamma}^*$  for the  $K_{eff}$  response are presented for the beginning of cycle and the next-to-last exposure step in Figs. 4.19 and 4.20, respectively. Recall that for the

Table 4.23. 5% Perturbation of  $\nu\Sigma_{f1}$  for a Fuel Cycle of 14,000 MWD/T

$\Delta K/K$		$\frac{\% \text{ Error}}{\text{(DPT)}}$
(DPT)	(Direct)	
$0.3972 \times 10^{-3}$	$0.3999 \times 10^{-3}$	-0.68

[Reference Value:  $K_{\text{eff}} = 0.985176$ ]

EOC Peak Exposure Response		
$\Delta E_p$ (GWD/T)		$\frac{\% \text{ Error}}{\text{(DPT)}}$
(DPT)	(Direct)	
-0.044	-0.053	-17.0

[Reference Value:  $E_p = E(1,7,2) = 17.861$  GWD/T]

final exposure step  $\underline{I}^*$  is equal to  $\underline{S}^*$  for the  $K_{\text{eff}}$  response. Each figure is a graph of the 2-D function at the axial center of the reactor for that particular case.

The fission source density  $\underline{S}$  and the adjoint function  $\underline{S}^*$  have generally similar shapes, both at the BOC and at the EOC, indicating a tendency of  $\underline{S}$  and  $\underline{S}^*$  to be self-adjoint. The adjoint function, however, does tend to peak nearer the center of the reactor than the fission source density at the BOC. Both the adjoint function and the fission source density are less in magnitude at the reactor axial center at the EOC. This occurs because both distributions are much flatter in the axial direction, due to the increased burnup at the axial center caused by the peak there in the fission source density throughout most of the cycle. The fission source density and the adjoint function are both

ORNL-DWG 80-18186

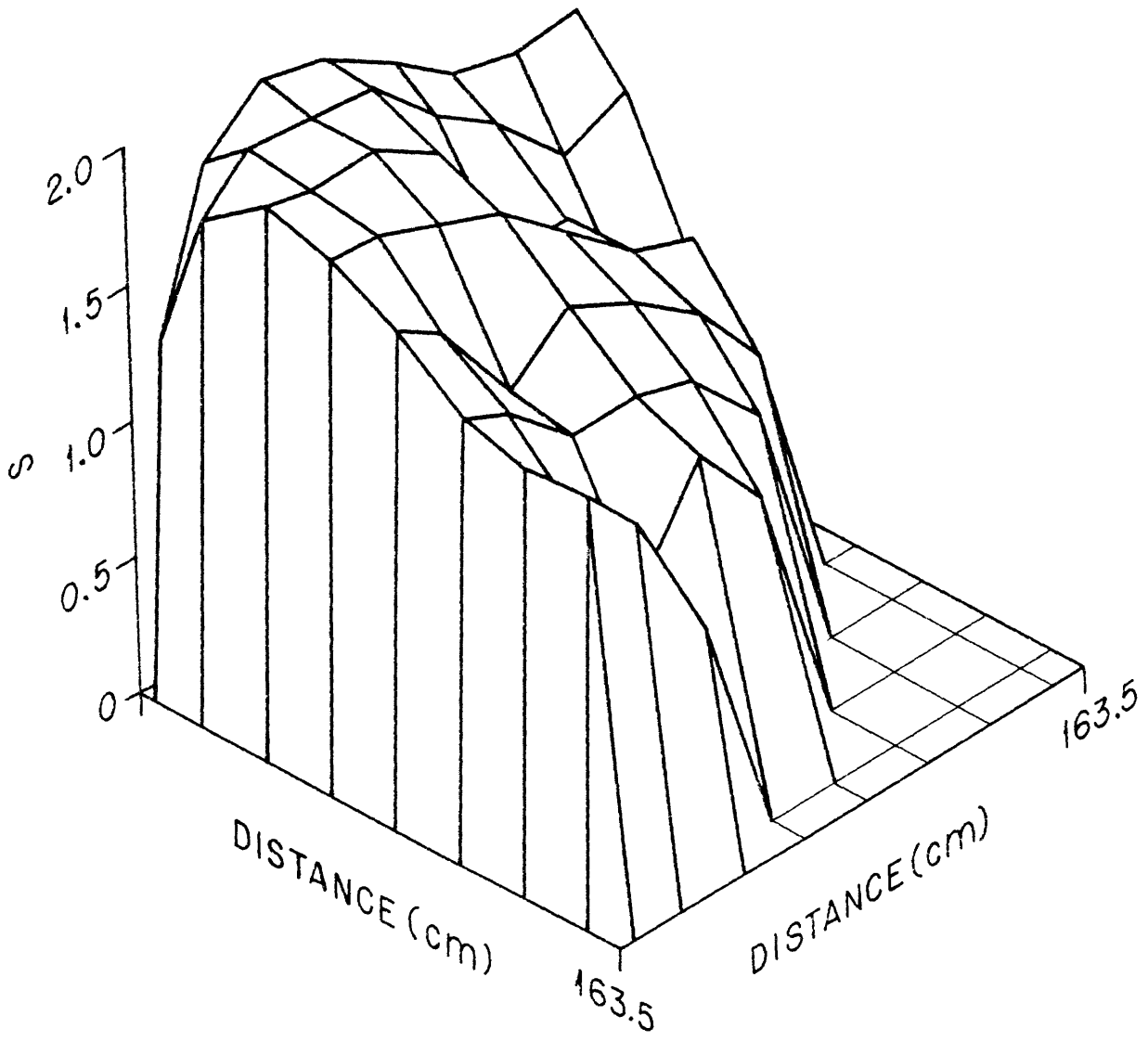


Fig. 4.15. BOC Fission Source Density

ORNL-DWG 80-18187

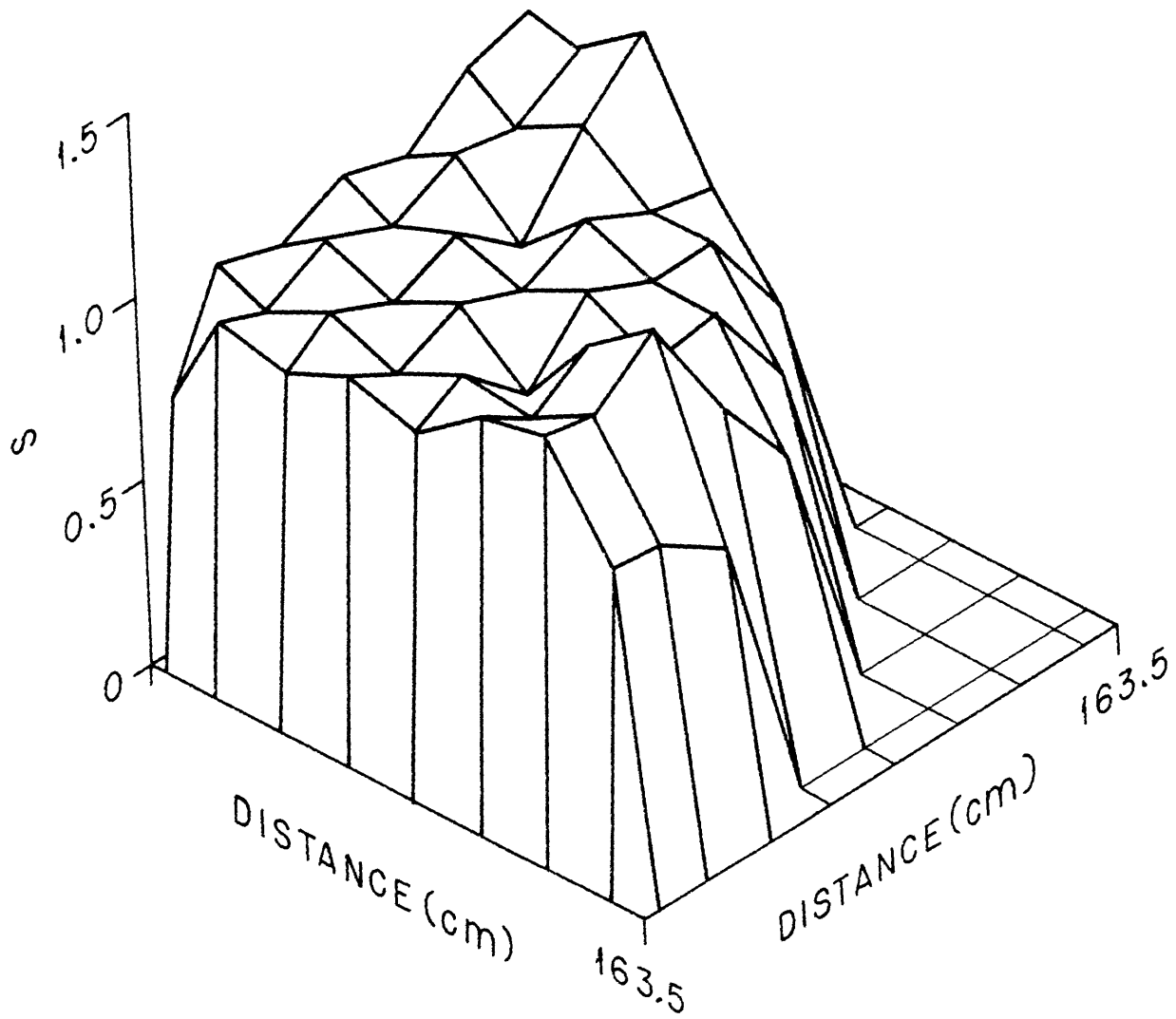


Fig. 4.16. EOC Fission Source Density



ORNL-DWG 80-18188

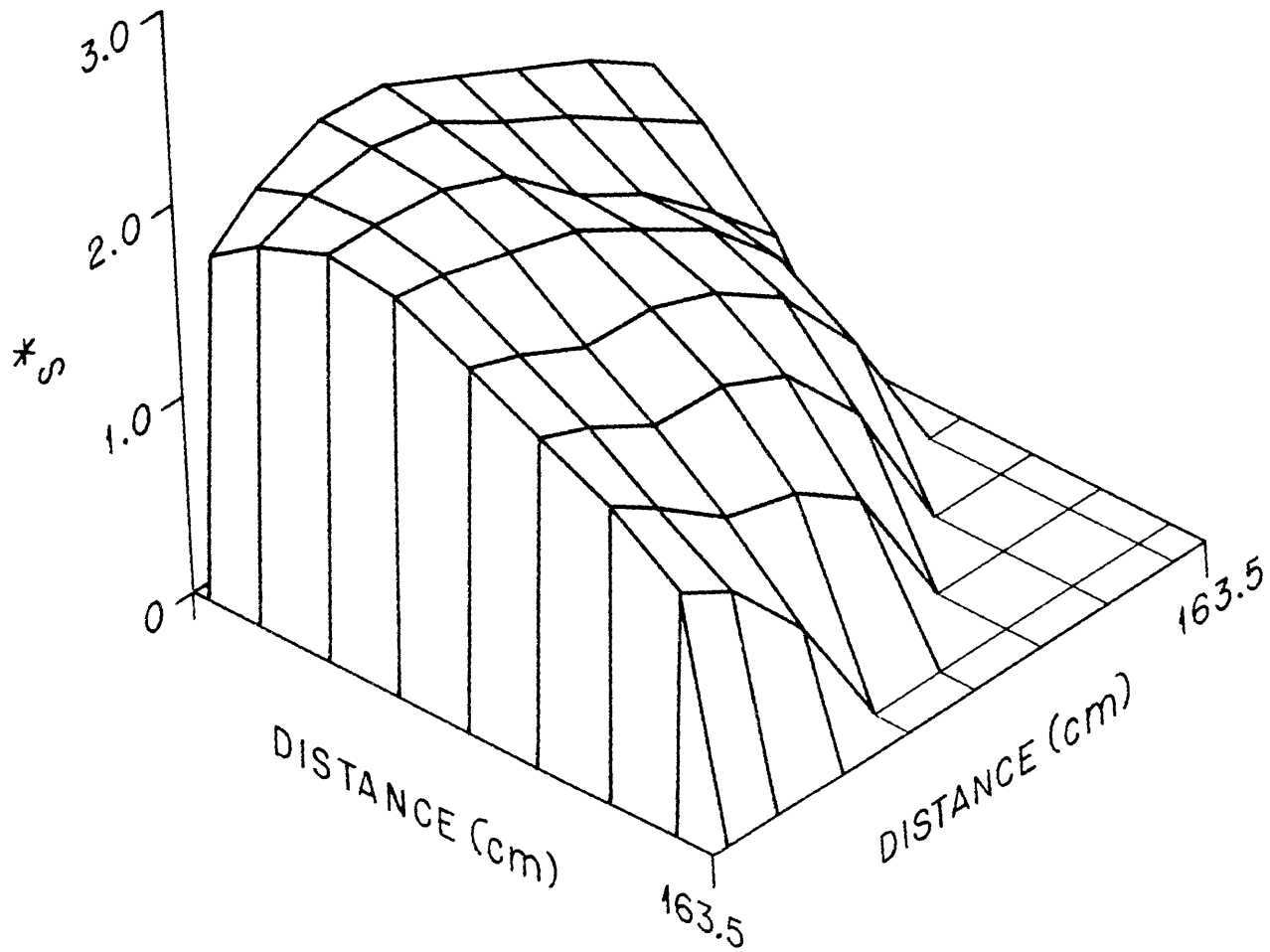


Fig. 4.17. BOC Adjoint Function

ORNL-DWG 80-18189

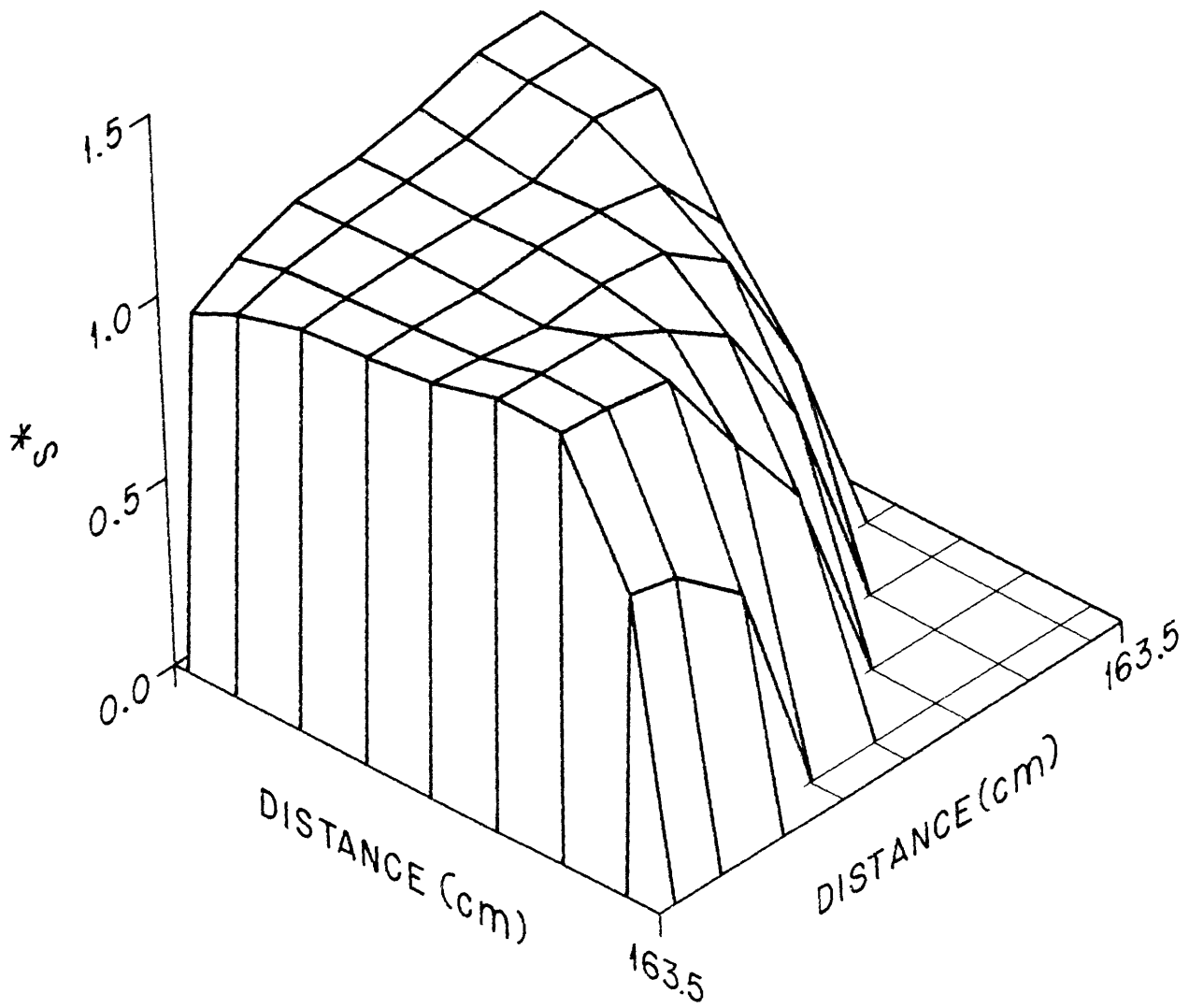


Fig. 4.18. EOC Adjoint Function

ORNL-DWG 80-18190

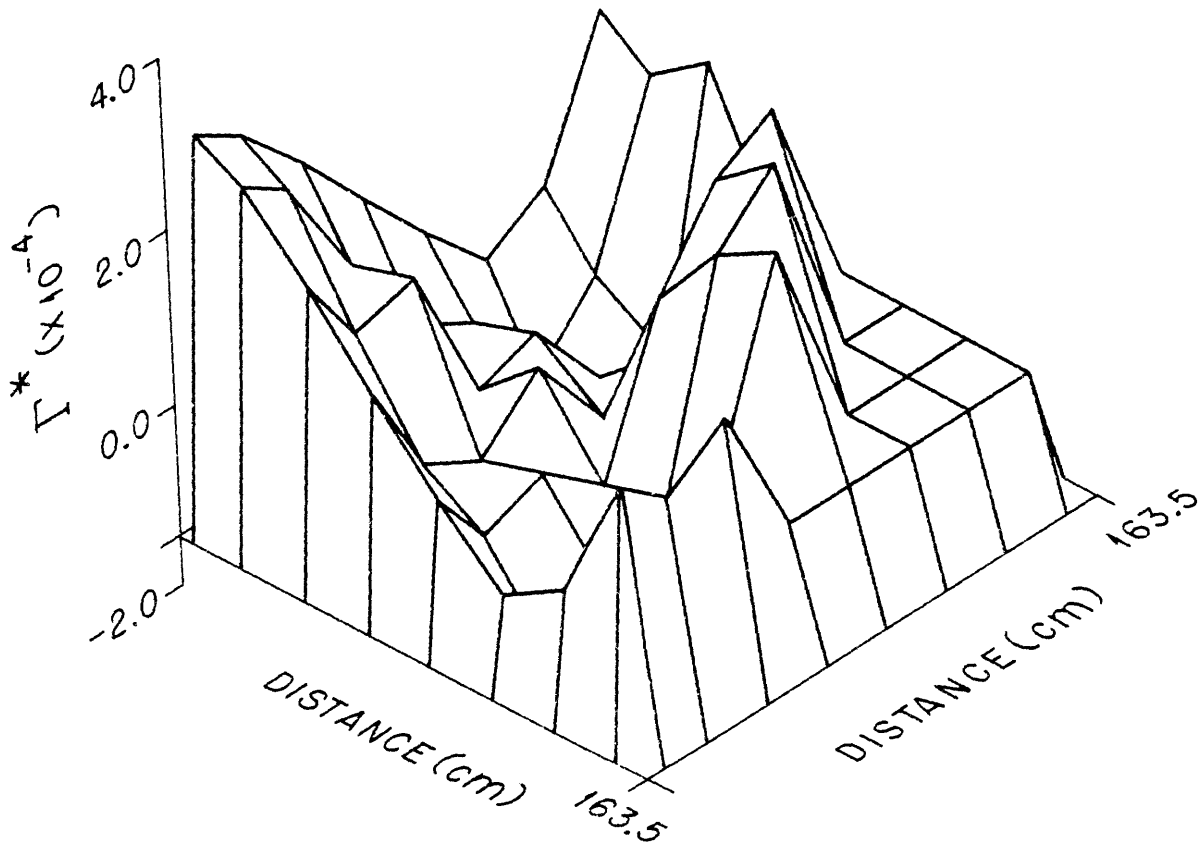


Fig. 4.19. BOC Generalized Adjoint Function

ORNL-DWG 80-18191

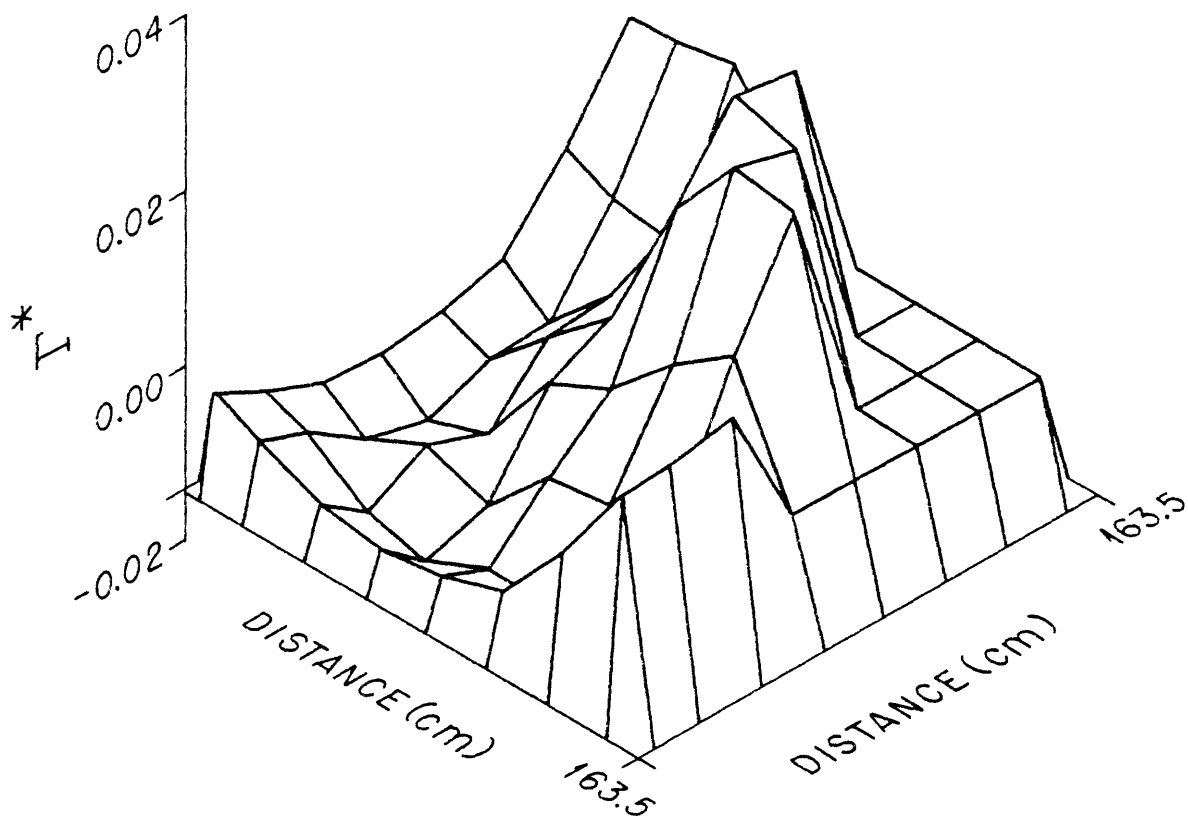


Fig. 4.20. Generalized Adjoint Function at Exposure Step ( $l-1$ )

flatter in the radial direction at the EOC, and the peaks are nearer the core periphery, as one may observe in Figs. 4.16 and 4.18, respectively. Thus, through the course of the fuel cycle, the fission source density and the adjoint function tend to become more evenly distributed throughout the core as a result of the increased burnup of the more reactive regions.

The BOC adjoint function  $\underline{S}^*$  represents the neutron importance to BOC  $K_{eff}$ . Neutrons near the core center at the beginning of cycle are more important to BOC  $K_{eff}$ , as one would expect. The dips in  $\underline{S}$  and  $\underline{S}^*$  at the center of the core are due to the control rod which is inserted there. The EOC adjoint function  $\underline{S}^*$  represents the neutron importance to EOC  $K_{eff}$ . Because of the fuel depletion near the core center at the end of cycle, the neutrons in the highly enriched fuel assemblies along the edge of the core are more important to EOC  $K_{eff}$ .

The generalized adjoint function  $\underline{I}^*$  is quite different in character since it assumes positive and negative values and is not normalized. The BOC distribution has its greatest values at the center of the core and in the high enrichment assemblies on the core periphery. Adding neutrons in these regions would increase EOC  $K_{eff}$ , while adding neutrons in the areas where  $\underline{I}^*$  is negative would decrease EOC  $K_{eff}$ . At the next-to-last exposure step, the distribution has its greatest values along the edge of the core and its least values near the core center. As the end of the fuel cycle is approached, adding neutrons to the high enrichment assemblies along the periphery of the core will increase EOC  $K_{eff}$ . However, adding neutrons near the center of the core would shift the

distribution of the fission source density away from the more reactive region near the edge, and would reduce EOC  $K_{\text{eff}}$ . Note the similarity in shape of this  $\underline{I}^*$  distribution and the EOC  $\underline{S}^*$  distribution (Fig. 4.18). This is expected, since  $\underline{I}^*$  is equal to  $\underline{S}^*$  at the end of cycle for the EOC  $K_{\text{eff}}$  response.

The generalized adjoint function is much less at the beginning of cycle than at the next-to-last exposure step, because the importance of the fission source density to EOC  $K_{\text{eff}}$  decreases as one goes backward in time. The boundary conditions for the fixed source adjoint calculations were identical to those for the forward calculations.

The example problems examined in this section show that depletion perturbation theory has been successfully implemented into SIMULATE. These problems also indicate that the use of depletion perturbation theory in LWR design analysis is restricted for some problems. Its validity is limited for problems involving large localized perturbations (e.g. in one fuel assembly). Such perturbations generally affect the fission source density only in a small region surrounding the location of the perturbation, and thus alter the shape of the overall fission source distribution in the vicinity of the perturbation. Depletion perturbation theory accounts only for the first order changes in the fission source distribution. Thus, the theory is only valid for perturbations which alter the fission source distribution in an approximately linear manner.

## V. SUMMARY

The goals of this work have been to develop a depletion perturbation theory formulation for a LWR nodal code, to implement this formulation into the code in a manner consistent with the solution of the forward nodal equations, and to evaluate the accuracy of depletion perturbation theory in LWR design analysis. These objectives have been achieved, but there remains a considerable amount of research which needs to be performed in the application of depletion perturbation theory to light water reactors. This section will summarize the conclusions of this work, and makes recommendations for future research.

### Conclusions

The depletion adjoint equations developed in Section II have been successfully implemented into the 3-D LWR nodal code SIMULATE. The solution of these equations by SIMULATE yields sensitivity coefficients which are space and time-dependent. These can be used to account for variations in the neutron and nuclide fields caused by perturbations in the initial reactor design at BOC in predicting responses at EOC.

A wide variety of numerical calculations have been performed to verify the accuracy of the coding added to SIMULATE, and to evaluate the applicability of depletion perturbation theory to LWR design calculations. The test cases studied varied from simple static problems to a realistic PWR model for an entire fuel cycle. The results of these calculations reveal that depletion perturbation theory is accurate for only small perturbations. In some cases, it may give very accurate

results. For example, the change in EOC  $K_{\text{eff}}$  due to the removal of a part length control rod at BOC was estimated with an error of only 1.05%. However, perturbations of greater than 10% to either  $\sum a_2$  or  $\nu \sum f_2$  generally seem to give poor results when one uses DPT. This restricts the types of LWR design changes which can be considered with DPT. In particular, some perturbations involving the movement of a full-length control rod or the swapping of a high enrichment and a low enrichment fuel assembly can be expected to produce an error of greater than 20% in the DPT approximation of the response change.

An important aspect of the depletion perturbation theory calculations is the comparative costs. The computational time required for the solution of the forward and backward marches through time for a specific response is approximately six times the amount required for a conventional series of forward calculations. Perturbation theory is desirable for studying the effects of many different design variations on only a few responses. Conversely, if the effects of only a few design changes on a large number of responses are desired, using direct calculations would be more practical (i.e., less costly).

Perturbation theory can also be useful for gaining insight into the physical phenomena which are associated with a given response. The sensitivity coefficients which are obtained from depletion perturbation theory can provide a better understanding of the neutronic behavior in LWR's, and could lead to improved core design and optimization techniques.



## Recommendations

It must be emphasized that a considerable amount of uncertainty remains about the applicability of depletion perturbation theory to LWR design calculations. These questions can only be answered by further research, especially in areas which could improve the accuracy of depletion perturbation theory.

One item which would improve the DPT accuracy in SIMULATE is the development of a separate code which could calculate the cross sections for perturbed cases using the reference case exposure distribution. This code should also calculate the changes in the matrix coupling coefficients for each perturbed case without storing the entire matrices in the computer. This would eliminate the first order Taylor Series approximation for the change in the nodal coupling coefficients, and should significantly increase the accuracy of the DPT formulation.

Another possible improvement in the DPT accuracy might be obtained by further modifying SIMULATE to solve for higher order eigenfunctions. The fission source density and the adjoint function are the fundamental eigenfunctions of their respective eigenvalue equations. By sweeping out the fundamental eigenfunction during the numerical solution of the forward and adjoint eigenvalue equations, it should be possible to solve for higher order eigenfunctions. These higher order eigenfunctions should improve the depletion perturbation theory results.<sup>10</sup> However, the gain in accuracy may not be worth the increased computational costs.

Further research is also needed to develop the appropriate adjoint equations for the thermal-hydraulic section of SIMULATE. Extending depletion perturbation theory to account for thermal-hydraulic feedback

would add some versatility to the DPT capability of SIMULATE. Analysis of boiling water reactors (BWR's) with the DPT options in SIMULATE also needs to be investigated.

If the DPT accuracy could be improved significantly by implementing the previous suggestions, then the DPT capability in SIMULATE should be extended to handle multicycle cases. This would involve accounting for fuel shuffling, removal, and loading between fuel cycles.<sup>11</sup>

Finally, the greatest potential which DPT possesses is the possibility of design optimization. For example, the optimum fuel loading pattern for a given LWR core design could be determined, given the allowable changes in fuel enrichments, control rod positions, and burnable poison concentrations. The development of such an optimization program which would use the DPT sensitivity coefficients and a set of constraints to determine an optimum design could be a very powerful tool in core design and fuel management analyses of light water reactors.

## LIST OF REFERENCES

## LIST OF REFERENCES

1. M. L. Williams, "Development of Depletion Perturbation Theory for Coupled Neutron/Nuclide Fields," *Nucl. Sci. Eng.*, 70, 20 (1979).
2. D. M. Ver Planck, "Manual for the Reactor Analysis Program SIMULATE," EPRI Report for RP710-2, 1978.
3. J. J. Duderstadt and L. J. Hamilton, *Nuclear Reactor Analysis*, John Wiley and Sons, Inc., New York, 1976.
4. D. L. Delp et al., "FLARE, A Three-Dimensional Boiling Water Reactor Simulator," GEAP-4598, General Electric Company (1964).
5. Z. M. Khalid, M. Becker, and D. R. Harris, "Influence of Axial Node Size on Modified Coarse-Mesh Nodal Methods," *Trans. Am. Nucl. Soc.*, 34, 827 (1980).
6. W. M. Stacey, *Variational Methods in Nuclear Reactor Physics*, Academic Press, New York, 1974.
7. R. L. Childs, "Generalized Perturbation Theory Using Two-Dimensional, Discrete Ordinates Transport Theory," ORNL/CSD-TM-127 (June 1980).
8. A. Ancona, M. Becker, M. D. Beg, D. R. Harris, A. DaC. Manzes, D. M. Ver Planck and E. Pilat, "Nodal Coupling by Response Matrix Principles," *Nucl. Sci. Eng.*, 64, 405-417 (1977).
9. Samuel H. Levine, personal communication, October 26, 1979.
10. A. Gandini, "Generalized Perturbation Theory for Non-Linear Systems from the Importance Conservation Principle," Comitato Nazionale Per L'Energia Nucleare (1980).
11. J. R. White, "The Development, Implementation, and Verification of Multicycle Depletion Perturbation Theory for Reactor Burnup Analysis," ORNL/TM-7305 (August 1980).
12. M. L. Williams and S. M. Bowman, "Development of the Depletion Adjoint Equations for SIMULATE," to be published, Oak Ridge National Laboratory.
13. L. A. Hageman, "The Estimation of Acceleration Parameters for the Chebyshev Polynomial and the Successive Overrelaxation Iteration Methods," WARD-TM-1038, Atomic Energy Commission (June 1972).

## APPENDICES

## APPENDIX A. ADJOINT MATRIX OPERATORS

The purpose of this appendix is to show how the adjoint matrix operators  $\underline{\underline{M}}^*$  and  $\underline{\underline{F}}^*$  for the eigenvalue equation solved by SIMULATE are determined, and why they are not necessarily identical to the transpose of the matrix operators.

Usually the adjoint of a matrix operator [e.g.,  $\underline{\underline{M}}^*$  or  $\underline{\underline{F}}^*$  in Eq. (2.13)] is simply the transpose of a matrix operator. This is not always the case in SIMULATE. Let us examine two simple problems to understand this.

Figures A.1 and A.2 show two simple reactor configurations. Both are quarter core symmetric, but the configuration in Fig. A.1 contains half nodes on the boundary while the other contains full nodes. The matrix of nodal coupling coefficients can be separated into two matrices, one containing the boundary coupling coefficients and the other containing the internal coupling coefficients

$$\underline{\underline{M}} = \underline{\underline{C}} + \underline{\underline{B}}, \quad (\text{A.1})$$

where

$\underline{\underline{C}}$  = internal coupling coefficients

$\underline{\underline{B}}$  = boundary coupling coefficients.

For both configurations discussed above

$$\underline{\underline{C}}_1 = \underline{\underline{C}}_2 = \begin{bmatrix} m_{1 \leftarrow 1} & m_{1 \leftarrow 2} & m_{1 \leftarrow 3} & 0 \\ m_{2 \leftarrow 1} & m_{2 \leftarrow 2} & 0 & m_{2 \leftarrow 4} \\ m_{3 \leftarrow 1} & 0 & m_{3 \leftarrow 3} & m_{3 \leftarrow 4} \\ 0 & m_{4 \leftarrow 2} & m_{4 \leftarrow 3} & m_{4 \leftarrow 4} \end{bmatrix} \quad (\text{A.2})$$

ORNL-DWG 80-18192

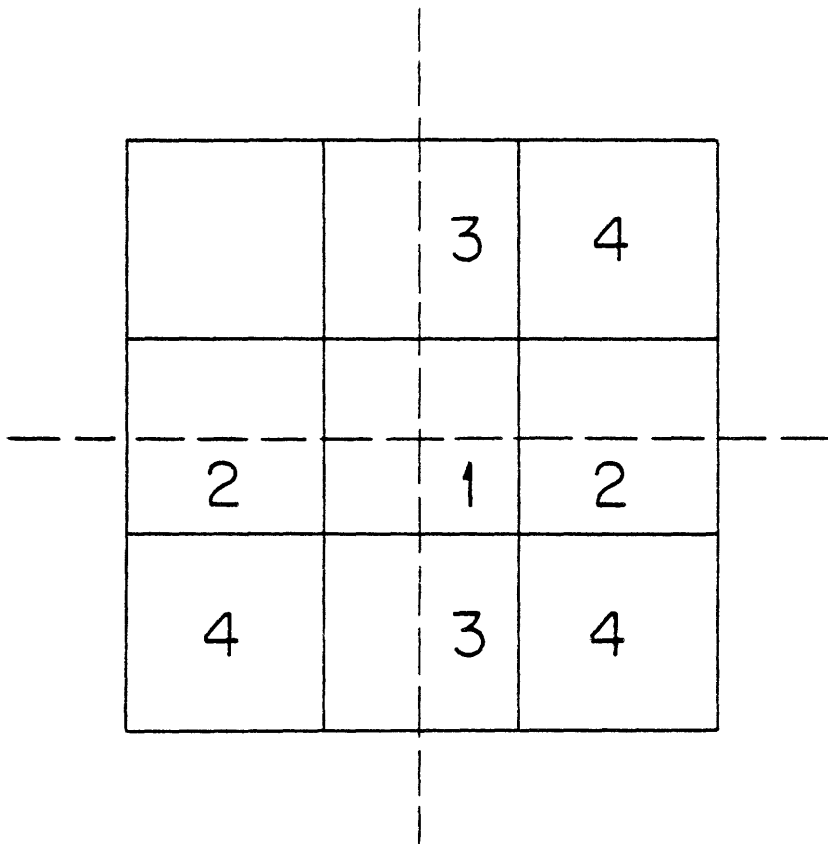


Fig. A.1. Half Nodes on Boundary



ORNL-DWG 80-18193

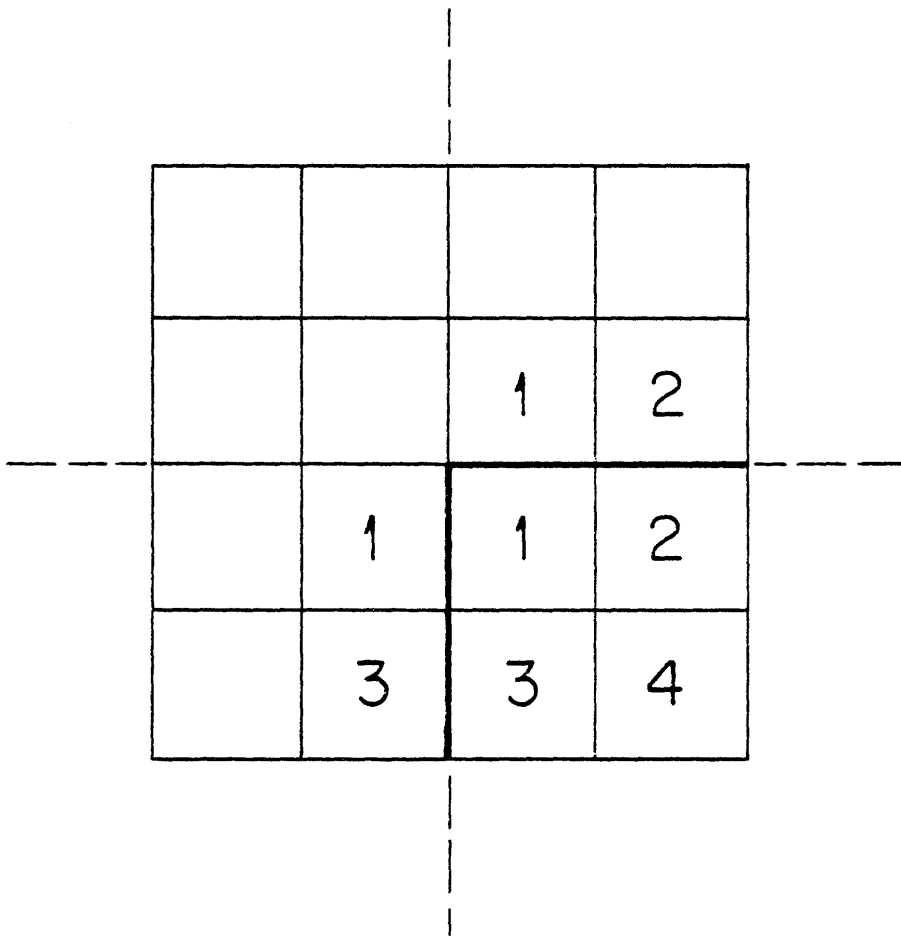


Fig. A.2. Full Nodes on Boundary

The boundary terms for Fig. A.1 are

$$\underline{\underline{B}}_1 = \begin{bmatrix} 0 & m_{1\leftarrow 2} & m_{1\leftarrow 3} & 0 \\ 0 & 0 & 0 & m_{2\leftarrow 4} \\ 0 & 0 & 0 & m_{3\leftarrow 4} \\ 0 & 0 & 0 & 0 \end{bmatrix} \quad (\text{A.3})$$

and for Fig. A.2 are

$$\underline{\underline{B}}_2 = \begin{bmatrix} 2m_{1\leftarrow 1} & 0 & 0 & 0 \\ 0 & m_{2\leftarrow 2} & 0 & 0 \\ 0 & 0 & m_{3\leftarrow 3} & 0 \\ 0 & 0 & 0 & 0 \end{bmatrix} \quad (\text{A.4})$$

The adjoint of the matrix operator is obtained by simply reversing the coupling. Thus,

$$\underline{\underline{C}}_1^* = \underline{\underline{C}}_2^* = \begin{bmatrix} m_{1\leftarrow 1} & m_{2\leftarrow 1} & m_{3\leftarrow 1} & 0 \\ m_{1\leftarrow 2} & m_{2\leftarrow 2} & 0 & m_{4\leftarrow 2} \\ m_{1\leftarrow 3} & 0 & m_{3\leftarrow 3} & m_{4\leftarrow 3} \\ 0 & m_{2\leftarrow 4} & m_{4\leftarrow 3} & m_{4\leftarrow 4} \end{bmatrix} = \underline{\underline{C}}^T \quad (\text{A.5})$$

$$\underline{\underline{B}}_1^* = \begin{bmatrix} 0 & m_{2\leftarrow 1} & m_{3\leftarrow 1} & 0 \\ 0 & 0 & 0 & m_{4\leftarrow 2} \\ 0 & 0 & 0 & m_{4\leftarrow 3} \\ 0 & 0 & 0 & 0 \end{bmatrix} \neq \underline{\underline{B}}_1^T \quad (\text{A.6})$$

$$\underline{\underline{B}}_2^* = \begin{bmatrix} 2m_{1 \leftarrow 1} & 0 & 0 & 0 \\ 0 & m_{2 \leftarrow 2} & 0 & 0 \\ 0 & 0 & m_{3 \leftarrow 3} & 0 \\ 0 & 0 & 0 & 0 \end{bmatrix} = \underline{\underline{B}}_2^T \quad (\text{A.7})$$

From these two examples, we see that the adjoint matrix operator is identical to the transpose of the matrix if the nodes on the boundaries are full nodes, but that the adjoint and the transpose of the matrix are different for partial nodes on the boundaries.

APPENDIX B. FUNDAMENTAL MODE CONTAMINATION

The "fundamental mode contamination" of the solution of a fixed source adjoint equation is simply the component of the computed solution which is actually the solution to the corresponding homogeneous adjoint equation.

When the fixed source adjoint equation

$$(\underline{M}^* - \lambda \underline{F}^*) \underline{\Gamma}^* = \underline{Q}^* \quad (\text{B.1})$$

is solved, the computed solution will be

$$\underline{\Gamma}^* = \underline{\tilde{\Gamma}}^* + a \underline{S}^* \quad (\text{B.2})$$

where

$\underline{\tilde{\Gamma}}^*$  = particular solution to Eq. (B.1)

$\underline{S}^*$  = solution to the corresponding homogeneous adjoint equation

$a$  = constant to be determined .

The fundamental mode contamination is ( $a \underline{S}^*$ ).

Multiply both sides of Eq. (B.2) by  $(\underline{F} \ \underline{S})^T$

$$\begin{aligned} (\underline{F} \ \underline{S})^T \underline{\Gamma}^* &= (\underline{F} \ \underline{S})^T \underline{\tilde{\Gamma}}^* + a (\underline{F} \ \underline{S})^T \underline{S}^* \\ &= \underline{\tilde{\Gamma}}^{*T} (\underline{F} \ \underline{S}) + a \underline{S}^{*T} (\underline{F} \ \underline{S}) \end{aligned}$$

But  $\underline{\tilde{\Gamma}}^{*T} \underline{F} \ \underline{S} = 0$  by orthogonality. Therefore

$$a = \frac{\underline{\Gamma}^{*T} \underline{F} \ \underline{S}}{\underline{S}^{*T} \underline{F} \ \underline{S}} .$$

The particular solution to Eq. (B.1) is

$$\tilde{\Gamma}^* = \Gamma^* - a\underline{S}^*$$

$$\tilde{\Gamma}^* = \Gamma^* - \left[ \frac{\underline{\Gamma}^* \underline{F} \underline{S}}{\underline{S}^* \underline{F} \underline{S}} \right] \underline{S}^* . \quad (\text{B.3})$$

Equation (B.3) is the equation for sweeping out the fundamental mode contamination.

## APPENDIX C. DERIVATION OF DEPLETION ADJOINT EQUATIONS

APPENDIX C. DERIVATION OF DEPLETION  
ADJOINT EQUATIONS

This appendix contains the complete derivation of the depletion adjoint equations for SIMULATE. This derivation is taken from Ref. 12 which was written by M. L. Williams and this author.

In this derivation we will:

- 1) neglect thermal-hydraulic feedback.
- 2) neglect the constraint of negative moderator coefficient.
- 3) Neglect criticality reset (i.e., it is assumed that the change in the time dependent boron concentration can be ignored).
- 4) consider a single fuel cycle (i.e., no refueling or fuel shuffling).

Definitions\*

$\underline{S}_i$	nodal fission source density at exposure step i
$\underline{P}_i$	relative nodal power (i.e. "power peaking factor") at exposure step i
$\underline{E}_i$	nodal exposure (GWD/T) at exposure step i
$\underline{M}_i, \underline{F}_i$	nodal coupling coefficient matrices
$\underline{A}_i$	diagonal matrix of $\frac{K_{\Sigma f, i}}{v_{\Sigma f, i}}$ node for conversion of nodal fission source to relative nodal power
$\underline{\Sigma}_i^x$	nodal macroscopic cross section of type $\chi$ , at exposure step i
	$\chi \equiv \Sigma_{tr_1}, \Sigma_{tr_2}, \Sigma_{a_1}, \Sigma_{a_2}, \Sigma_{r_1}, v_{\Sigma f_1}, v_{\Sigma f_2}, K_{\Sigma f_1}, K_{\Sigma f_2}$

---

\* Vector components refer to nodes.



$\underline{h}_i$	fission source normalization ( $\underline{h} = (V_1, V_2, \dots, V_M)$ )
$V_j$	relative volume of node j <span style="float: right;">M</span>
N	magnitude of integrated fission source ( $N = \sum_{i=1}^M V_i$ )
$\underline{C}_k$	concentration of k <sup>th</sup> control variable (e.g. boron concentration)
i	refers to exposure step number. ( $0 \leq i \leq \ell$ )
$\underline{f}^X(\underline{E}, \underline{C}_1, \dots)$	polynomial for $\sum^X$ fitted against exposure $\underline{E}$ and control variables $\underline{C}_1, \dots, \underline{C}_k, \dots$
$\lambda_i$	lambda mode eigenvalue at exposure step i
$T_i$	length (GWD/T) of i <sup>th</sup> exposure step
$\ell$	total number of exposure steps in calculation
$R_i$	power normalization constant for exposure step i

### Governing Equations

Forward Eigenvalue Equation

$$(\underline{M}_i - \lambda_i \underline{F}_i) \underline{S}_i = 0 \quad (i = 0, 1, \dots, \ell) \quad (C.1)$$

Power Equation

$$\underline{P}_i = R_i \cdot \underline{A}_i \underline{S}_i \quad (i = 0, 1, \dots, \ell) \quad (C.2)$$

Exposure Equation

$$\begin{aligned} \underline{E}_i &= \underline{E}_{i-1} + \underline{P}_{i-1} \cdot T_{i-1} & (i = 1, 2, \dots, \ell) \\ \underline{E}_i &= \underline{E}_0 & (i = 0) \end{aligned} \quad (C.3)$$

Exposure Equation (in terms of  $\underline{S}$ )

$$\underline{E}_{i-1} = \underline{E}_i + (R_i \cdot \underline{A}_i \cdot \underline{S}_i) \cdot T_i \quad (i = 0, 1, \dots, \ell) \quad (C.4)$$

Cross Section Fitting Equation

$$\begin{aligned} \sum_i^X &= \underline{f}^X(\underline{E}_i, \underline{C}_1, \dots, \underline{C}_k, \dots) & (i = 0, 1, \dots, \ell) \\ & & (X = 1, 2, \dots, 9) \end{aligned} \quad (C.5)$$

where

$\underline{f}(\underline{E}_i)$  = vector with components of  $\underline{f}$  evaluated at each node.

Source Normalization Equation

$$\underline{h}_i \underline{S}_i = N_i \quad (i = 0, 1, \dots, \ell) \quad (C.6)$$

( $\underline{S}_i$  is normalized to an average value of 1.0 for each full node)

Power Normalization Equation

$$R_i \underline{h}_i \underline{A}_i \underline{S}_i = \underline{h}_i \underline{P}_i = N_i \quad (i = 0, 1, \dots, \ell) \quad (C.7)$$

( $\underline{P}_i$  is also normalized to an average value of 1.0 for each full node)

### Adjoint Equations and Sensitivity Coefficients for EOC $K_{eff}$

We now proceed to derive the appropriate adjoint equations from a variational principle. The first case we will consider is that of the response corresponding to the  $\lambda$  eigenvalue (or  $K_{eff}$ ) at exposure step  $\ell$  (end of cycle). The development for this case and the following one is similar to the method used to derive the original depletion perturbation theory (DPT) equations.

Consider the functional

$$\begin{aligned} K = & \sum_{i=0}^{\ell} \underline{S}_i^* (\underline{M}_i - \lambda_i \underline{F}_i) \underline{S}_i + \sum_{i=1}^{\ell} \underline{E}_i^* (\underline{E}_i - \underline{E}_{i-1} - R_{i-1} \underline{A}_{i-1} \underline{S}_{i-1} \underline{T}_{i-1}) \\ & + \sum_{i=0}^{\ell} \left\{ \sum_{x=1}^9 \underline{S}_i^x (\sum_j^x - \underline{f}^x(\underline{E}_i, \underline{C}_1, \dots, \underline{C}_k, \dots)) \right\} \\ & + \sum_{i=0}^{\ell} a_i (\underline{h}_i \cdot \underline{S}_i - N_i) + \sum_{i=0}^{\ell} b_i (R_i \cdot \underline{h}_i \underline{A}_i \underline{S}_i - N_i) \end{aligned} \quad (C.8)$$

where the parameters  $\underline{S}_i^*, \underline{E}_i^*, \underline{S}_i^X, a_i$ , and  $b_i$  are as yet unspecified, and where the summations are over the exposure steps  $i=0 \rightarrow \lambda$  and over the two-group cross section types  $i=1 \rightarrow 9$ .

Note that when  $\underline{S}_i, \underline{E}_i, \sum_i^X$  satisfy the relations in Eqs. (C.1), (C.4), (C.5), (C.6) and (C.7), then  $K = 0$  regardless of the values of  $\underline{S}_i^*, \underline{E}_i^*, \underline{S}_i^X, a_i$ , or  $b_i$ .

Suppose that some perturbation or combination of perturbations is made to Eqs. (C.1)-(C.7). This, in turn, will cause a complex series of perturbations (due to the coupling between exposure steps, between nodes, and between the equations) as

$$\underline{S}_i \longrightarrow \underline{S}_i + \Delta \underline{S}_i$$

$$\underline{E}_i \longrightarrow \underline{E}_i + \Delta \underline{E}_i$$

$$\sum_i^X \longrightarrow \sum_i^X + \Delta \sum_i^X$$

$$\lambda_i \longrightarrow \lambda_i + \Delta \lambda_i, \text{ etc.}$$

However, the perturbed variables must still obey exactly the perturbed set of equations:

$$(\underline{M}_i' - \lambda_i' \underline{F}_i') \underline{S}_i' = 0$$

$$\underline{E}_{i+1}' = \underline{E}_i' + R_{i-1}' \underline{A}_{i-1}' \underline{S}_i' \underline{T}_i'$$

$$(\sum_i^X)' = f^X(\underline{E}_i', \dots, \underline{C}_k', \dots)$$

$$\underline{h}_i' \cdot \underline{S}_i' = \underline{N}_i'$$

$$R_{i-1}' \underline{h}_{i-1}' \underline{A}_{i-1}' \underline{S}_i' = \underline{N}_i'$$

If these perturbed equations are used in Eq. (8), we see that  $K' = 0$  exactly and

$$K' - K = \Delta K = 0 .$$

We now proceed to obtain a first-order estimate for  $\Delta K$ , which will then define the necessary adjoint equations for the EOC  $\lambda$ . Writing out the expression for  $\Delta K$  and neglecting second order terms gives

$$\begin{aligned}
\Delta K \approx & \sum_{i=0}^{\ell} \underline{S}_i^* \left\{ (\Delta \underline{M}_i - \lambda_i \Delta \underline{F}_i) \underline{S}_i + (\underline{M}_i - \lambda \underline{F}_i) \Delta \underline{S}_i - (\Delta \lambda_i \underline{F}_i \underline{S}_i) \right\} \\
& + \sum_{i=1}^{\ell} \underline{E}_i^* \left\{ \Delta \underline{E}_i - \Delta \underline{E}_{i-1} - R_{i-1} \cdot \Delta \underline{A}_{i-1} \underline{S}_{i-1} \cdot \underline{T}_{i-1} - R_{i-1} \underline{A}_{i-1} \Delta \underline{S}_{i-1} \cdot \underline{T}_{i-1} \right. \\
& \left. - R_{i-1} \cdot \underline{A}_{i-1} \underline{S}_{i-1} \cdot \Delta \underline{T}_{i-1} - \Delta R_{i-1} \underline{A}_{i-1} \underline{S}_{i-1} \cdot \underline{T}_{i-1} \right\} \\
& + \sum_{i=0}^{\ell} \left\{ \sum_{x=1}^9 \underline{S}_i^x \left[ \Delta \underline{\Sigma}_i^x - \left( \underline{f}^x(\underline{E}_i + \Delta \underline{E}_i, \underline{C}_1 + \Delta \underline{C}_1, \dots, \underline{C}_k + \Delta \underline{C}_k, \dots) \right. \right. \right. \\
& \left. \left. \left. - \underline{f}^x(\underline{E}_i, \underline{C}, \dots, \underline{C}_k, \dots) \right) \right] \right\} \\
& + \sum_{i=0}^{\ell} a_i (\Delta \underline{h}_i \cdot \underline{S}_i + \underline{h}_i \cdot \Delta \underline{S}_i - \Delta N_i) \\
& + \sum_{i=0}^{\ell} b_i (\Delta R_i \cdot \underline{h}_i \underline{A}_i \underline{S}_i + R_i \underline{h}_i \underline{A}_i \Delta \underline{S}_i + R_i \Delta \underline{h}_i \underline{A}_i \underline{S}_i \\
& + R_i \underline{h}_i \Delta \underline{A}_i \underline{S}_i - \Delta N_i) \tag{C.9}
\end{aligned}$$

The matrix operators  $M_i$ ,  $F_i$  and  $A_i$  are implicitly perturbed due to the perturbations in nodal coupling coefficients caused by changing the various cross sections. These can be approximated by a first-order Taylor Series expansion

$$\Delta \underline{M}_i \approx \sum_{x=1}^9 \frac{\partial \underline{M}_i}{\partial \underline{\Sigma}_i^x} \Delta \underline{\Sigma}_i^x \tag{C.10}$$

$$\Delta \underline{F}_i \cong \sum_{x=1}^9 \frac{\partial \underline{F}_i}{\partial \underline{\Sigma}_i^x} \Delta \underline{\Sigma}_i^x \quad (\text{C.11})$$

$$\Delta \underline{A}_i \cong \sum_{x=1}^9 \frac{\partial \underline{A}_i}{\partial \underline{\Sigma}_i^x} \Delta \underline{\Sigma}_i^x \quad (\text{C.12})$$

The value for  $f^X(\underline{E}_i + \Delta \underline{E}_i, \dots, \underline{C}_k + \Delta \underline{C}_k, \dots)$  can also be estimated by a first order Taylor series expansion  $f^X(\underline{E}_i + \Delta \underline{E}_i, \dots, \underline{C}_k + \Delta \underline{C}_k, \dots) - f^X(\underline{E}_i, \dots, \underline{C}_k, \dots)$

$$\cong \left( \frac{\partial f^X}{\partial \underline{E}_i} \right)_{\underline{C}_k} \Delta \underline{E}_i + \sum_k \left( \frac{\partial f^X}{\partial \underline{C}_k} \right)_{\underline{E}_i} \Delta \underline{C}_k \quad (\text{C.13})$$

Assume that the normalization vector is a constant, i.e.,

$$\Delta \underline{h}_i = 0$$

Substituting Eqs. (C.10), (C.11), (C.12), (C.13) and (C.14) into Eq. (C.9) and redefining the summation on the  $\underline{E}_{i+1}^*$  term from  $i=0$  to  $i=\ell-1$  gives

$$\begin{aligned} \Delta K = & \sum_{i=0}^{\ell} \underline{S}_i^* \left\{ \left[ \sum_{x=1}^9 \left( \frac{\partial \underline{M}_i}{\partial \underline{\Sigma}_i^x} - \lambda_i \frac{\partial \underline{F}_i}{\partial \underline{\Sigma}_i^x} \right) \Delta \underline{\Sigma}_i^x \right] \underline{S}_i \right. \\ & \left. + (\underline{M}_i - \lambda_i \underline{F}_i) \Delta \underline{S}_i - \Delta \lambda_i \underline{F}_i \underline{S}_i \right\} \\ & + \sum_{i=0}^{\ell-1} \underline{E}_{i+1}^* \left\{ \Delta \underline{E}_{i+1} - \Delta \underline{E}_i - \left( \sum_{x=1}^9 \frac{\partial \underline{A}_i}{\partial \underline{\Sigma}_i^x} \Delta \underline{\Sigma}_i^x \right) \underline{R}_i \cdot \underline{S}_i \cdot \underline{T}_i \right. \\ & \left. - \underline{R}_i \cdot \underline{A}_i \Delta \underline{S}_i \underline{T}_i - \underline{R}_i \cdot \underline{A}_i \underline{S}_i \Delta \underline{T}_i - \Delta \underline{R}_i \underline{A}_i \underline{S}_i \underline{T}_i \right\} \\ & + \sum_{i=0}^{\ell} \left\{ \sum_{x=1}^9 \underline{S}_i^x \left[ \Delta \underline{\Sigma}_i^x - \left( \frac{\partial f^X}{\partial \underline{E}_i} \right)_{\underline{C}_k} \Delta \underline{E}_i - \sum_k \left( \frac{\partial f^X}{\partial \underline{C}_k} \right)_{\underline{E}_i} \Delta \underline{C}_k \right] \right\} \end{aligned}$$

$$\begin{aligned}
& + \sum_{i=0}^{\ell} a_i \left\{ \underline{h}_i \cdot \Delta \underline{S}_i - \Delta N_i \right\} \\
& + \sum_{i=0}^{\ell} b_i \left\{ R_i \cdot \underline{h}_i \underline{A}_i \Delta \underline{S}_i + R_i \cdot \underline{h}_i \sum_{x=1}^9 \left( \frac{\partial \underline{A}_i}{\partial \underline{\Sigma}_i^x} \right) \Delta \underline{\Sigma}_i^x \underline{S}_i \right. \\
& \left. + \Delta R_i \cdot \underline{h}_i \underline{A}_i \underline{S}_i - \Delta N_i \right\} \tag{C.14}
\end{aligned}$$

It is convenient to separate out the last term in the exposure step summation ( $i=\ell$ ):

$$\begin{aligned}
\Delta K & \equiv \underline{S}_\ell^* \left\{ \left[ \sum_{x=1}^9 \left( \frac{\partial \underline{M}_\ell}{\partial \underline{\Sigma}_\ell^x} - \lambda_\ell \frac{\partial \underline{F}_\ell}{\partial \underline{\Sigma}_\ell^x} \right) \Delta \underline{\Sigma}_\ell^x \right] \underline{S}_\ell + (\underline{M}_\ell - \lambda_\ell \underline{F}_\ell) \Delta \underline{S}_\ell - \Delta \lambda_\ell \underline{F}_\ell \underline{S}_\ell \right\} \\
& + \underline{E}_\ell^* \Delta \underline{E}_\ell + \sum_{x=1}^9 \underline{S}_\ell^* \left[ \Delta \underline{\Sigma}_\ell^x - \frac{\partial \underline{f}^x}{\partial \underline{E}_\ell} \Delta \underline{E}_\ell - \sum_k \left( \frac{\partial \underline{f}^x}{\partial \underline{C}_k} \right) \underline{E}_\ell \Delta \underline{C}_k \right] \\
& + a_\ell \left\{ \underline{h}_\ell \Delta \underline{S}_\ell - \Delta N_\ell \right\} \\
& + b_\ell \left\{ R_\ell \cdot \underline{h}_\ell \underline{A}_\ell \Delta \underline{S}_\ell + R_\ell \cdot \underline{h}_\ell \left( \sum_{x=1}^9 \frac{\partial \underline{A}_\ell}{\partial \underline{\Sigma}_\ell^x} \Delta \underline{\Sigma}_\ell^x \right) \underline{S}_\ell + \Delta R_\ell \cdot \underline{h}_\ell \underline{A}_\ell \underline{S}_\ell - \Delta N_\ell \right\} \\
& + \sum_{i=0}^{\ell-1} \left\{ \left[ \underline{S}_i^* (\underline{M}_i - \lambda_i \underline{F}_i) - \underline{E}_{i+1}^* \cdot \underline{T}_i \cdot \underline{A}_i \cdot R_i + a_i \underline{h}_i + b_i R_i \cdot \underline{h}_i \underline{A}_i \right] \Delta \underline{S}_i \right\} \\
& + \sum_{i=1}^{\ell-1} \left\{ \left[ \underline{E}_i^* - \underline{E}_{i+1}^* - \sum_{x=1}^9 \underline{S}_i^x \left( \frac{\partial \underline{f}^x}{\partial \underline{E}_i} \right) \underline{C}_k \right] \Delta \underline{E}_i \right\} - \left[ \underline{E}_1^* + \sum_{x=1}^9 \underline{S}_0^x \left( \frac{\partial \underline{f}^x}{\partial \underline{E}_0} \right) \right] \Delta \underline{E}_0 \\
& + \sum_{i=0}^{\ell-1} \left\{ \sum_{x=1}^9 \left[ \underline{S}_i^* \left( \frac{\partial \underline{M}_i}{\partial \underline{\Sigma}_i^x} - \lambda_i \frac{\partial \underline{F}_i}{\partial \underline{\Sigma}_i^x} \right) \underline{S}_i - \underline{E}_{i+1}^* \frac{\partial \underline{A}_i}{\partial \underline{\Sigma}_i^x} \underline{S}_i \cdot R_i \underline{T}_i \right. \right. \\
& \left. \left. + \underline{S}_i^x + b_i R_i \cdot \underline{h}_i \frac{\partial \underline{A}_i}{\partial \underline{\Sigma}_i^x} \underline{S}_i \right] \Delta \underline{\Sigma}_i^x \right\} - \sum_{i=0}^{\ell-1} \Delta \lambda_i (\underline{S}_i^* \underline{F}_i \underline{S}_i)
\end{aligned}$$

$$\begin{aligned}
& - \sum_{i=0}^{\ell-1} \left\{ (E_{i+1}^* R_i \cdot A_i S_i) \Delta T_i + \sum_k \left( \sum_{x=1}^9 s_i^x \left( \frac{\partial f^x}{\partial C_k} \right) E_i \right) \Delta C_k \right. \\
& \left. + a_i \Delta N_i + (E_{i+1}^* A_i S_i \cdot T_i + b_i \cdot h_i A_i S_i) \Delta R_i \right\} \quad (C.15)
\end{aligned}$$

The first five terms in Eq. (15) which corresponds to the  $i=\ell$  exposure step can be written

$$\begin{aligned}
& S_\ell^* (M_\ell - \lambda_\ell F_\ell) \Delta S_\ell + a_\ell (h_\ell \Delta S_\ell - \Delta N_\ell) \\
& + \sum_{x=1}^9 \left\{ S_\ell^* \left( \frac{\partial M_\ell}{\partial \Sigma_\ell^x} - \lambda_\ell \frac{\partial F_\ell}{\partial \Sigma_\ell^x} \right) S_\ell + s_\ell^x \right\} \Delta \Sigma_\ell^x \\
& + \left\{ E_\ell^* - \sum_{x=1}^9 s_\ell^x \left( \frac{\partial f^x}{\partial E_\ell} \right) C_k \right\} \Delta E_\ell \\
& + b_\ell \left[ R_\ell \cdot h_\ell A_\ell \Delta S_\ell + R_\ell \cdot h_\ell \sum_{x=1}^9 \left( \frac{\partial A_\ell}{\partial \Sigma_\ell^x} \Delta \Sigma_\ell^x \right) S_\ell + \Delta R_\ell \cdot h_\ell A_\ell S_\ell - \Delta N_\ell \right] \\
& - \sum_k \left[ \sum_{x=1}^9 s_\ell^x \left( \frac{\partial f^x}{\partial C_k} \right) E_\ell \right] \Delta C_k - \Delta \lambda_\ell S_\ell^* F_\ell S_\ell \quad (C.16)
\end{aligned}$$

Since the values of  $S_\ell^*$ ,  $E_\ell^*$ ,  $s_\ell^x$ ,  $a_i$  and  $b_i$  are completely arbitrary at this point, we can assign any value to them that is useful. Let us define them as follows for the final exposure step ( $i=\ell$ ):

$$(M_\ell^* - \lambda_\ell F_\ell^*) S_\ell^* = 0 \quad (C.17)$$

$$s_\ell^x = - S_\ell^* \left( \frac{\partial M_\ell}{\partial \Sigma_\ell^x} - \lambda_\ell \frac{\partial F_\ell}{\partial \Sigma_\ell^x} \right) \quad (C.18)$$

$$E_\ell^* = \sum_{x=1}^9 s_\ell^x \left( \frac{\partial f^x}{\partial E_\ell} \right) C_k \quad (C.19)$$

$$a_\ell = 0 \quad (C.20)$$

$$b_\ell = 0 \quad (C.21)$$

Substituting Eqs. (C.17)-(C.21) into the expression in (C.16)

reduces it to

$$-\sum_k \left[ \sum_{x=1}^g \frac{s_x^X}{s_\ell} \left( \frac{\partial f^X}{\partial C_k} \right) E_\ell \right] \Delta C_k - \Delta \lambda_\ell \frac{S_\ell^* E_\ell S_\ell}{s_\ell}$$

We now examine the remaining terms in Eq. (C.15) which correspond to all exposure steps prior to the last one at  $i=\ell$ . Again, we are free to choose any values for  $a_i$ ,  $s_i^X$ ,  $S_i^*$ , and  $E_i^*$ . We define the following relations for exposure step  $i$ :

$$\left( \frac{M_i^*}{s_i} - \lambda_i \frac{F_i^*}{s_i} \right) S_i^* = R_i T_i \cdot \frac{A_i^* E_{i+1}^*}{s_{i+1}} - a_i h_i - b_i R_i \frac{A_i^* h_i}{s_i} = Q_i^* \quad (0 \leq i < \ell) \quad (C.22)$$

$$s_i^X = R_i T_i E_{i+1}^* \frac{\partial A_i}{\partial \sum_i^X} S_i - S_i^* \left( \frac{\partial M_i}{\partial \sum_i^X} - \lambda_i \frac{\partial F_i}{\partial \sum_i^X} \right) S_i - b_i R_i h_i \frac{\partial A_i}{\partial \sum_i^X} S_i \quad (0 \leq i < \ell) \quad (C.23)$$

$$E_i^* = E_{i+1}^* + \sum_{x=1}^g s_x^X \frac{\partial f^X}{\partial E_i} (E_i, \dots, C_k, \dots) \quad (1 \leq i < \ell) \quad (C.24)$$

$$S_i^* F_i S_i = 0 \quad (0 \leq i < \ell) \quad (C.25)$$

$$b_i = \frac{T_i E_{i+1}^* A_i S_i}{h_i A_i S_i} \quad (0 \leq i < \ell) \quad (C.26)$$



Substituting Eq. (C.26) into Eq. (C.23) gives

$$\underline{s}_i^x = -\underline{s}_i^* \left( \frac{\partial \underline{M}_i}{\partial \underline{\Sigma}_i^x} - \lambda_i \frac{\partial \underline{F}_i}{\partial \underline{\Sigma}_i^x} \right) \underline{S}_i \quad (0 \leq i < \ell) \quad (\text{C.27})$$

We will define  $a_i$  such that the adjoint source,  $\underline{Q}_i^*$  is orthogonal to the forward solution, i.e.,

$$\begin{aligned} \underline{S}_i \underline{Q}_i^* &= 0 \quad (0 \leq i < \ell) \\ \underline{S}_i (R_i T_i A_i^* E_{i+1}^* - a_i h_i - \frac{T_i E_{i+1}^* A_i S_i}{h_i A_i S_i} R_i A_i^* h_i) &= 0 \\ R_i T_i S_i A_i^* E_{i+1}^* - a_i h_i S_i - \frac{R_i T_i E_{i+1}^* A_i S_i}{h_i A_i S_i} S_i A_i^* h_i &= 0 \end{aligned} \quad (\text{C.28})$$

But  $E_{i+1}^* A_i S_i = S_i A_i^* E_{i+1}^*$ , and  $S_i A_i^* h_i = h_i A_i S_i$ .

Substituting these relations into (C.28) gives

$$a_i = 0 \quad (0 \leq i < \ell) \quad (\text{C.29})$$

When Eqs. (C.17)-(C.22), (C.24)-(C.27) and (C.29) are substituted into Eq. (C.15), we obtain

$$\begin{aligned} \Delta K \cong & -\Delta \lambda_\ell \left[ \underline{S}_{\ell-2}^* \underline{F}_{\ell-2} \underline{S}_{\ell-2} \right] - \left[ \underline{E}_1^* + \sum_{x=1}^9 \underline{s}_0^x \frac{\partial \underline{f}^x}{\partial \underline{E}_0} \right] \Delta \underline{E}_0 \\ & - \sum_{i=0}^{\ell-1} (R_i E_{i+1}^* A_i S_i) \Delta T_i - \sum_k \left[ \sum_{i=0}^{\ell} \sum_{x=1}^9 \underline{s}_i^x \left( \frac{\partial \underline{f}^x}{\partial \underline{C}_k} \right) \underline{E}_i \right] \Delta \underline{C}_k \end{aligned} \quad (\text{C.30})$$

Assume that the initial exposure distribution is fixed (i.e.,  $\Delta \underline{E}_0 = 0$ ) and that the exposure step length remains constant ( $\Delta T_i = 0$ ). Recalling that  $\Delta K = 0$ , we can solve Eq. (C.30) for  $\Delta \lambda_\ell$ :

$$\Delta \lambda_\ell \cong \frac{-\sum_k \alpha_{C_k} \Delta \underline{C}_k}{\underline{S}_{\ell-2}^* \underline{F}_{\ell-2} \underline{S}_{\ell-2}} \quad (\text{C.31})$$

where  $\alpha_{C_k} = \sum_{i=0}^{\ell} \sum_{x=1}^9 \underline{s}_i^x \frac{\partial f^x}{\partial C_k} \equiv$  sensitivity coefficient for control variable  $K$ . Since  $\Delta \lambda_{\ell} = \frac{1}{k_{\text{eff},\ell}'} - \frac{1}{k_{\text{eff},\ell}} = \frac{\Delta k_{\text{eff},\ell}}{k_{\text{eff},\ell}' k_{\text{eff},\ell}} \approx \frac{\Delta k_{\text{eff},\ell}}{(k_{\text{eff},\ell}')^2}$ ,

Eq. (C.31) can be written

$$\left( \frac{\Delta k_{\text{eff}}}{k_{\text{eff}}} \right)_{\ell} \approx \frac{\sum_k \alpha_{C_k} \cdot \Delta C_k}{(1/k_{\text{eff}})_{\ell} (S_{\ell}^{*F} S_{\ell})} \quad (\text{C.32})$$

Suppose that one is interested in the effect of changing the cross sections of one or more assemblies (e.g., change in BOC fuel enrichment or lumped burnable poisons). We will now determine the sensitivity coefficients for the cross sections. If we set  $\underline{s}_i^x = 0$  ( $0 \leq i \leq \ell$ ) instead of using Eqs. (C.18) and (C.27), Eq. (C.32) will become

$$\left( \frac{\Delta k_{\text{eff}}}{k_{\text{eff}}} \right) \approx \frac{\sum_{i=0}^{\ell} \left\{ \sum_{x=1}^9 \left[ S_i^* \left( \frac{\partial M_i}{\partial \Sigma_i^x} - \lambda_i \frac{\partial F_i}{\partial \Sigma_i^x} \right) S_i \right] \Delta \Sigma_i^x \right\}}{(1/k_{\text{eff}})_{\ell} (S_{\ell}^{*F} S_{\ell})} \quad (\text{C.33})$$

If we substitute the definitions from Eqs. (C.18) and (C.27) into Eqs. (C.33), we obtain

$$\frac{\Delta k_{\text{eff}}}{k_{\text{eff}}} \approx \frac{\sum_{i=0}^{\ell} \left( \sum_{x=1}^9 \underline{s}_i^x \Delta \Sigma_i^x \right)}{(1/k_{\text{eff}})_{\ell} (S_{\ell}^{*F} S_{\ell})} \quad (\text{C.34})$$

Thus  $\underline{s}_i^x$ , as we originally defined it, is the cross section sensitivity coefficient for cross section type  $X$  and exposure step  $i$ .

Adjoint Equations and Sensitivity Coefficients  
for Responses Other than  $k_{eff}$

For this case we need a slightly different functional than the one defined in Eq. (8). Consider the functional L, given by

$$L = R [S_{\ell}, H_{\ell}, N_{\ell}] - K ,$$

where R is some final time response (evaluated at exposure step  $\ell$ ) which may depend on the nodal source  $S_{\ell}$ , the nodal "realization vector"  $H_{\ell}$ , and the source normalization  $N_{\ell}$ .

As discussed earlier, if the exact solutions to Eqs. (C.1),(C.4), (C.5),(C.6) and (C.7) are used to evaluate L, then  $K = 0$  and  $L = R$ . Similarly, if the exact perturbed values are used to evaluate  $L'$ , then  $K' = 0$  and  $L' = R'$ . Therefore,

$$\Delta L = \Delta R,$$

which is exactly true, if the exact perturbed and unperturbed values are known. Proceeding as before we will attempt to obtain a first order estimate for  $\Delta L$ , for which  $(\Delta L)_{\text{first order}} \cong \Delta R$ .

Because we are only considering a final time response defined at some arbitrary exposure step  $\ell$ , the only difference between this case and the previous one for  $k_{eff}$  at  $\ell$  will be in defining the stationary condition at  $i=\ell$  (i.e., the equations derived for  $i<\ell$  are still valid). At  $i=\ell$  we have the following expression, neglecting second order terms:

$$\begin{aligned} & S_{\ell}^* (M_{\ell} - \lambda_{\ell} F) \Delta S_{\ell} - \frac{\partial R}{\partial S_{\ell}} \Delta S_{\ell} + a_{\ell} (h_{\ell} \Delta S_{\ell} - \Delta N_{\ell}) \\ & + \sum_{x=1}^9 \left\{ S_{\ell}^* \left( \frac{\partial M_{\ell}}{\partial \sum_{i,\ell}^x} - \lambda_{\ell} \frac{\partial F_{\ell}}{\partial \sum_{i,\ell}^x} \right) S_{\ell} + S_{\ell}^x \right\} \Delta \sum_{i,\ell}^x \end{aligned}$$

$$\begin{aligned}
& + \left\{ \underline{E}_\ell^* - \sum_{x=1}^9 \underline{s}_\ell^x \left( \frac{\partial \underline{f}^x}{\partial \underline{E}_\ell} \right) \underline{C}_k \right\} \Delta \underline{E}_\ell \\
& + b_\ell \left\{ R_{\ell-2} h_{\ell-2} \underline{A} \Delta \underline{S}_\ell + \Delta R_{\ell-2} h_{\ell-2} \underline{A} \underline{S}_\ell - \Delta N_\ell + R_{\ell-2} h_{\ell-2} \left( \sum_{x=1}^9 \frac{\partial \underline{A}_\ell^x}{\partial \underline{\Sigma}_\ell^x} \Delta \underline{\Sigma}_\ell^x \right) \underline{S}_\ell \right\} \\
& - \sum_k \left[ \sum_x \underline{s}_\ell^x \left( \frac{\partial \underline{f}^x}{\partial \underline{C}_k} \right) \underline{E}_\ell \right] \Delta \underline{C}_k - \Delta \lambda_{\ell-2} \underline{S}_\ell \underline{F}_\ell \underline{S}_\ell \\
& - \sum_{x=1}^9 \left( \frac{\partial R}{\partial \underline{H}_\ell} \right) \left( \frac{\partial \underline{H}_\ell}{\partial \underline{\Sigma}_\ell^x} \right) \Delta \underline{\Sigma}_\ell^x - \frac{\partial R}{\partial N_\ell} \Delta N_\ell \tag{C.35}
\end{aligned}$$

Rearranging terms gives

$$\begin{aligned}
& \left[ \underline{S}_\ell^* \left( \underline{M}_\ell - \lambda_{\ell-2} \underline{F}_\ell \right) - \frac{\partial R}{\partial \underline{S}_\ell} + a_{\ell-2} h_{\ell-2} \right] \Delta \underline{S}_\ell \\
& - \left[ a_\ell + \frac{\partial R}{\partial N_\ell} \right] \Delta N_\ell \\
& + \left[ \sum_{x=1}^9 \left\{ \underline{S}_\ell^* \left( \frac{\partial \underline{M}_\ell}{\partial \underline{\Sigma}_\ell^x} - \lambda_{\ell-2} \frac{\partial \underline{F}_\ell}{\partial \underline{\Sigma}_\ell^x} \right) \underline{S}_\ell + \underline{s}_\ell^x - \left( \frac{\partial R}{\partial \underline{H}_\ell} \right) \left( \frac{\partial \underline{H}_\ell}{\partial \underline{\Sigma}_\ell^x} \right) \right\} \Delta \underline{\Sigma}_\ell^x \right] \\
& + \left\{ \underline{E}_\ell^* - \sum_{x=1}^9 \underline{s}_\ell^x \left( \frac{\partial \underline{f}^x}{\partial \underline{E}_\ell} \right) \underline{C}_k \right\} \Delta \underline{E}_\ell - \sum_k \left[ \sum_{x=1}^9 \underline{s}_\ell^x \left( \frac{\partial \underline{f}^x}{\partial \underline{C}_k} \right) \underline{E}_\ell \right] \Delta \underline{C}_k \\
& + b_\ell \left\{ \Delta R_{\ell-2} h_{\ell-2} \underline{A} \underline{S}_\ell + R_{\ell-2} h_{\ell-2} \sum_{x=1}^9 \frac{\partial \underline{A}_\ell}{\partial \underline{\Sigma}_\ell^x} \Delta \underline{\Sigma}_\ell^x \underline{S}_\ell + R_{\ell-2} h_{\ell-2} \underline{A} \Delta \underline{S}_\ell \right\}
\end{aligned}$$

Since the normalization is fixed,  $\Delta N_\ell = 0$ .

The appropriate stationary conditions for  $i=\ell$ , corresponding to a final time response at  $i=\ell$ , are

$$\left( \underline{M}_\ell^* - \lambda_{\ell-2} \underline{F}_\ell^* \right) \underline{S}_\ell^* = \frac{\partial R}{\partial \underline{S}_\ell} \tag{C.36}$$

$$a_\ell = 0 \quad (C.37)$$

$$s_\ell^x = -s_\ell^* \left( \frac{\partial M}{\partial \underline{\Sigma}_\ell^x} - \lambda_\ell \frac{\partial F_\ell}{\partial \underline{\Sigma}_\ell^x} \right) s_\ell + \left( \frac{\partial R}{\partial H_\ell} \right) \left( \frac{\partial H_\ell}{\partial \underline{\Sigma}_\ell^x} \right) \quad (C.38)$$

$$E_\ell^* = \sum_{x=1}^9 s_\ell^x \left( \frac{\partial f^x}{\partial E_\ell} \right) \underline{C}_k \quad (C.39)$$

$$s_\ell^* F s_\ell = 0 \quad (C.40)$$

$$b_\ell = 0 \quad (C.41)$$

Recalling that  $\Delta L = \Delta R$ , we obtain the following expression for the change in the response due to control variable perturbations:

$$\left( \frac{\Delta R}{R} \right)_\ell \cong \frac{\sum_k \alpha_{C_k} \cdot \Delta C_k}{R} \quad (C.42)$$

where

$$\alpha_{C_k} \equiv \sum_{i=0}^{\ell} \sum_{x=1}^9 \left[ s_{-i}^x \left( \frac{\partial f^x}{\partial \underline{C}_k} \right) E_j \right] .$$

The change in the final time response due to cross section perturbations is given by

$$\left( \frac{\Delta R}{R} \right)_\ell \cong \frac{\sum_{i=0}^{\ell} \left( \sum_{x=1}^9 s_{-i}^x \Delta \underline{\Sigma}_i^x \right)}{R} . \quad (C.43)$$

APPENDIX D. IMPLEMENTATION OF DEPLETION PERTURBATION THEORY  
INTO SIMULATE

SIMULATE is a FORTRAN-IV program. Version 215, the most recent version, consists of approximately 120 subroutines. The implementation of depletion perturbation theory into SIMULATE has effected modifications to more than ten of the existing subroutines and the creation of seven new subroutines. In this section, the important modifications are outlined, and the functions performed by the new subroutines are discussed. We also examine the effects of these changes on the code performance and the new options which are available to the user.

### Modifications to Existing Subroutines

One of the first and most important modifications which had to be made was enabling SIMULATE to solve the adjoint of the forward eigenvalue equation, Eq. (2.13). This involved reversing the coupling between nodes for  $\underline{\underline{M}}$  and  $\underline{\underline{F}}$ . SIMULATE solves the eigenvalue equation in a series of inner and outer iterations. At each outer iteration, the subroutine CALSRC calculates  $\underline{\underline{F}} \underline{\underline{S}}^{(i)}$ , where  $\underline{\underline{S}}^{(i)}$  is the source guess for the  $i^{\text{th}}$  outer iteration. Between the  $i^{\text{th}}$  and  $i+1^{\text{th}}$  outer iterations, a set of inner iterations is performed in the subroutine GUTS to iteratively invert  $\underline{\underline{M}}$  in order to obtain the source guess for the  $i+1^{\text{th}}$  outer iteration

$$\underline{\underline{S}}^{(i+1)} = 1/k_{\text{eff}} \underline{\underline{M}}^{-1} \underline{\underline{F}} \underline{\underline{S}}^{(i)}$$

A flow chart for the inner and outer source iterations is illustrated in Fig. D.1. The inner and outer iterations are so named because of a set of inner iterations is performed between every two outer iterations.

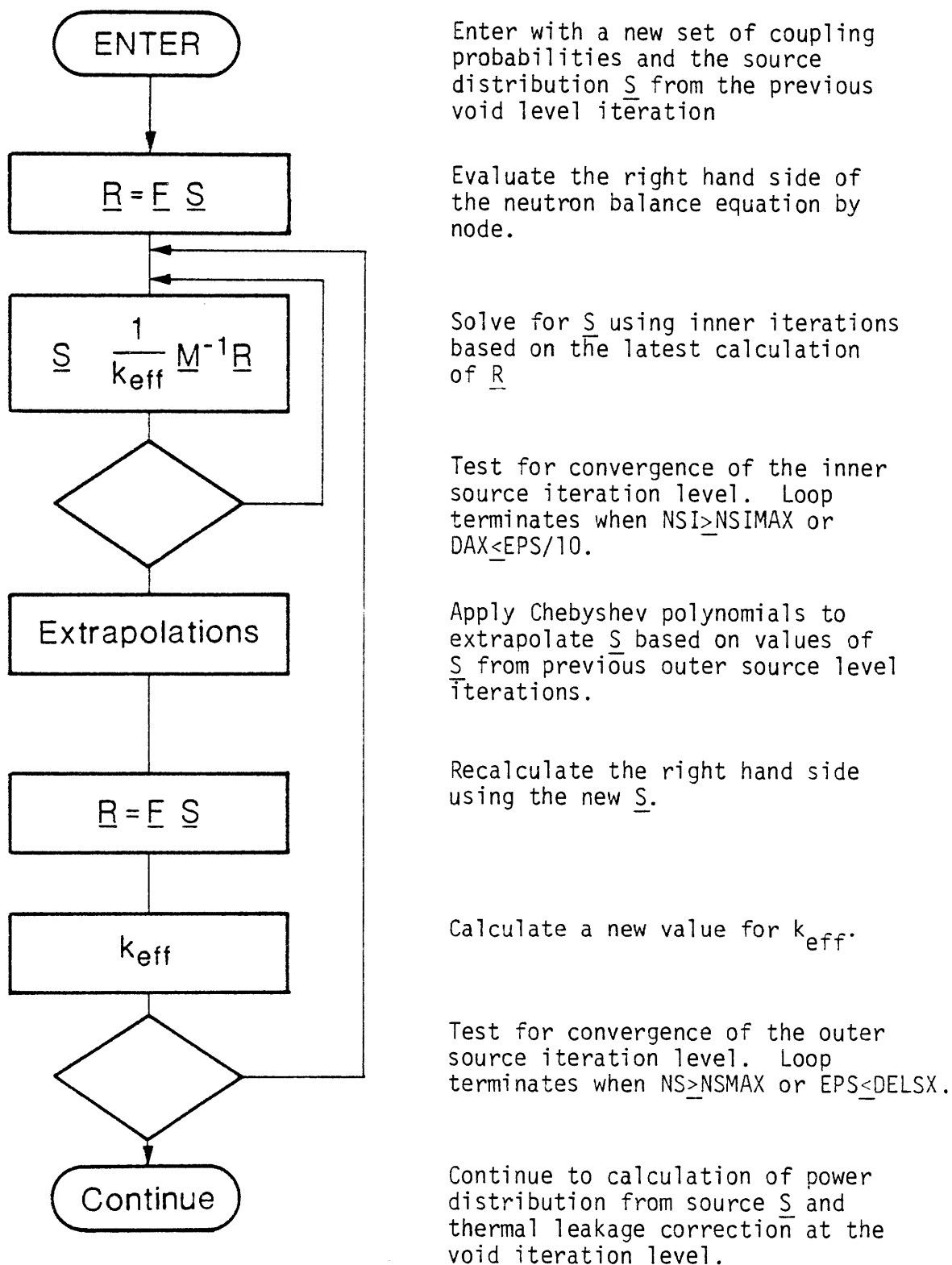


Fig. D.1. Flow Chart for the Inner and Outer Source Iteration Levels



The matrices  $\underline{\underline{M}}$  and  $\underline{\underline{F}}$  are not stored explicitly in core due to their size (e.g., 40,000 words of storage each for a 200-node problem), but are calculated during each of these iterations. CALSRC and GUTS were modified to reverse the coupling when solving an adjoint problem in order to obtain the adjoint matrices.

The subroutine NBTCAL determines the core configuration for any problem according to the given boundary conditions. It assigns to each fuel bundle an identification number. This set of I.D. numbers is the NBT array. A typical configuration for a core with 1/8 core symmetry is shown in Fig. D.2. The 1/8 core region is outlined in the figure. On any boundary where there is a reflection boundary condition, NBTCAL assigns the bundles outside the boundary the same identification number as the corresponding fuel bundles inside the boundary. All bundles not lying in the region of interest on the boundary are set to zero. Notice in Fig. D.2 that there are no bundles assigned the numbers 2-7, 11-16, 20-24, 29-32, 38-40, 47-48, or 54-56. These fuel bundles have all been "zeroed out," because they did not lie within the region of interest. However, to simplify the indexing of the matrices in the depletion adjoint equations, we want to number only the fuel bundles which are not "zeroed out." The subroutine NBTCAL has been modified to do this also, as shown in Fig. D.3 for the same configuration as that in Fig. D.2. This set of I.D. numbers is the NBD array. Both arrays are stored in memory and used at different points throughout the solution of a problem.

The subroutine SOURCE controls the source iterations, and naturally, contains several modifications. Most of these modifications

0	9	10	18	26	34	42	50	58	0
9	1	9	17	25	33	41	49	57	0
10	9	10	18	26	34	42	50	58	0
18	0	18	19	27	35	43	51	59	0
0	0	0	27	28	36	44	52	0	0
0	0	0	0	36	37	45	53	0	0
0	0	0	0	0	45	46	0	0	0
0	0	0	0	0	0	0	0	0	0
0	0	0	0	0	0	0	0	0	0
0	0	0	0	0	0	0	0	0	0

Fig. D.2. Fuel Bundle ID Numbers - Old Method

0	2	3	5	8	12	17	23	28	0
2	1	2	4	7	11	16	22	27	0
3	2	3	5	8	12	17	23	28	0
5	0	5	6	9	13	18	24	29	0
0	0	0	9	10	14	19	25	0	0
0	0	0	0	14	15	20	26	0	0
0	0	0	0	0	20	21	0	0	0
0	0	0	0	0	0	0	0	0	0
0	0	0	0	0	0	0	0	0	0
0	0	0	0	0	0	0	0	0	0

Fig. D.3. Fuel Bundle ID Number - New Method

are concerned with the solution of the fixed source adjoint equation, Eq. (2.17). The fundamental mode contamination is swept out according to Eq. (2.19) in SOURCE. The calculation of a new  $k_{\text{eff}}$ , which ordinarily occurs at the end of each outer iteration in SOURCE, is bypassed for the fixed source case, so that the eigenvalue from the forward case is used throughout the calculation. The source normalization, Eq. (2.30), is also bypassed in this subroutine for the solution of the fixed source case, since multiplying the solution of a non-homogeneous equation by a constant will not necessarily be a solution to the equation.

SOURCE calls the subroutine CHEBY, which tests for convergence and applies Chebyshev polynomial acceleration.<sup>13</sup> Ordinarily, CHEBY calculates the minimum and maximum ratios of the source solutions from the present and previous iterations. This is not possible for fixed source solutions, because the solution can be very small, or even zero, for some nodes. For such cases, these ratios can approach infinity. Therefore, CHEBY has been modified to calculate the maximum and minimum differences of the solutions from the present and previous iterations for the fixed source adjoint case only.

The subroutine PARTB is the largest in SIMULATE and controls all the nuclear and thermal-hydraulic calculations. It also handles the control searches, depletion calculations, and the setting of the memory pointers. Most of the modifications made to the original SIMULATE code are located in this subroutine. These modifications are often in the forms of flags which signal the program at the times that it is to perform various routines in the forward and backward marches through

time. Statements also have been added to call the new subroutines which have been added to the code. During each exposure step forward in time, PARTB writes the forward and adjoint sources and the exposure distribution onto I/O units for use during the backward march through time. It also allocates additional storage for the new variables that appear in the development of the depletion adjoint equations. The forward and backward marches through time are outlined in the flowcharts in Figs. D.4 and D.5, respectively.

PARTB is followed by the subroutine DPART, which was originally a dummy subroutine placed in SIMULATE for possible use by the user. At the end of the forward march through time, DPART prepares for the backward march through time by calling a new subroutine which transfers the source and exposure distributions which have been stored sequentially on I/O units to direct access I/O units, so that these distributions can be recalled into memory at the corresponding exposure step in the backward march through time.

When a fixed source is input to SIMULATE for a response other than  $k_{eff}$ , the subroutine INPUT1 writes the fixed source onto disk, from which it will be read at a later point in the program. It then sets the initial source guess for  $\underline{\Gamma}^*$  to zero in order to minimize the initial fundamental mode contamination.

### New Subroutines

Seven new subroutines have been created and added to SIMULATE for DPT calculations. Three of these subroutines are very simple and written to perform a particular task. BUGTAP writes the sensitivity

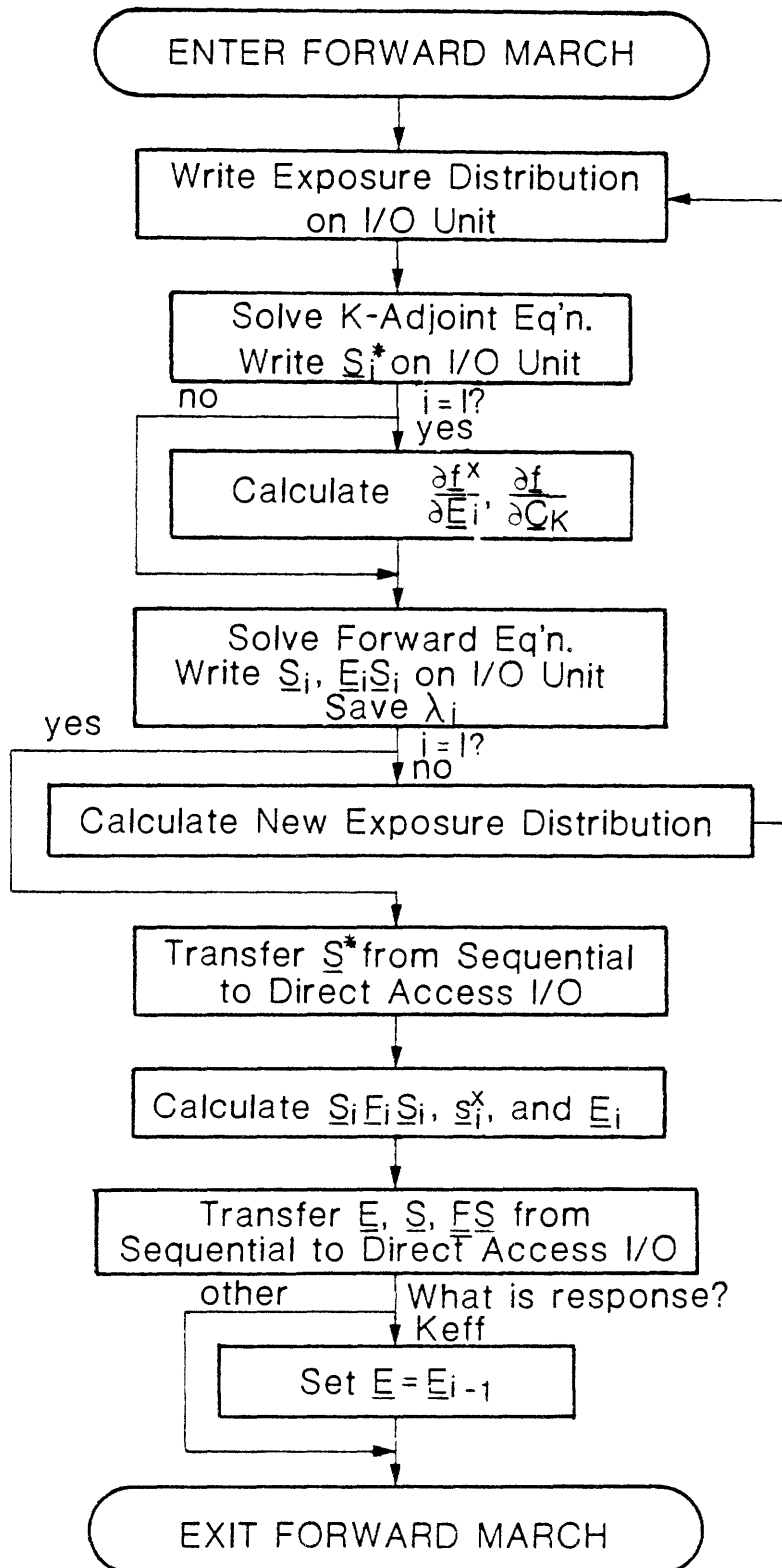


Fig. D.4. Forward March Through Time

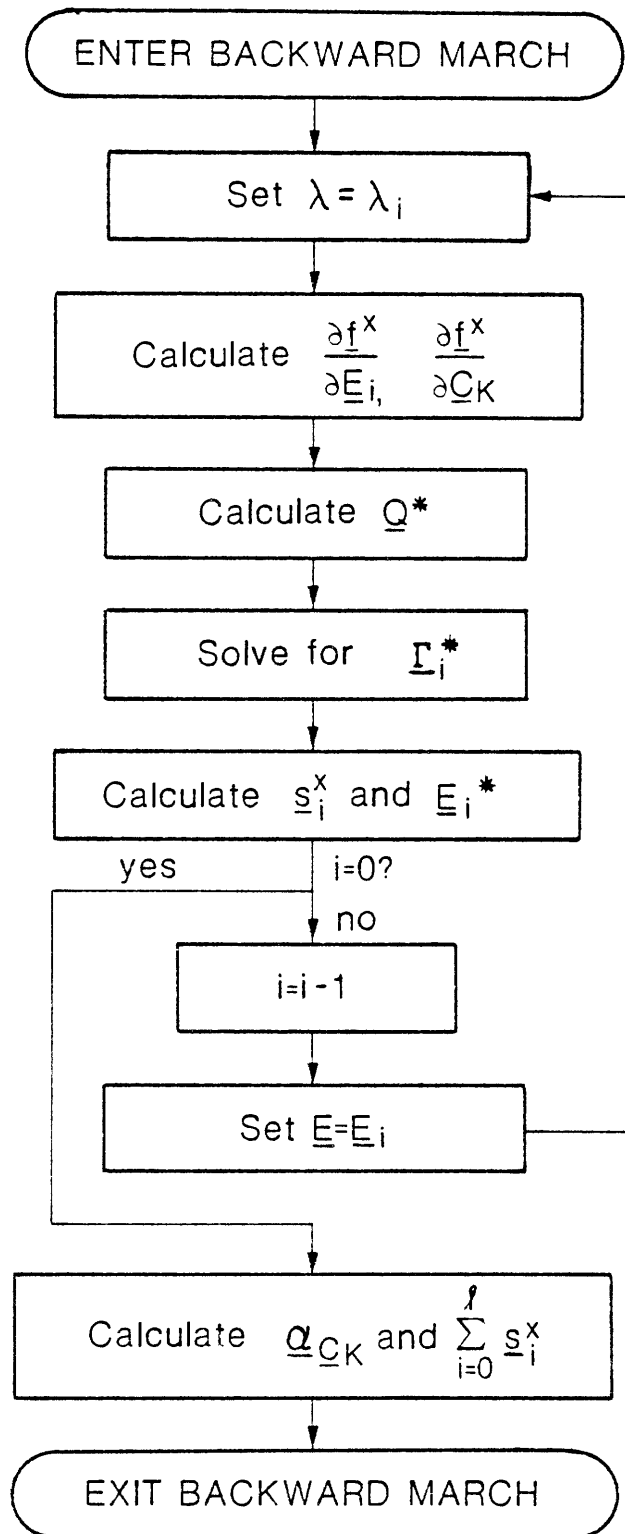


Fig. D.5. Backward March Through Time

coefficients on I/O units for later use in perturbation calculations. The subroutine REPLAC replaces the present exposure distribution with the exposure distribution from another exposure step which has been stored on disk. This subroutine is called prior to each exposure step backward in time to set the exposure distribution equal to that from the corresponding exposure step in the forward calculations. STACK reads a set of arrays which have been stored on a sequential I/O unit during the end of each forward exposure step and writes them on a direct access I/O unit for recall during the backward march through time. STACK is called at the end of the forward march through time.

CALMAT is a new subroutine which uses the same logic as CALSRC and GUTS to calculate explicitly and print the coefficients of  $\underline{\underline{M}}$  and  $\underline{\underline{F}}$ . This subroutine can be called when requested by the user. It should only be used for debug purposes, since it requires a great deal of additional storage.

The new subroutine DERIV calculates the partial derivatives given in Eqs. (3.51)–(3.95) and uses these derivatives to calculate  $\frac{\partial \underline{\underline{M}}}{\partial \underline{\underline{\Sigma}}^x}$  and  $\frac{\partial \underline{\underline{F}}}{\partial \underline{\underline{\Sigma}}^x}$  for  $x = 1, \dots, 7$ . Note that in the original derivation of the depletion adjoint equations outlined in Section II, the variable  $x$  took on the values  $1, \dots, 9$ , where these numbers corresponded to the macroscopic cross sections I.D. numbers in Table 2.1. However, the derivatives of the coefficients of  $\underline{\underline{M}}$  and  $\underline{\underline{F}}$  with respect to  $K\Sigma_{f1}$  and  $K\Sigma_{f2}$  are zero. Therefore, these two cases are omitted in DERIV, and the cross section sensitivities  $\underline{s}^x$ , which are also calculated in DERIV are only listed for seven cross sections using the newly defined macroscopic cross section I.D. numbers listed in Table D.1. In addition to



Table D.1. Macroscopic Cross Sections  
with Sensitivity Coefficients

Identification Number	Macroscopic Cross Section
1	$\Sigma_{tr_2}$
2	$\Sigma_{a_1}$
3	$\Sigma_{r_1} = \Sigma_{s_{1 \rightarrow 2}}$
4	$\nu \Sigma_{f_1}$
5	$\Sigma_{tr_2}$
6	$\Sigma_{a_2}$
7	$\nu \Sigma_{f_2}$

calculating the cross section sensitivity coefficients  $s_i^x$  at each exposure step  $i$ , DERIV calculates the sum of these coefficients over all exposure steps,  $\sum_{i=0}^{\ell} s_i^x$ ,  $x = 1, \dots, 7$ . This subroutine also calculates the control variable sensitivity coefficients  $\alpha_{c_k}$  defined in Eq. (2.49), the product  $\underline{S}_{\ell}^* \underline{F}_{\ell} \underline{S}_{\ell}$  in Eq. (2.50), and the exposure importance  $\underline{E}^*$  in Eqs. (2.35), (2.41), and (2.48).

The new subroutine DIREFF is called by DERIV at the final exposure step whenever SIMULATE conducts a backwards march through time for a response other than  $k_{eff}$ . DIREFF calculates the contribution of the "direct effect" to the sensitivity coefficients at the final exposure step, which is the expression

$$\frac{\partial R}{\partial H_{\ell}} \frac{\partial H_{\ell}}{\partial \Sigma_{\ell}^x} \quad (D.2)$$

in Eq. (2.40). Recall that R is defined as

$$R \equiv \frac{H_1 \cdot S_\ell}{H_2 \cdot S_\ell} , \quad (D.3)$$

so that

$$\frac{\partial R}{\partial H_\ell} = \frac{\partial R}{\partial H_1} + \frac{\partial R}{\partial H_2} . \quad (D.4)$$

The expression in Eq. (D.2) can be written

$$\frac{\partial R}{\partial H_\ell} \frac{\partial H_\ell}{\partial \Sigma_\ell^x} = \frac{\partial R}{\partial H_1} \frac{\partial H_1}{\partial \Sigma_\ell^x} + \frac{\partial R}{\partial H_2} \frac{\partial H_2}{\partial \Sigma_\ell^x} \quad (D.5)$$

Since  $H_1$  and  $H_2$  will differ for each response of interest, general equations for each term on the RHS of Eq. (D.5) cannot be programmed into SIMULATE. The specific equations for these terms *must be supplied by the user* whenever such depletion perturbation theory reference cases are to be solved. This is done in the subroutine DIREFF, which is ordinarily a dummy subroutine which sets all these terms equal to zero. When the user supplies the proper equations to DIREFF, the subroutine DERIV then uses the solutions of these equations to solve Eq. (D.5) which is substituted into Eq. (2.40).

EXPOSE is a new subroutine which uses logic based on that of SIGDAT, the subroutine in SIMULATE which evaluates the macroscopic cross sections at each exposure step. EXPOSE calculates  $\frac{\partial f^x}{\partial E_i}$  and  $\frac{\partial f^x}{\partial C_K}$ , the derivatives of the cross section polynomial fitting function with respect to exposure and control variable K, respectively. The possible identification numbers are listed in Table D.2.

Table D.2. Identification Numbers of Available Control Variables

ID Number	Variable	Comments
1	$E_{ijk}$	Nodal Exposure, GWD/T
2	$CT_{ijk}$	Control Flag, = 1 for uncontrolled = -1 for controlled
3	$P^*_{ijk}$	Node power relative to core average rated value
4	$U_{ijk}$	Relative Water Density
5	$V_{ijk}$	Void History
6	$\sqrt{T}_{fijk}$	Square root of fuel temperature, °K
7	$C_B$	Boron number density related variable ( $C_B$ is input on Card 1)
8	$C_B^U_{ijk}$	Boron concentration related variable
9	$h$	Axial position in cm from bottom surface of core
10 - 20	Spares	
21	$N_I$	Nuclide concentrations, atoms/bn-cm Iodine, $I^{135}$
22	$N_{Xe}$	Xenon, $Xe^{135}$
23	$N_{Pm}$	Promethium, $Pm^{149}$
24	$N_{Sm}$	Samarium, $Sm^{149}$

EXPOSE is only programmed to handle a maximum of two control variables for each reference case. This should be sufficient for most users, but the limit can be easily expanded by the user, if necessary. The polynomial fitting function may be a function of up to three variables, but EXPOSE can calculate the derivatives of any particular polynomial with respect to only one control variable. Thus, if a polynomial is a function of exposure and any other variable, the derivative of that polynomial with respect to that second variable cannot be calculated by EXPOSE because the derivative with respect to exposure is required for the solution of the depletion adjoint equations. This is not viewed as a serious restriction since the polynomials are generally a function of one variable each.

The subroutine FIXSRC calculates the fixed source for the fixed source adjoint equation. If the fixed source  $Q^*$  was input to SIMULATE for a response other than  $k_{\text{eff}}$  (Eq. (2.38)), FIXSRC reads  $Q^*$  from disk (where it was placed by INPUT1) and stores it in memory. For the solution of Eq. (2.44), which is for exposure steps prior to the final step ( $i < \ell$ ), the fixed source  $Q^*$  is calculated by FIXSRC for each exposure step.

The new subroutines which have been added to SIMULATE are listed in Table D.3 with a brief description. The subroutine(s) which call each one are written in parentheses.

The names and numbers assigned to the various I/O units used for storing data during the forward and backward marches through time are listed in Table D.4. Units 21-32 are required for any forward and backward march through time. Units 33 and 34 are required if the

Table D.3. New Subroutines Added to SIMULATE

Name	Purpose
BUGTAP	Writes sensitivity coefficients on I/O unit for calculations external to SIMULATE. (DERIV)
CALMAT	Calculates the coefficients of $\underline{M}$ & $\underline{E}$ explicitly. (SOURCE)
DERIV	Calculates the partial derivatives of the nodal coupling coefficients and the sensitivity coefficients. (PARTB)
DIREFF	Calculates the direct effect contribution to the sensitivity coefficients for responses other than $k_{eff}$ . (DERIV)
EXPOSE	Evaluates the derivatives of the cross section fitting functions with respect to exposure and other control variables. (PARTB)
FIXSRC	Calculates the fixed source for the depletion adjoint equations. (PARTB)
REPLAC	Replaces the present exposure distribution with that of the previous exposure step. (DPART, PARTB)
STACK	Transfers source and exposure distributions of all forward exposure steps from sequential to direct access I/O units. (DPART, DERIV)

Table D.4. I/O Units for Forward and Backward March Through Time

I/O No.	I/O Name	Variable Speed	Type I/O
21	ITAPAA	$\underline{S}_i$	Sequential
22	ITAPBB	$\underline{S}_i^*$	Sequential
23	ITAPCC	$\underline{F}_i \underline{S}_i$	Sequential
24	ITAPDD	$\underline{Q}_i^*$	Sequential
25	ITAPEE	$\underline{E}_i$	Sequential
26	ITAPFF	$\underline{S}_i^*$	Direct Access
27	ITAPGG	$\underline{F}_i \underline{S}_i$	Direct Access
28	ITAPHH	$\underline{E}_i$	Direct Access
29	ITAPII	$\underline{S}_i$	Direct Access
30	ITAPJJ	$\underline{E}_i^*$	Sequential
31	ITAPKK	$\frac{\partial f^x}{\partial \underline{E}_i}$	Sequential
32	ITAPLL	$\sum_{i=0}^{\lambda} \underline{S}_i^x$	Sequential
33	ITAPMM	$\underline{\alpha}_{c_1}$	Sequential
34	ITAPNN	$\frac{\partial f}{\partial \underline{c}_1}$	Sequential
35	ITAPOO	$\underline{\alpha}_{c_2}$	Sequential
36	ITAPPP	$\frac{\partial f}{\partial \underline{c}_2}$	Sequential

sensitivity coefficients for a single control variable are desired. If sensitivity coefficients for a second control variable are desired, units 35 and 36 will also be required.

### User Options

SIMULATE can be used to solve any number of different variations on a problem. The data for an "independent case" must be submitted first. This data has to contain all necessary information for SIMULATE to solve the initial problem, whether static or burnup-dependent. This case can be followed by any number of "dependent cases," where only the data which the user wishes to change must be submitted.

A user will submit an independent case to begin a forward march through time for a particular fuel cycle for a given reactor design. The forward march may be executed entirely from the independent case, but usually it will require several dependent cases since many input parameters may change during the course of a fuel cycle (e.g., boron concentration).

Once the forward march has been completed, a dependent case must be submitted to begin the backward march through time. Usually the number of cases required to execute the backward march will equal the number of cases for the forward march, because the input parameters changed during the forward march must be changed in reverse order during the backward march.

SIMULATE reads its input from numbered cards with free format input. The card number identifies the data which appear on the card. Free format input does not have fixed fields as do normal input. The

input data are assigned to the proper variable names according to the order in which they appear on the card.

Card Type 25 is an extra card type available for the user in the original version of SIMULATE. The data from this card are assigned to the MODEF array, which can store a maximum of twenty values. SIMULATE has been modified to use the MODEF array as input user options for the solution of the depletion adjoint equations. The options available to the user are listed in Table D.5. The default value for all members of the MODEF array is zero. The user should never submit input values for MODEF(5)–MODEF(10), which are used internally by SIMULATE during the forward and the backward marches through time. The purposes of these internal flags are listed in Table D.6.

If Card 25 is not submitted by the user, this new version of SIMULATE will operate like the original version of the code. Executing a forward and backward march through time will use approximately six times the CPU time and will cost approximately six times as much as the same forward run using the original version of SIMULATE. This is expected, since the forward and backward march solves three equations (forward, k-adjoint, and fixed source adjoint) for every equation that the original code solves. The CPU time is also increased by the calculation of the partial derivatives and the increased use of I/O devices.

The fixed source adjoint solution generally takes significantly more iterations to converge than the solutions of the other two equations. Several methods of convergence acceleration were tested (including overrelaxation, Chebyshev polynomial, and no acceleration) to see if the rate of convergence could be improved. It was determined



Table D.5. Control Options for Depletion Adjoint Equations  
Card Type 25, Array MODEF

---

MODEF(1) = 0	Solve only the forward equation.
= 1	Solve the k-adjoint and the forward equations.
= 2	Solve the fixed source adjoint equation. Use this for response other than $k_{eff}$ for static case and for all responses for backward march through time.
MODEF(2) = 0	All cases except the following:
= 1	Set to this value when MODEF(1) = 2 for static case.
= 2	Set to this value when MODEF(1) = 2 and $Q^*$ is <u>not</u> being input (i.e., for $i \neq \ell$ ) for burnup-dependent case.
= 3	Set to this value when MODEF(1) = 2 and $Q^*$ is being input (i.e., for $i = \ell$ ) for burnup-dependent case.
MODEF(3) = 0	Exposure distribution is set to $E_{\ell-1}$ at end of forward march in preparation for backward march through time ( $k_{eff}$ response).
= 1	Exposure distribution is left at $E_{\ell}$ at end of forward march in preparation for backward march through time (response other than $k_{eff}$ ).
MODEF(4) = 0	Bypass calculation of <u>M&amp;F</u>
= 1	Calculate <u>M&amp;F</u> explicitly. Use only for debug - requires large amount of storage.
MODEF(5) - (10)	Reserved for internal flags.
MODEF(11) = 0	Do not write cross section sensitivity coefficients $s_i^X$ on I/O unit for later use.
= m	Write cross section sensitivity coefficients on I/O unit number m for later use.

Table D.5 (Continued)

---

MODEF(12) = 0	Do not write macroscopic cross sections on I/O unit for later use.
= n	Write macroscopic cross sections on I/O unit number n for later use.
MODEF(13) = 0	Do not calculate any control variable sensitivity coefficients.
= p	Calculate sensitivity coefficients $\alpha_{c_1}$ for control variable p (see Table 4.2).
MODEF(14) = 0	Do not calculate sensitivity coefficients for a second control variable.
= q	Calculate sensitivity coefficients $\alpha_{c_2}$ for control variable q.
MODEF(15) = 0	Do not write sensitivity coefficients $\alpha_{c_1}$ on I/O unit for later use.
= r	Write sensitivity coefficients $\alpha_{c_1}$ on I/O unit number r for later use.
MODEF(16)	Same as MODEF(15) for $\alpha_{c_2}$ .
MODEF(17) = 0	All cases except the following:
= 1	This is the final case (independent or dependent) in the forward march through time. (If this is a static case, MODEF(17) = 1, too).

---

Table D.6. Internal Flags for Depletion Adjoint Equations

---

MODEF(5) = NSTEP =	Exposure step $i$
MODEF(6) =	1, if MODEF(1) = 1 initially
MODEF(7) = NREC =	Total number of records for each of the source and the exposure distributions
MODEF(8) = IREC =	location on direct access I/O unit where array for step $i$ is stored = $2 - i + 1$
MODEF(9) = LSREC =	number of records per time step for each array = $\left( \frac{ID * JD * KD}{1600} \right) + 1$
MODEF(10) = 0	Calculate the NBT array in NBTCAL
= 1	Calculate the NBD array in NBTCAL

---

that the Chebyshev acceleration already in SIMULATE was the best method of convergence acceleration.

The printing of the output edits are controlled by Card Type 19, the IEDIT array. Several of the new arrays developed in the depletion adjoint equations have been put under user control in this array. Some are printed and some are suppressed by default, but any array can be printed if the user desires. A value of 0 signals the code to print the output edit, and a value of 1 suppresses the printing of that edit. The new variables which can be controlled by the IEDIT array are listed in Table D.7 with their control flag numbers and their default values.

Table D.7. Edits of New Arrays

DPT Variable Name	FORTTRAN Array Name	Control Flag	Default Value
$s^x$	SX	IEDIT(35)	0 (ON)
$\sum_{i=0}^{\ell} s^x$	SXSUM	IEDIT(36)	0 (ON)
$\alpha_{c_1}$	ALPHC1	IEDIT(37)	0 (ON)
$\alpha_{c_1}$	ALPHC2	IEDIT(38)	0 (ON)
$Q^*$	QSTAR	IEDIT(39)	0 (ON)
$\frac{\partial f^x}{\partial E}$	DFDE	IEDIT(96)	1 (OFF)
$\frac{\partial f^x}{\partial c_1}$	DFD1	IEDIT(97)	1 (OFF)
$\frac{\partial f^x}{\partial c_2}$	DFD2	IEDIT(98)	1 (OFF)
$A^*$	ASTAR	IEDIT(99)	1 (OFF)
$E^*$	ESTAR	IEDIT(99)	1 (OFF)
$F$	F	IEDIT(100)	1 (OFF)
$M$	AM	IEDIT(100)	1 (OFF)

In this section, we have presented the major modifications which have been made to SIMULATE in order to solve the depletion adjoint equations. Information concerning the use of this modified version of SIMULATE has also been presented. This information is supplemental to that given in the SIMULATE manual.<sup>2</sup>

## VITA

Stephen M. Bowman was born in Chattanooga, Tennessee, on March 8, 1956. He attended elementary schools in that city and was graduated from Red Bank High School in June 1974. The following September he entered The University of Tennessee, and in June 1979 he received a Bachelor of Science degree in Nuclear Engineering.

In the summer of 1979 he accepted a research assistantship at The University of Tennessee and began study toward a Master of Science degree, with a major in nuclear engineering. This degree was awarded in March 1981.

The author is a member of Phi Kappa Phi, Tau Beta Pi, and Phi Eta Sigma. Mr. Bowman will be employed with the Tennessee Valley Authority after graduation.

He is married to the former Joanna Fleenor of Huntsville, Alabama.